

„Structural characterisation of tBLMs”

—

From anchor modifications to a biomimetic platform

D i s s e r t a t i o n
zur Erlangung des Grades
„Doktor der Naturwissenschaften”

Am Fachbereich Biologie
Der Johannes Gutenberg-Universität in Mainz

Ann Falk
geb. am 18. Februar 1981 in Mittweida

Mainz, 2009

Dekan:

1. Gutachter:

2. Gutachter:

Tag der mündlichen Prüfung: 24. Juni 2009

Contents

1	Abstract & Motivation	1
2	Membranes	5
2.1	Biological membranes	5
2.2	Model membranes	6
2.2.1	Vesicles	6
2.2.2	Bilayer lipid membranes	7
2.2.3	Solid supported lipid bilayers	7
2.3	Model membranes and proteins	10
2.3.1	Solid-liquid interface	10
2.3.2	Air/Oil-liquid interface	11
3	Material and Methods	13
3.1	Neutron Reflectivity (NR)	13
3.1.1	Interactions	14
3.1.2	Contrast matching & variation	16
3.1.3	Measurements	17
3.1.4	Data	18
3.1.5	Fitting	19
3.2	Surface Plasmon Resonance (SPR)	23
3.2.1	Surface Plasmon excitation	23
3.2.2	Sample Preparation	24
3.2.3	Data evaluation	24
3.3	Electrical Impedance Spectroscopy (EIS)	26
3.3.1	Measurement	26

3.3.2	Equivalent circuit models	27
3.3.3	Representation of impedance spectra	28
3.4	Isotherms	29
3.4.1	Surface pressure measurement	30
3.4.2	π - A - isotherms	31
3.4.3	Brewster angle microscopy	33
3.5	Procedure	35
3.5.1	Buffer preparation	35
3.5.2	Metal evaporation	35
3.5.3	Template stripped gold	35
3.5.4	Self assembly	36
3.5.5	Vesicle preparation	36
3.5.6	Rapid solvent exchange	36
4	β-lactoglobulin	39
4.1	Introduction	39
4.1.1	Properties of β -lactoglobulin	40
4.1.2	Milk fat globule membrane	41
4.1.3	β lg - lipid interactions	42
4.2	Experimental	45
4.3	Results	47
4.3.1	Pre-investigations	47
4.3.2	β lg interaction with mono- and bilayers	49
4.3.3	Native vs. urea denatured β lg	56
4.3.4	Effect of cholesterol in the bilayer	60
4.3.5	Lipid layer packing density	64
4.3.6	pH influence	77
4.3.7	Comparison DPhyPC - DPhyPG	80
4.4	Summary	83
5	Model membranes	87
5.1	DPTL	87
5.2	Anchor modifications	88

5.3	DPTT – DPHT – DPOT	92
5.4	DPHDL	98
5.5	DDPTT	100
	5.5.1 Comparison: DPTT vs. DDPTT	102
5.6	CholPEG	103
	5.6.1 Comparison: DPTL vs. DPTL-CholPEG	104
5.7	Cholesterol	105
5.8	Summary	107
Appendix		109
6.1	Abbreviations	109
6.2	Chemicals	111
6.3	DSC	112
6.4	EIS values	112
6.5	GaRefl setup.c protocols	113
Acknowledgements		118
Bibliography		120

Chapter 1

Abstract & Motivation

Biological membranes are one of the vital key elements of life. They define the boundaries of cells and control the interactions of a cell with its environment. Thus, they are involved in processes such as cell motility, energy transduction, immune reactions, nerve conduction, cell-cell signalling or biosynthesis. Additionally, they have applications in various fields, from biosensing applications to food science processes. [1]

The generic structure of a biological membrane is a lipid bilayer. In nature, the bilayer is composed of a large variety of different lipids. The structure then supports incorporated transmembrane as well as peripheral proteins. Biological membranes are thus highly complex architectures. Therefore, various model membrane systems have been developed to enable systematic investigations of different membrane related processes. These investigations include fundamental thermodynamic questions up to approaches from more medical problems. A biomimetic model architecture should provide a simplified system, which allows for systematic investigation of the membrane while maintaining the essential membrane characteristics such as membrane fluidity or electrical sealing properties. [2]

This work has been focused on two complementary parts. In a **first part**, the behaviour of the whey protein β -lactoglobulin at a membrane interface has been investigated. β lg is the major component in bovine milk [3]. It coexists with the milk fat globular membrane [4]. During the homogenisation

of milk, β lg adsorbs at the interface of fat globules and thus stabilises the oil-in-water emulsion [5, 6]. The interactions between the protein and the membrane have thus important implications in food processing processes such as the stabilisation of emulsions [7], gelation [8] or foaming [9].

Additionally, β lg is proposed to facilitate the digestion of milk fat [10], but is also supposed to be one of the allergens for human infant milk allergy [11].

Protein-lipid interactions have been investigated using Langmuir monolayers at the air-water interface and tethered bilayer lipid membranes. A combination of different surface analytical techniques such as surface plasmon spectroscopy, neutron reflectivity and electrochemical techniques allowed for a detailed analysis of the underlying processes.

In the **second part** of this work, the structure of different model membrane systems has been investigated. Solid supported membrane systems have been established as powerful biomimetic architectures, which allow for the systematic investigation of various membrane related processes. Additionally, these systems have been proposed for biosensing applications. Tethered bilayer lipid membranes (tBLMS) are one type of solid supported membranes. In principle, these architectures consist of a lipid bilayer that is covalently attached to a solid support *via* an oligomeric spacer group. [12] tBLMs are membranes with excellent stability and high electrical sealing properties. They have been used to study a wide variety of incorporated ion channel proteins. [13–15]

The structure of the anchor lipid that anchors the membrane to the solid support has a significant impact on the membrane properties. Especially the sub-membrane part, which is defined by the spacer group, is important for the biological activity of incorporated membrane proteins. In principle, the spacer region should provide a hydrophilic reservoir and accommodate extra-membrane protein domains, thus avoiding denaturation of proteins upon direct interaction with the substrate. [16]

Previously, different anchor lipids have been synthesised with different spacer and anchor groups [14, 17, 18]. Additionally, a cholesterol-spacer has been designed to modulate the membrane fluidity [19]. The structures of tBLMs with different anchor lipids have been analysed using the same com-

bination of techniques as in the first part of the work.

This manuscript comprises 5 chapters. In chapter 2, a general introduction to membranes and model membrane systems is given. Chapter 3 gives an overview of the techniques used. In chapter 4, results of the interaction of β lg with different model membrane architectures are given. Finally, chapter 5 summarises results of the structural investigations of various tBLMs.

Chapter 2

Biological and model membranes

2.1 Biological membranes

Membranes are the most widespread structures in plant and animal cells. They are composed of different lipids and proteins, that are directly linked to their functional diversity [20]. This variety is depicted in a descriptive model known as the ‘fluid mosaic model’ by Singer and Nicolson (fig. 2.1) [21].

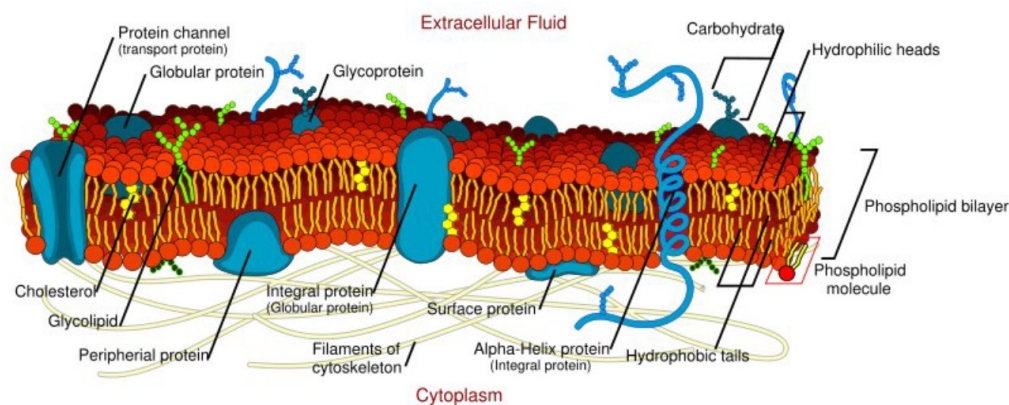


Figure 2.1: Illustration of the cell membrane – Fluid-Mosaic-Model by Singer & Nicolson [21] (Picture: Open source)

The lipid bilayer provides the structural framework of the membrane and

enables motion of incorporated proteins. Although the model is widely accepted, its simple thermodynamic considerations underestimate for example lipid heterogeneity and it tends to stress the planar bilayer and the independence of proteins. A more accurate model would have to take into account the dynamic organisation of the membrane as well as interactions between lipids and proteins. However, it is yet not possible to elucidate the full structure-function relationship of the membrane architecture. Nevertheless, an understanding of the physical principles that govern the molecular organisation of membranes is essential to comprehend their physiological roles. [2]

Due to the high complexity of a biological membrane, most experiments are performed using simpler model systems. These can be lipid bilayers, as well as vesicles or multilayers, which allow to study the system under well-controlled conditions.

2.2 Model membranes

2.2.1 Vesicles

Amphiphilic molecules in an aqueous solution aggregate spontaneously to reduce the system free energy when the critical micelle concentration is reached. The emerging structures are determined by the thermodynamic interplay of entropy (small structures) and packing constraints. For example, if double chained lipids with small head-group areas are present, planar lipids are formed. In the case of single-chained lipids with large head-group areas micelles are preferred, if the lipids are double chained with fluid chains vesicles are formed. [2]

Isolated, natural vesicles are composed of a complex mixture of different lipids and proteins, exhibiting fundamental similarities to the cell membrane. Due to this, vesicles are extensively used for studying specific biological phenomena. In a living cell, lipids are transported as vesicles, making them important model systems for gene and (target) drug delivery. The major drawback of vesicles as model systems is that they are experimentally difficult to access.

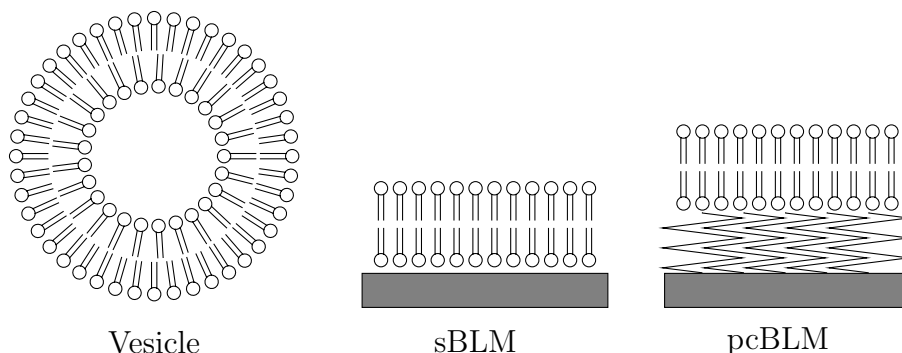


Figure 2.2: Examples for model membranes

2.2.2 Bilayer lipid membranes

Black, bimolecular or bilayer lipid membranes (BLM) are one of the earliest model bilayer systems [22].

In a BLM setup, both lipid leaflets are separately accessible, making them well suited for electrical measurements. (Resistance typically $M\Omega$ Ohms or higher for intact bilayers, capacitance $\approx 2\mu\text{F}/\text{cm}^2$.) Such electrical characterisations are particularly important in the study of voltage gated ion channels. Another advantage is that asymmetric membranes can be formed by adjoining two lipid monolayers of different chemical composition.

BLMs are highly susceptible to mechanical vibrations and suffer from short lifetimes (≤ 1 d), but advancements could be made by encapsulating a BLM in situ within a hydrogel, which extended the lifetime up to 11 d [23].

2.2.3 Solid supported lipid bilayers

To overcome the extreme fragility of bilayer lipid membranes and to extend their life-time from hours to weeks and months [24,25], solid supported bilayer lipid membranes (sBLMs) were developed. This also expanded the range of characterisation tools to methods that require a direct physical interaction with the sample. Additionally, attaching bilayers to functional materials also enables the use of specific techniques, such as surface plasmon resonance on gold or magnetic contrast neutron reflectivity on magnetic materials.

Various methods can be employed to form the bilayer, either in one step

by vesicle fusion onto the substrate [26–29] or successively monolayer and bilayer. The monolayer can be constituted by e.g. Langmuir-Blodgett transfer [30–32], self-assembly [17, 33, 34], adsorption of charged lipids onto oppositely charged surfaces [35] or spontaneous thinning of lipid/decane mixtures [36–38]. The bilayer can be completed by Langmuir-Schäfer transfer [39–42], vesicle fusion [35, 43, 44] or rapid solvent exchange [15, 45, 46].

Supported bilayer lipid membranes

Supported bilayers (sBLMs) are planar structures with the upper part exposed to solution and the lower leaflets sitting, cushioned by a small water gap, on a solid substrate. This water layer is, depending on substrate and lipid, in the range of nanometres [47, 48] and limits the utility of sBLMs in studying integral membrane proteins with large domains, as they often denature on the substrate surface and lose their functionality. Membrane processes of ion carriers and channels cannot be characterised because an adequate ionic reservoir on the lower side of the membrane is missing. [16]

Another drawback is the hydrophobic coupling between the bilayer and the substrate that reduces the fluidity of the membrane, compared to other model systems presented below [49].

Polymer cushioned bilayer lipid membranes

In a polymer cushioned BLM (pcBLMs), a bilayer is applied onto a network of soft hydrated polymers or onto a hydrogel. This polymer layer acts as a spacer as well as support for the biomembrane, similar to the the cytoskeletal support found in mammalian cells. [41, 49–51]

However, the roughness of the polymer cushion might influence the bilayer quality as often the formed bilayers are not complete, inhomogeneous and not well-sealing.

Tethered bilayer lipid membranes

Tethered bilayer lipid membranes (tBLMs) combine the advantages of solid supported membranes with a defined ionic reservoir and sub-membrane space. Their principal composition (fig. 2.3) consists of a spacer molecule that binds the membrane to the solid surface and controls the sub-membrane space. The inner part of the bilayer is connected to this anchor. The bilayer is usually completed by mobile lipids. They are relatively easy to build and there is a growing interest in various research fields as well as for industrial applications. [15, 17, 46, 52, 53] To summarise the advantages of tBLMs they:

- are accessible to wide range of characterisation techniques
- possess a ionic reservoir on each side of the membrane
- prevent direct contact of membrane compounds and the solid substrate
- are insulating, but still fluid
- are highly stable
- feature easy and reproducible fabrication

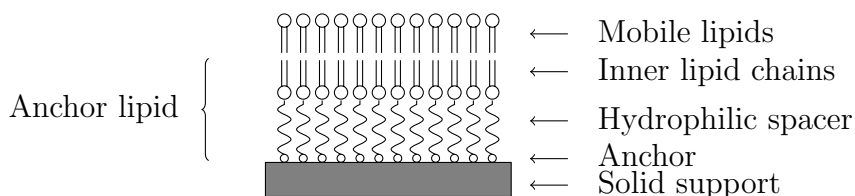


Figure 2.3: Schematic illustration of a tBLM

The inner bilayer leaflet is attached to the solid support via a spacer group. The upper bilayer leaflet is made of mobile lipids.

Protein tethered bilayer lipid membranes

A special class of tBLMs are protein tethered BLMs (ptBLMs), where the incorporated protein itself acts as the tethering moiety [54]. This is especially useful for biosensing/lab on a chip applications, as it is ensured that the sensing protein is in the right configuration and position.

2.3 Model membranes and proteins

Proteins at interfaces play an important role for fundamental biophysical and biochemical issues, as well as for a variety of technological applications.

Approximately 30% of all proteins are membrane associated. Precise investigations of the interactions between those proteins and the lipid bilayers are not only of interest for academics, but also lead to important applications, e.g. drug targeting in the pharmaceutical industry. [55]

Most studies on proteins at solid surfaces concentrate on biomaterial research such as the integration of an implant etc. [56–61].

Biomimetic investigations, exploring the interactions of proteins on phospholipid-covered surfaces and relating them to in vivo activity are rather rare. [62, 63]

2.3.1 Solid-liquid interface

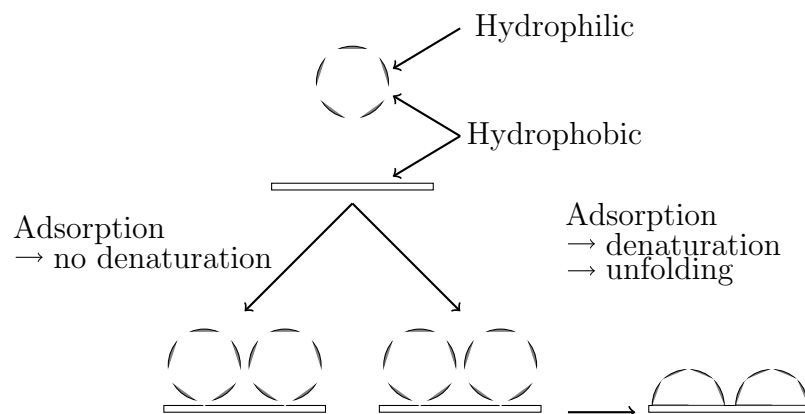


Figure 2.4: Schematic illustration of the adsorption of proteins to hydrophobic surfaces [63]. The protein, which possesses hydrophobic and hydrophilic patches, can either adsorb and remain in its native conformation, or denature and unfold.

The interface between two different phases has a higher free energy than the bulk phase. Adsorbing solutes from solution will thermodynamically stabilise this interface [58].

Additionally, the driving forces for protein adsorption are generally very complex, including van der Waals interactions, hydrophobic interactions, and electrostatic interactions between oppositely charged surfaces and proteins or protein domains [57].

The adsorption behaviour depends also on the surface characteristics as well as on the type of protein. Throughout the adsorption process, environmental conditions such as salt concentration, protein charge, dipole moment, hydrophobicity and especially surface charges play a vital role. It has been observed that proteins maintain more structure on electrostatically neutral hydrophilic surfaces than on hydrophobic or charged surfaces. [60]

During the adsorption to solid hydrophobic surfaces (fig. 2.4), presumably hydrophobic patches on the surface of the protein interact with hydrophobic regions on the surface. This is often followed by conformational changes of the protein, hence exposure of the hydrophobic core to the hydrophobic surface [63].

Although protein adsorption is well studied, detailed information about the relation of structure, activity and function after surface interactions is often missing.

2.3.2 Air/Oil-liquid interface

The interaction of proteins with solid surfaces has attracted more attention than the protein behaviour at air-liquid interfaces. However, such experiments provide a high level of simplification and enable clear determination of effects involved in protein-lipid interaction such as charge, hydrophobicity, pH, ionic strength.

The characteristics of protein adsorption is not as “straightforward” and differs in many aspects from those observed for surfactant monolayers [64]. For example, a protein at or close to an air-water interface, can undergo structural changes up to a complete denaturation.

Due to their amphipathic nature, proteins are surface sensitive [65]. If a water soluble protein is injected into an aqueous subphase, an increase in surface pressure π_S is observed, indicating that some interactions between

protein and interface occurred [66]. To be able to lower the surface tension, the protein has to undergo conformational changes namely unfolding to expose its hydrophobic regions. This is caused by hydrophobic interactions [67] and promotes protein-protein interactions [65] which lead to the formation of an adsorbed protein layer. The state of denaturation decreases with distance from the interface and eventually proteins encounter an environment very similar to the bulk, and net adsorption ceases [67].

As the denaturation can be a very slow process, and as protein molecules take more time to diffuse to the interface due to their size, the lowering of the interfacial tension is much slower than for surfactants [68]. Denaturation is facilitated at lower surface pressure and the rate of change can be connected to the amount of interfacial area available [64, 68].

If additional surface active material is present, e.g. lipids, the protein has to compete for interface space. Usually this leads to less interface available and therefore less protein unfolding and aggregation [65].

But native proteins are able to bind to lipids, either through hydrophobic patches on the molecule outside or inside a cavity. Thus, at the water-oil interface the protein may unfold as well. Additionally, lipid binding sites can be introduced by e.g. heat, pH or ionic strength. [68]

Chapter 3

Material and Methods

3.1 Neutron Reflectivity (NR)

Neutron reflectivity (NR) allows to probe the properties of samples up to 5000 Ångström in depth. In a neutron reflectometry experiment, the intensity of the neutron beam reflected by a surface is measured as a function of the scattering vector \vec{q} . The obtained scattering profile can be connected to the scattering length density (sld) of the sample. Neutrons are sensitive to differences in contrast (i.e. refractive index) in layers on top the substrate.

Neutrons can either be produced by spallation with the help of a particle accelerator or a controlled nuclear chain reaction in a reactor.

In a water tank that surrounds the reactor, neutrons collide with the atomic nuclei of the water, transfer energy to it and are therefore slowed down. After this “moderation” the energy of the neutrons is in a range that corresponds to ambient conditions and they are referred to as cold (or thermal) neutrons. The wavelengths of cold neutrons are in the range of 0.1 - 1 nm, which is approximately the same as the atomic spacings in soft matter. As the cross-section of neutrons is reciprocally proportional to their energy, thermal neutrons lead to more effective scattering in the sample, compared to faster neutrons. Due to the wave-particle dualism, neutrons scatter in solid

materials similar to X-rays and Bragg's law can be applied:

$$2 d \sin\alpha = n\lambda \quad (3.1)$$

where d is the distance of the planes in the atomic lattice, α is the angle between the incident ray and the scattering planes, n an integer to determine the scattering order and λ the used neutron wavelength.

When a collimated ray of particles ($p=mv$ and $\lambda = h/p$) strikes a plane under the angle α , constructive interference can be observed when the distance between the planes is $n\lambda$. Scattering leads to interferences that can be connected to the atomic structure of the probe. [69–71]

3.1.1 Interactions

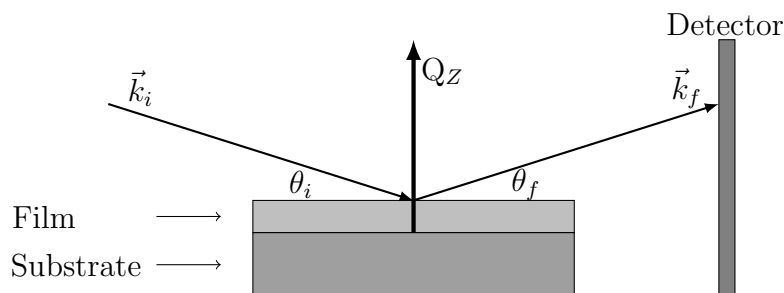


Figure 3.1: Incoming and outgoing wave vectors

In specular reflectivity measurements (fig. 3.1), neutrons strike upon the sample surface at an angle θ_i and are scattered at an angle θ_f . The incident and exit angles are equal ($\theta = \theta_i = \theta_f$).

The wave-vector transfer is defined as the difference between the final and initial wave-vectors $\vec{q} = \vec{k}_f - \vec{k}_i$. For elastic scattering of neutrons, the magnitudes of the incoming and outgoing wave vectors are the same and equal to the wave number,

$$|\vec{k}_i| = |\vec{k}_f| = 2\pi/\lambda \quad (3.2)$$

With $\theta = \theta_i = \theta_f$ follows $q_x = 0$ and this gives the wave vector Q_z

$$Q_z = 2 \sin \theta \cdot \vec{q} = (4\pi \sin \theta) / \lambda \quad (3.3)$$

In reflectometry, neutrons strike on a surface at a grazing angle of less than 3° . At these small angles, the potential for scattering can be approximated by a continuous value which is called the scattering length density ρ (sld). The neutron scattering length density is defined as:

$$\rho = \frac{\sum_{i=1}^n b_c}{v_M} \quad (3.4)$$

where b_c is the bound coherent scattering length of the i th of n atoms in a molecule with molecular volume v_M .

For cold neutrons, the very small angles of incidence can be sufficiently low to cause the neutrons to be totally reflected from the surface. This angle is the critical edge (fig. 3.2) and gives information about the average sld of the substrate material. At angles higher than the critical edge, the reflected

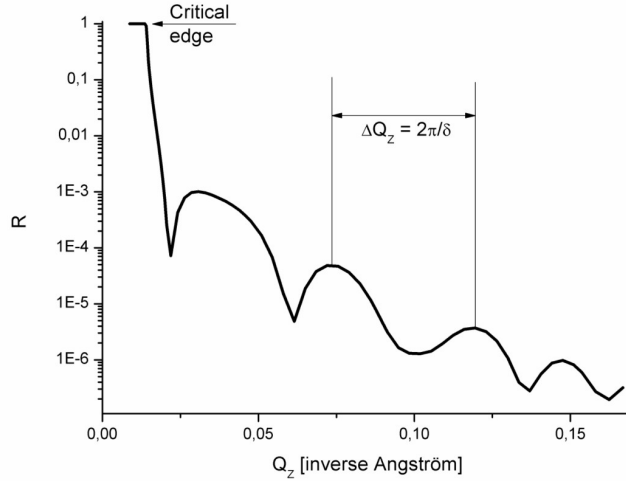


Figure 3.2: Neutron reflectivity profile

intensity comprises information about the change in scattering length density with depth. The data shows finite-size fringes that can be analysed to

determine total thickness of the film, material composition, periodicity, and roughness.

After subtraction of the off-specular background, these data can be fitted (or inverted) to obtain a real-space profile of the scattering length density as a function of depth.

3.1.2 Contrast matching & variation

Contrary to X-Ray methods, in neutron scattering the sld does not increase with atomic number but depends on the properties of the nucleus, which makes it possible to distinguish different nuclides and isotopes.

Biological materials are rich in hydrogen which is nearly invisible to X-rays, therefore neutron scattering is more descriptive for such samples. Using contrast matching or variation, we are able to increase the information obtained during the experiments significantly by using different ratios of H₂O/D₂O and highlight or blend out one element. This can be achieved due to the very different neutron cross section (cs), and therefore slds, of

- hydrogen ($cs = 82/sld = -0.56 \cdot 10^{-6} \text{Å}^2$ at $\lambda = 5 \text{Å}$ and $T = 20^\circ\text{C}$) and
- deuterium ($cs = 7.6/sld = 6.37 \cdot 10^{-6} \text{Å}^2$ at $\lambda = 5 \text{Å}$ and $T = 20^\circ\text{C}$).

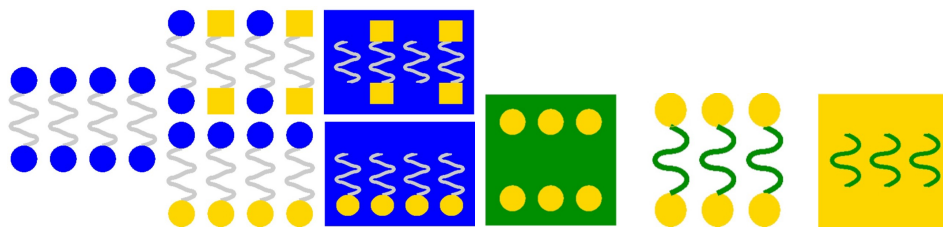


Figure 3.3: Contrast variation (left) and contrast matching (right)
 During contrast variation, hydrogen (\circ) in the sample is replaced by deuterium (\square). The so marked parts stick out or disappear, according to the buffer used.

In contrast matching, the sld of the buffer media is changed so that parts of the sample, with the same sld, fade out.

Contrast matching (or null scattering) describes the method to adjust the sld of the media to the value of a component of the system by mixtures of

D₂O and H₂O, so that certain parts of the structure, with different molecular composition, “stick out” (fig. 3.3). This is always under the assumption that the chemical structure of the interface is unchanged.

Mixtures used in this work are CM4 (3 H₂O : 7 D₂O, sld $\approx 4 \cdot 10^{-6} \text{Å}^2$) and CM5 (1 H₂O : 7 D₂O, sld $\approx 5 \cdot 10^{-6} \text{Å}^2$).

Contrast variation denotes the approach to substitute hydrogen to deuterium, similar to staining in biology. This requires complex preparation and is usually done in specialised laboratories associated with neutron facilities. However, for samples containing labile protons, such as in -OH groups, deuteration of certain groups is easily achieved.

Contrast matching/variation is not only suitable to distinguish otherwise similar molecular compositions, but also from the data analysis point it is useful to measure the sample in different contrasts. Due to the loss of phase information with the inversion of experimental data into scattering length density values, a measured reflectivity curve cannot be uniquely described by exactly one scattering length density profile. If at least two sets of data, with different contrast, were obtained, the phase information can be recovered and a unique sld profile can be calculated.

3.1.3 Measurements

Measurements were performed on the reflectometers AndR (fig. 3.4), NG1 and NG7 at the NIST Center for Neutron Research, National Institute for Standards and Technology, Gaithersburg, MD/USA.

Samples were placed in a silicon wet cell (Fig. 3.5), mounted on the instrument and aligned. Prior to the neutron reflectivity measurement an incident beam scan through the thick fronting wafer is performed in order to measure the direct beam intensity. The later-on measured specular reflectivity will be normalised to the direct beam incident intensity.

The cell is first filled with D₂O-based buffer and the specular reflectivity is typically measured between momentum transfers $0 \leq Q_z \leq 0.35 \text{Å}^{-1}$. The background intensity offset to both sides of the specular ridge is measured separately. The background neutron radiation mainly originates from in-

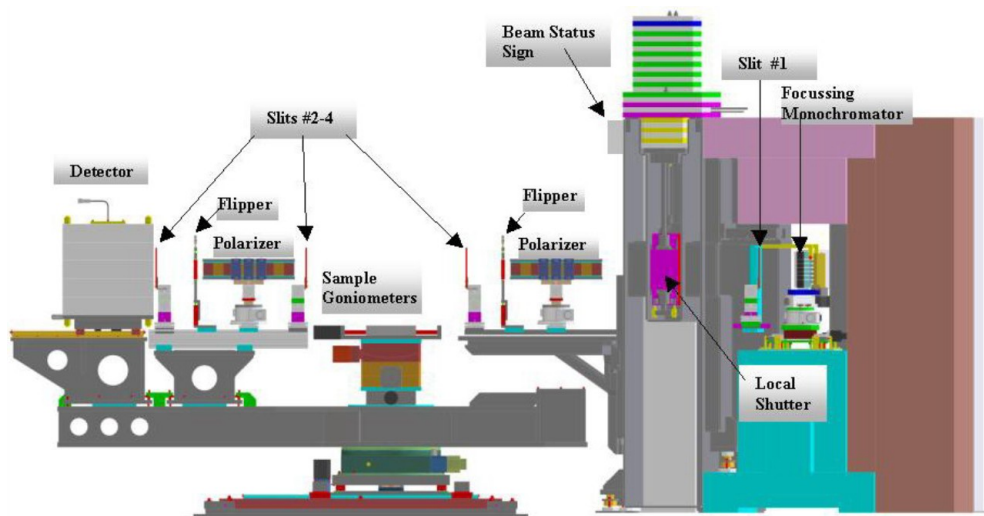


Figure 3.4: Elevation view of the AndR instrument.
 (Provided by J.A. Dura, NCNR Gaithersburg/USA)

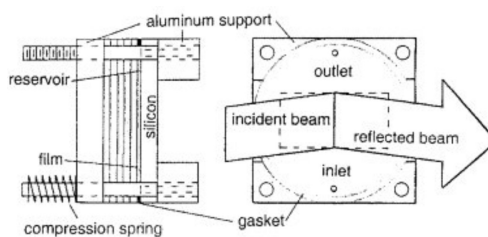


Figure 3.5: Drawing of the NCNR wet cell [72].

coherent scattering from the bulk solvent reservoir. The measurement is repeated after filling the wet cell with D_2O/H_2O -based buffer. If necessary, different mixtures of D_2O and H_2O are used. This way, distinct data sets of the same sample in contact with isotopically different bulk solvents are recorded.

The neutron reflectivity is calculated from the measured specular raw data, the background data and the incident beam data.

3.1.4 Data

The reflectivity profile, hence the plotted intensity of reflected radiation as a function of angle, provides information about the structure of the surface,

including thickness, density, and roughness.

The position of the critical edge gives information about the nuclear (chemical) composition of the substrate of the sample. The periodicity of the fringes is related to the layer thickness δ (approx. $2\pi/\delta$) and their amplitude can be connected to the nuclear (chemical) contrast across the interface (fig. 3.6, left). The attenuation of the reflected intensity is dependant on the roughness of the surface (fig. 3.6, right). These parameters additionally are all depend on the sample substrate and the solvent (fig. 3.7, left). All those factors superimpose and result in a complicated reflectivity profile (fig. 3.7, right).

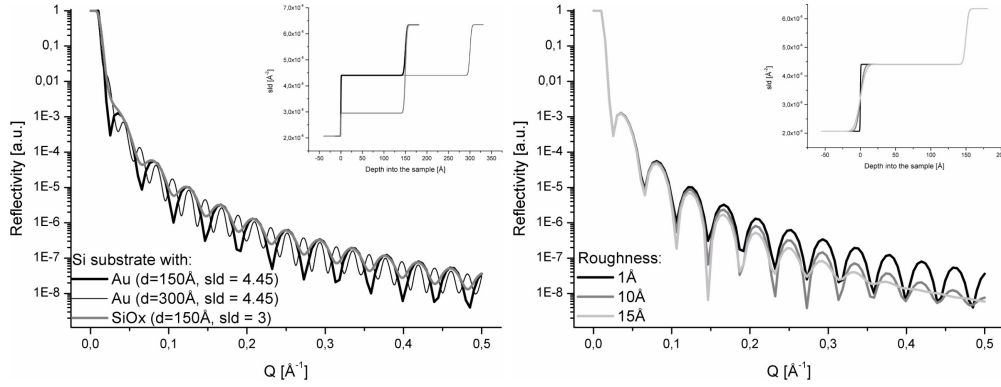


Figure 3.6: Reflectivity curves of a perfect interface between D_2O and a silicon substrate and corresponding scattering length density profiles (inset). left: Comparison of samples with 150 Å (black), 300 Å (thin black) gold ($sld = 4.45 \cdot 10^{-6} \text{Å}^2$), and 150 Å (dark grey) SiOx ($sld = 3 \cdot 10^{-6} \text{Å}^2$). Thicker layers lead to smaller periods, films with smaller nuclear contrast to smaller amplitudes.

right: Comparison between sample roughness 1 Å (black), 10 Å (dark grey) and 15 Å (light grey). The attenuation increases with increasing roughness.

3.1.5 Fitting

Parratt's Recursion Relation

One method of calculating reflectivity profiles is based on Parratt's recursion relation [73], which was originally conceived for X-ray reflectivity data evaluation.

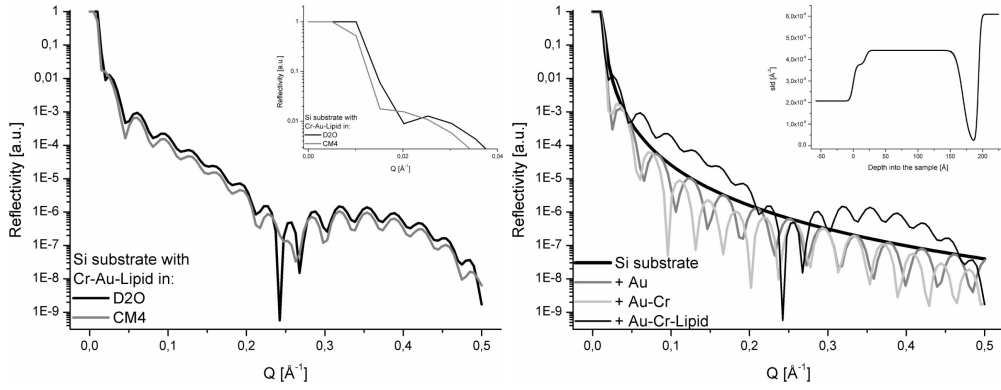


Figure 3.7: Reflectivity curves of a perfect interface between D_2O and a silicon substrate with a 150 \AA Au layer.
left: Solvent influence on reflectivity curves. The differences are especially visible at the critical edge and small Q (inset), as well as in the region of interest resulting from the lipids ($0.2 - 0.3 \text{ \AA}^{-1}$).
right: Calculated reflectivity curves of Si substrate (black) with 150 \AA Au (dark grey), additional 20 \AA Cr (light grey) and 25 \AA lipid layer (thin black) and corresponding scattering length density profiles (inset).

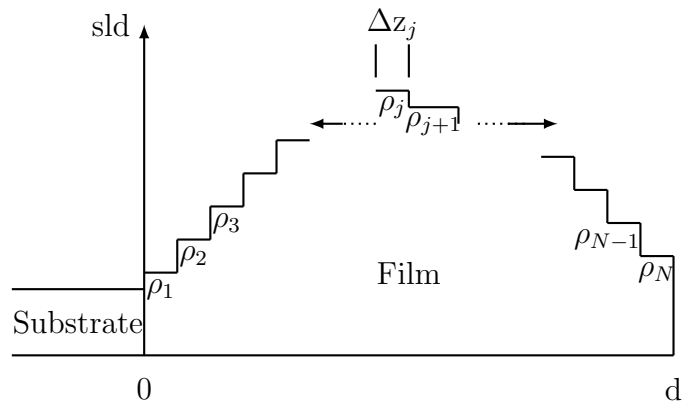


Figure 3.8: Scattering length density profile used for calculating reflectivities from Parratt's recursion relation. The profile is divided into N layers, and the wave is calculated in each layer.

It is an iterative technique where the model scattering length density profile is broken up into a series of layers as shown in Fig. 3.8.

Since all of the phase information is lost in a conventional experiment, direct inversion of the recorded data into the scattering length profile $\rho(z)$, is mathematically not possible. An iterative fitting procedure must be used to deduce $\rho(z)$ from the reflectivity data.

Data reduction using the NCNR 'refpak' reflectometry package

The NCNR 'refpak' reflectometry package [74] is one of many different methods to fit reflectivity data. It uses Parratt's recursion relation to calculate reflectivities from a model profile and parameters are varied in a systematic way.

In order to calculate the neutron reflectivity, the background intensity is first subtracted from the specular reflectivity and the difference is divided by the incident beam intensity. This is called data reduction.

The data is fitted by 'Reffit' to a model of neutron scattering length density profile along the axis perpendicular to the substrate surface.

The fitted sld profile is structurally interpreted in terms of chemically distinct layers. In case of a solid supported lipid bilayer, the following order of layers was used: the silicon substrate, the silicon oxide layer, the chromium layer, the gold layer, the spacer region, the inner headgroup layer, the outer headgroup layer, and the bulk solvent phase (fig. 3.9).

As 'Reffit' only simulates single data sets, it was only used for a rough calculation of the parameters. These parameters were then fed into 'Gareff'. This software is also part of the 'refpak' package, and allows to simultaneously fit data sets with isotopically different bulk solvents.

"Ga_refl" is a C++-based system for modelling reflectivity data using Parratt-formalism and model refinement using a genetic algorithm. It has been designed to enable the simultaneous fitting of multiple data sets. The initial model, data sets, constraints and beam details are adjusted in setup c-file. An example for such a protocol can be found in the appendix (Sec. 6.5). After compiling the setup file, the fitting procedure is started, which involves

solution of a coupled linear equation system by GNU octave. Sets of possible values of fitting parameters are created randomly, the reflectivity is calculated for each data set and then evaluated against a test function (χ^2). Genetic algorithms are normally maximising functions, so the quality defined for each set of parameter values is calculated as $\chi_{max}^2 - \chi^2$ where χ_{max}^2 is a user-defined constant value (by default 5000 x number of data sets). Parameter sets which give rise to $\chi^2 > \chi_{max}^2$ are given a quality of zero. Each time the quality of a fit is better than the current best, the old data set is substituted and the new parameter values are stored. Fitting a 4 stack data set requires simulation time in the range of hours to days. The post-processing is done by e.g. gnuplot or Origin.

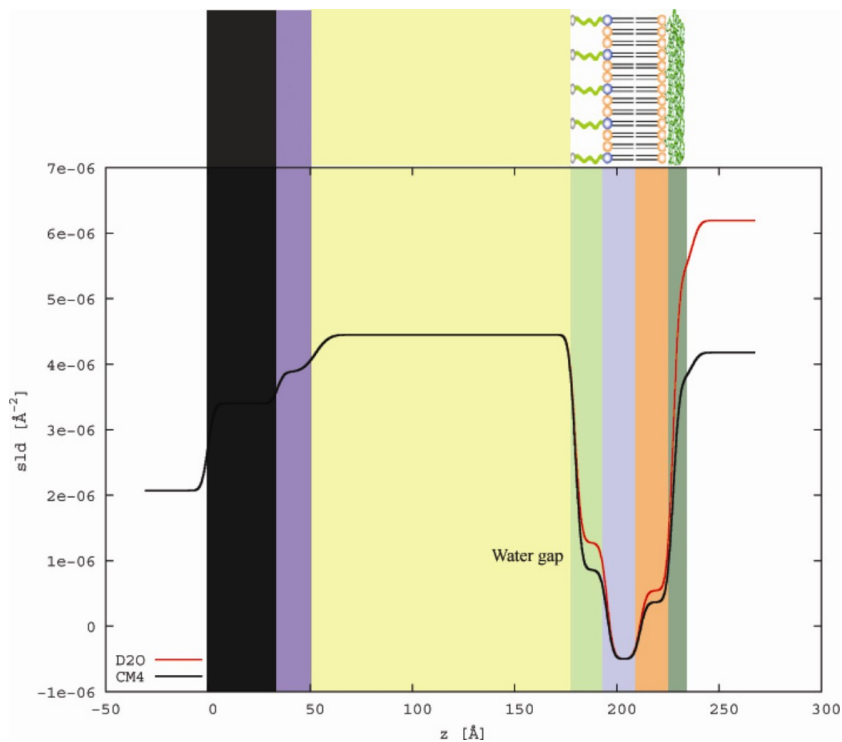


Figure 3.9: Model sld profiles with corresponding tBLM parts

The sld and thickness of the hydrocarbon layer can be utilised to calculate the area per lipid molecule. From simultaneous fits of the data sets with isotopically different bulk solvent phases, the hydration of the various layers and the completeness of the lipid bilayer can be calculated. This is an in-build

function of the ‘Gareff’ software.

3.2 Surface Plasmon Resonance (SPR)

Surface plasmon polaritons (SP) are sensitive to molecular changes in the environment near a metal-dielectric interface making SPR a valuable tool to observe adsorption kinetics and their parameters.

An SPR experiment allows to detect changes in the local index of refraction and this can provide information about layer growth [75]. In the scan mode, changes in the reflected intensity are measured as a function of the scattering angle, while in the kinetic mode, changes at a fixed angle are detected as a function of time.

3.2.1 Surface Plasmon excitation

Surface plasmons polaritons are transverse electromagnetic oscillations along the interface of two media with different reflective index, e.g. a metal and a dielectric.

Excitation in a smooth metal surface by photons requires the use of a coupling medium such as a prism as the propagation constant of a surface plasmon at a metal-dielectric interface is larger than the wave number of the light wave in the dielectric. Due to the direction of their wave vectors \vec{k} , SP can only be excited by p-polarised light.

In the here used Kretschmann configuration (fig. 3.10), the coupling wave to excite the surface plasmons is generated by a light wave that passes through a high refractive index prism where it is totally reflected at the prism base. The created evanescent wave propagates along the metal-dielectric interface with a propagation constant that can be adjusted to match that of the surface plasmon by controlling the angle of incidence θ . If parallel monochromatic light is used, reflection under certain incident angles is strongly decreased because the surface plasmons adsorb the irradiated energy. Varying the incident angle of light shows that the position, width and depth of the characteristic reflection minimum of the surface plasmon res-

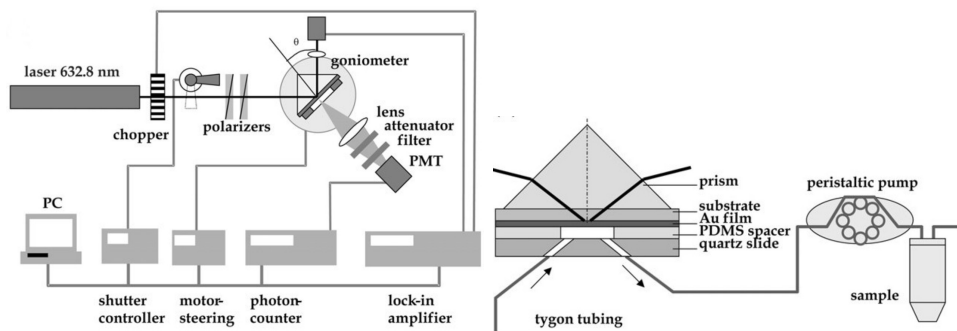


Figure 3.10: Simplified SPR setup and sample mounting. Picture taken from Knoll et al. (2003) [77]

onance is strongly dependent on the refractive index and layer thickness of the system (fig. 3.11).

Hence, surface plasmon adsorption is a valuable function to determine optical constants [76].

3.2.2 Sample Preparation

An LaSfN9 prism was assembled in a Kretschmann-like configuration. The prism was directly coupled to the sample using an immersion oil with the same refractive index as the glass. Lipid mono- and bilayers were assembled on gold coated LaSfN9 glass slides. A thin (2.5 nm) chromium layer was used to enhance the adhesion of the gold layer.

A customised SPR setup with a 632 nm He/Ne laser was used. Measurements were performed in a Teflon flow cell, where the sample could be flushed with different solution, e.g. containing the protein.

3.2.3 Data evaluation

Data was evaluated using the WINSPALL program (MPI for Polymer Research, Mainz/Germany).

Each layer was fitted independent and subsequently. When an additional layer was introduced and fitted (e.g. DPhyPC) the values of the layers underneath (e.g. LaSfN9, Cr +Au) were imported from the previous fit (e.g.

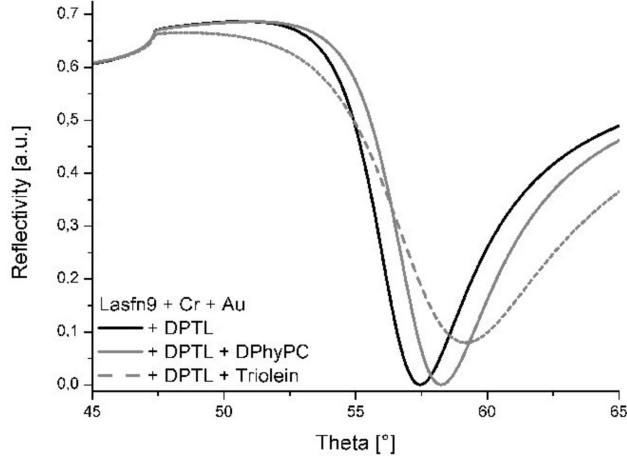


Figure 3.11: Simulated SPR scans for DPTL (—), DPTL + DPhyPC (---) and DPTL + Triolein (· · ·) on aLaSfN9 glass slide with Au and Cr

Layer	Thickness [nm]	ϵ' (real)	ϵ'' (imag)
LaSfN9	∞	3.404	0
Cr	2.5	-6.3	9.3
Au	50	-12.3	1.33
DPTL	3	2.25	0
DPhyPC	3	2.1025	0
Triolein	3	2	1.8
β lg	3.2	2 [79]	0
Air	∞	1	0
Water	∞	1.777	0

Table 3.1: Theoretical SPR values at $\lambda=633$ nm (Source: www.luxpop.com)

without DPhyPC) and kept constant.

The system was analysed in terms of a box model using the refractive indices shown in table 3.1. The imaginary part ϵ'' of the propagation constant is associated with the attenuation of the surface plasmon in the direction of propagation. Triolein, due to its “trident” structure, does not form a homogeneous upper bilayer, which leads to internal scattering, causing the minima to shift to higher intensities (fig. 3.11). Therefore, $\epsilon'' = 1.8$ has been used [78].

3.3 Electrical Impedance Spectroscopy (EIS)

Electrical Impedance Spectroscopy (EIS) studies the response of a system to the application of a periodic, small amplitude AC signal. The impedance $Z(f)$ of a system, which is the AC analogy to resistance in DC, is measured over a range of frequencies. Those measurements provide information about the interface, its structure and reactions taking place, including energy storage and dissipation properties. [80]

Impedance

The impedance can be seen as the AC analogy to resistance in DC, although it is a more general concept because it takes phase differences into account. In general, the opposition to the flow of an alternating current is not only resistive, but also includes energy dissipater (resistor) and energy storage (capacitor) elements.

$$Z = \frac{E(t)}{I(t)} = \frac{E_0 \cos(\omega t)}{I_0 \cos(\omega t - \varphi)} = Z_0 \frac{\cos(\omega t)}{\cos(\omega t - \varphi)} = Z_0 e^{j\varphi} = Z_0(\cos \varphi + j \sin \varphi) \quad (3.5)$$

3.3.1 Measurement

Measurements were conducted using a impedance analyser that provided the voltage signal, measured the voltage perturbation and the current responds, and calculated the impedance.

The analyser is connected to the sample in a Faraday cage. This is necessary to reduce interfering electromagnetic noise.

Membranes were assembled on gold slides, which also served as working electrodes in a three electrode setup (fig. 3.12). The Teflon measurement cell had an inner volume of approx. 1 ml. The counter electrode was made of a coiled platinum wire and a Ag/AgCl (World Precision Instruments, Berlin, Germany) electrode was placed close to the bilayer in order to create a defined electrochemical potential.

In the here used frequency domain method, a sinusoidal voltage

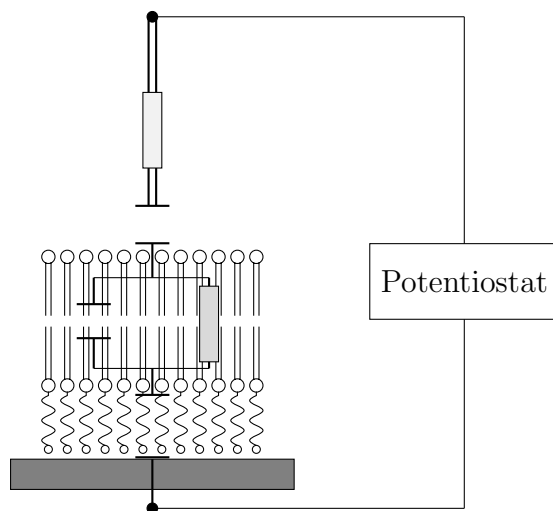


Figure 3.12: Principle set-up of a three electrode electrochemical cell for impedance measurement.

signal $U(t) = U_0(\omega) \sin(\omega t)$ is applied, causing a current response of $I(t) = I_0(\omega) \sin(\omega t + \varphi t)$. (The applied voltage signal should be small, in the range of thermodynamic fluctuations $\approx 25\text{mV}$, in order to maintain a linear response of the system.) The applied single frequency voltage U is measured, as well as the phase shift and amplitude (or real and imaginary part) of the resulting current I at that frequency.

Between two consecutive frequencies, a time delay allows the system to adapt and equilibrate to the frequency change.

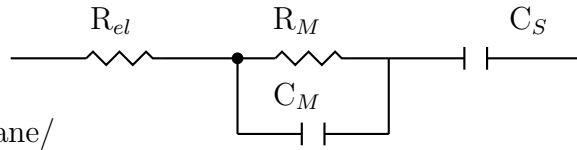
From the physical model, an equivalent circuit is derived which is fitted to the measured spectra.

3.3.2 Equivalent circuit models

Equivalent circuits, mostly made of resistors and capacitors, are simplistic models to mimic the behaviour of the investigated system. They are derived from physical considerations of the system, fitted to the measured data and interpreted in terms of the applied model [81].

The here used membrane architecture can be simplified represented by:

R_{el} : Electrolyte resistance
 R_M : Membrane resistance
 C_M : Membrane capacitance
 C_S : Capacitance at the membrane/
 electrolyte interface



3.3.3 Representation of impedance spectra

The aim of the various plot possibilities for impedance spectra is the optimal visual presentation of the characteristic features of a system and their changes.

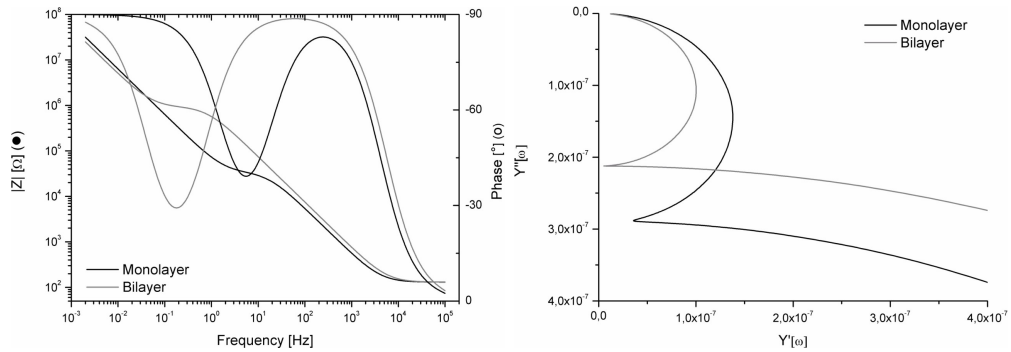


Figure 3.13: Bode (left) + Admittance (right) plot
 Bode: Impedance and phase shift vs. $\log \omega$
 Admittance: Capacitance of the system

Bode

A Bode (or polar) plot (3.13, left) includes two different sets of data:

- The absolute $Z_0(f)$ value of the impedance and the
- The phase shift $\varphi(f)$ of the impedance

both against the logarithmic plotted frequency, so that a wide range of frequencies and corresponding values of impedance can be viewed.

Admittance

The admittance $Y(\omega)$ is the reciprocal of the impedance. If the imaginary part of the admittance is plotted over the real part of the admittance this is known as ‘(Complex) Admittance plot’ (3.13, right), where the capacitance can be read.

3.4 Isotherms

A Langmuir monolayer is a one-molecule thick insoluble layer of an organic material spread onto an aqueous subphase [82]. Simplified, monolayers are (half)-membranes and can be used as model systems for biological membranes. They are suitable for the study of long-range interaction on microscopic length scales as they form an isolated quasi-two dimensional system at the air-water interface. Langmuir monolayers have been extensively studied and well described in the literature, e.g. [82–86].

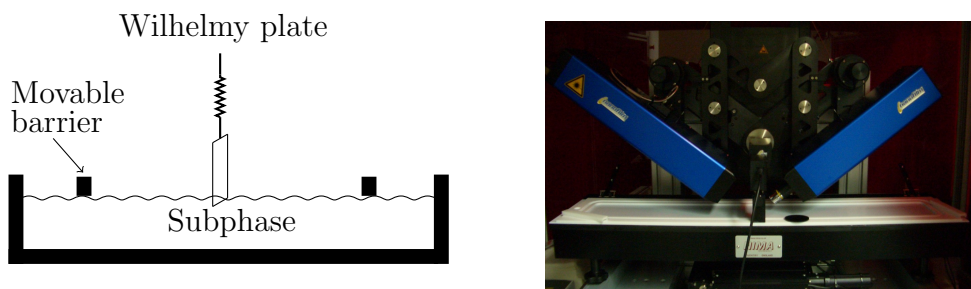


Figure 3.14: Schematic representation of a Langmuir trough (left) and used Langmuir trough with Brewster angle microscope (right).

A Langmuir film balance is a device for the study, analyse and manipulation of monomolecular organic layers such as amphiphilic molecules, fatty acids and lipids. The Langmuir trough (fig. 3.14) has one or two movable barrier(s) to control the trough area and a force measuring device for determining the surface pressure (surface tension).

Traditional compounds used to prepare Langmuir monolayers are amphiphilic materials that possess a hydrophilic headgroup that submerges into the water and a hydrophobic tail that remains outside to interact with other

tails to form a layer. Hydrophilic groups are attracted to polar media and the forces acting upon them in the liquid state are predominantly Coulomb type (r^{-2}). Hydrophobic groups such as hydrocarbon chains, fats and lipids are much less (if at all) water soluble and the forces acting upon them are predominantly van der Waals type (r^{-13} and r^{-7}). Amphiphilic molecules are trapped at the interface due to these two very different types of bonding within the one molecular structure. Lipids, because of the very long carbon chains, are almost always immiscible with water and therefore form monomolecular layers on the air-water interface. To create a monolayer, the amphiphiles are dissolved in a water-immiscible solvent such as chloroform and spread with a syringe onto the air-water interface. The chloroform evaporates and leaves a monomolecular layer of the spread molecules. Spontaneous spreading will continue until the surface pressure of the monolayer is equal to the ‘equilibrium spreading pressure’. At this point, the entire available surface is covered and any further droplets of solution remain embedded in the monolayer as floating lenses, as no more spreading out can take place. Upon closing of the barrier, the surfactant is compressed causing a change in the surface pressure. Plotting the surface pressure π as a function of trough area A is known as a π - A isotherm. Analysis of these isotherms provides information on the arrangement of the surfactant at the interface.

The lipid monolayer at the air-water interface represents only one half of the naturally occurring bilayer of the membrane, but allows the packing density of the spread lipid molecules to be varied by changing the available area per molecule. Thus, information on membrane constituents that are organised in a membrane-like environment can be obtained, but direct information on membrane functionality is only sparsely provided.

3.4.1 Surface pressure measurement

Any liquid will always try to reduce its surface area - this is known as surface tension γ [82]. The surface pressure π of a monolayer is defined as the lowering of the surface tension γ due to the presence of the monolayer on the

water surface [82]:

$$\pi = \Delta\gamma \quad (3.6)$$

It can be interpreted as the two-dimensional analogue of the three dimensional pressure.

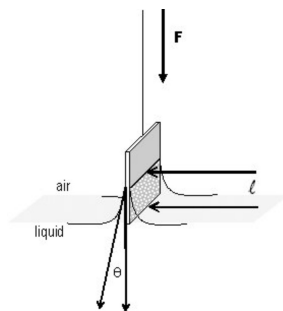


Figure 3.15: Wilhelmy plate,
© Nima Technology Ltd [87]

The Wilhelmy plate technique is a frequently used method to determine the surface pressure. The force due to surface tension is determined on a plate which is suspended so that it is partially immersed in the water subphase.

3.4.2 π - A - isotherms

The characteristics of a monolayer on the water surface are studied by measuring the changes in surface tension upon compressing. The shape of the isotherm is characteristic of the molecules that make up the film and hence provides a two-dimensional 'fingerprint'.

Molecules in solution are subject to attractive forces; in the bulk these forces are counterbalanced. However, at a surface or interface the forces are unequal and the net effect is to pull the peripheral molecules into the bulk of the solution. This effect gives rise to surface tension. The tendency of surface-active molecules to accumulate at interfaces favours the expansion of the interface and hence lowers the surface tension. Such behaviour makes it possible to monitor the surface pressure as a function of the area occupied per molecule provided that the number of molecules deposited on the surface is known. By quasi-statically moving the barrier of the Langmuir trough and simultaneously measuring the surface pressure, the surface pressure can be determined as a function of the area of water available to each molecule. Because the temperature is kept constant, this relation is known

as the surface pressure vs. area isotherm, usually abbreviated to “isotherm”, the two dimensional analogue of the three dimensional volume-pressure diagram (fig. 3.16).

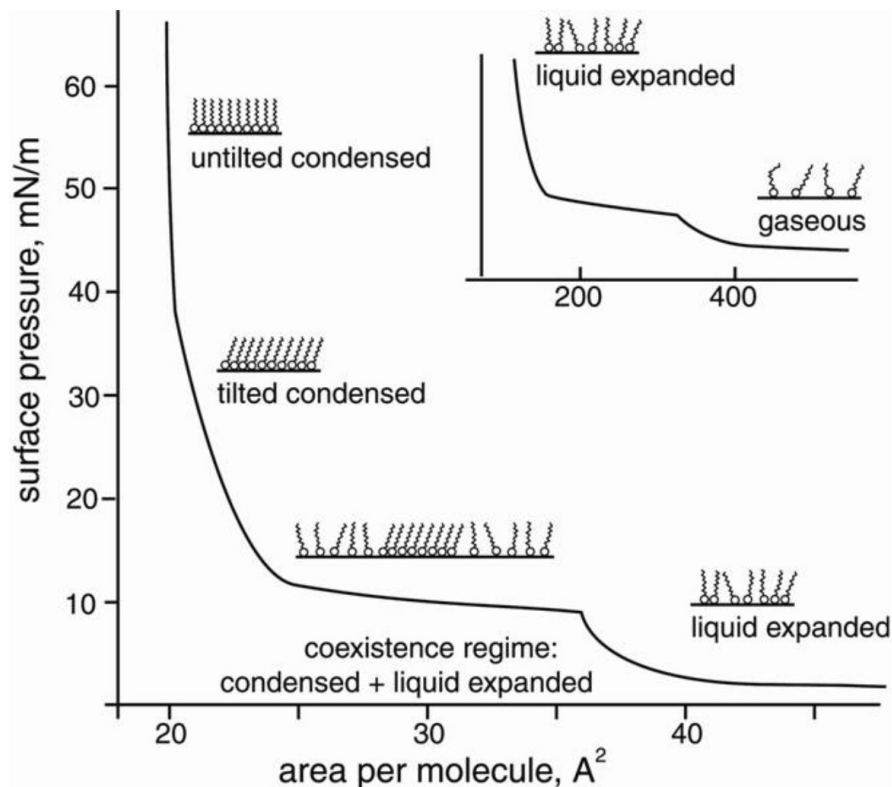


Figure 3.16: Schematic isotherm of a Langmuir monolayer, from Kaganer et al. [88]

Outlay: Transition from liquid to condensed phase with coexistence region
 Inlay: Transition from gaseous to liquid phase

The study of the surface pressure of monolayer provides information about the surface-active properties of the components, and also on the area occupied by them in the film. Analysis of the experimental results of the study of the surface pressure and the potential adsorption of proteins to phospholipid monolayers might enable to determine the nature of the interaction of the protein with lipids and the structure of the complex formed in this process.

3.4.3 Brewster angle microscopy

Brewster angle microscopy (BAM) is a form of reflectometry that was derived from ellipsometry and which is mostly applied to monolayers at an air-water interface. BAM makes it possible to directly and label-free observe ultra-thin films at air-water interfaces in situ and in real time.

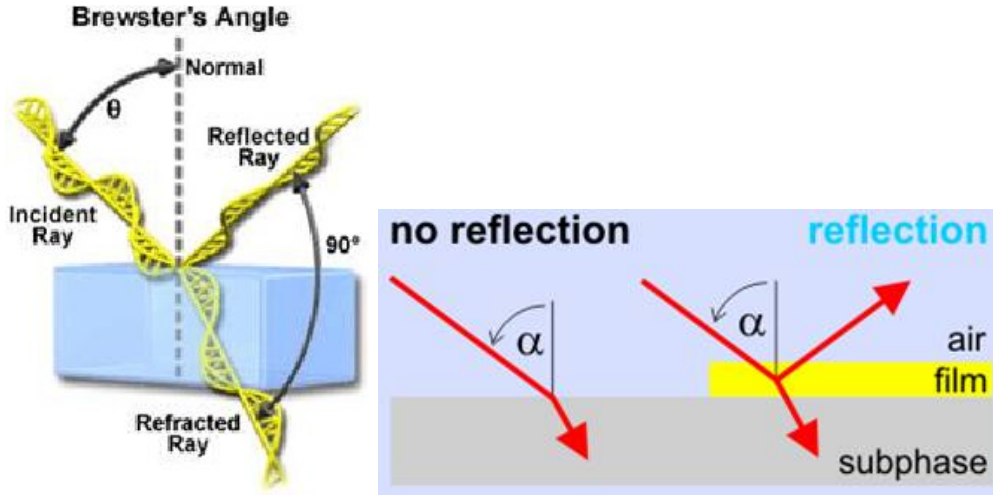


Figure 3.17: Brewster angle condition [89] and reflection on thin films

When light moves between two media of different refractive indices, light which is p-polarised with respect to the interface will not be reflected from the interface at one particular incident angle, known as Brewster's angle ω_B , but completely refracted into the subphase (fig. 3.17, left).

This can be expressed as [90] :

$$\theta_1 + \theta_2 = 90^\circ \quad (3.7)$$

where θ_1 is the angle of incidence and θ_2 is the angle of refraction.

Using Snell's law one finds [90]:

$$n_1 \sin \omega_B = n_2 \sin\left(\frac{\pi}{2} - \omega_B\right) = n_2 \cos \omega_B \quad (3.8)$$

and thus,

$$\tan \omega_B = \frac{n_1}{n_2} \quad (3.9)$$

Where n_1 and n_2 are the refractive indices of the two media.

If a thin film is present, the refractive index differs slightly from that of the substrate value. Then the Brewster angle condition is no longer fulfilled, neither at the air-film nor the film-water interface. Therefore, some reflections occur on both interfaces, and there are also multiple reflections within the film (fig. 3.17, right). All these beams superimpose coherently and produce a signal that can be detected with a sensor, e.g. a CCD camera. The reflected intensity depends on the film thickness and its optical parameters as well as the roughness of the water surface caused by thermal fluctuations (about 0.3 nm) [91].

Modelling film thickness

The software provided by Nanofilm, Göttingen/Germany includes the package ‘BAM tools’ which enables modelling of the thickness of a film at the air-water interface as a function of the reflective index of the adsorbed material.

During calibration at the bare subphase, the software calculates the “experimental Brewster angle”, a “calibration factor”, and a “dark signal”. With those values the BAM tools model converts the intensity of the reflected light into film thickness, in a range of a minimum and a maximum of the refractive index of the film.

3.5 Procedure

All experiments were executed at ambient conditions. For all steps, ultra pure water, filtered with a Millipore device (Billerica, MA/USA) was used.

3.5.1 Buffer preparation

PBS at varying pH was prepared with an ionic strength of 0.1 M NaCl prepared with Na_2HPO_4 and NaH_2PO_4 or citric acid respectively. The pH was checked with a Mettler Toledo, Giessen/Germany pH meter.

3.5.2 Metal evaporation

As the lipids used for monolayer formation are optimised for gold, a 50 nm layer of gold was electro-thermal evaporated onto previously cleaned glass slides. To enhance the stability of the layer, and to allow for rinsing with ethanol, a 2.5 nm layer of chromium was added between the glass slide and the gold layer.

High refractive index glass slide (LaSfN9/Schott) were chosen for SPR measurements as they allow for multiple uses if cleaned properly.

For neutron reflectivity measurements, 10 mm thick silicon wafers (Si-Mat, Landsberg/Lech, Germany) with a diameter of 76.2 mm were used. A 15 nm thin layer of gold was evaporated instead of 50 nm for SPR, but otherwise sample treatment was the same as for SPR substrates.

3.5.3 Template stripped gold

Surface flatness is an important issue when assembling membranes with high sealing properties, as small defects or unevenness prevents the formation of a complete bilayer. Glass substrates on which the metallic layer is directly evaporated are not flat enough. Therefore a special preparation technique that exploits the ultra flatness ($\leq 0.5\text{nm}$) of silicon is used. The so called ‘template stripped gold’ (tsg) [92] was used for all EIS measurements.

After cleaning the silicon substrates (CrysTeC, Berlin/Germany) in basic pi-

ranha, approximately 50 nm of gold were evaporated on the silicon chip. Each one is immediately glued to a cleaned glass slide with epoxy glue (EpoTek 353ND4, de-gased for 1 h). The sandwich was set to harden for 2 h at 150°C. After exposing the ultra-flat gold, the slides were cleaned with nitrogen and placed in the self assembly solution.

3.5.4 Self assembly

Lipid monolayers were formed by self assembly (SA). After the evaporation of chromium and gold, the substrates were immediately immersed in a lipid solution (0.2 mg/ml in ethanol) for 24 h. Before use, samples were rinsed in abundance with ethanol and dried with nitrogen.

An overview of the anchor lipids used, as well as their chemical structure, theoretical length and sld can be found in table 3.2.

3.5.5 Vesicle preparation

Highly insulating bilayers can be formed by vesicles. If the osmotic pressure is high enough, vesicles added onto the monolayer will break open and complete the bilayer.

Vesicles were produced by the extrusion technique [93] using a pore size of 50 nm and 2 mg lipid per ml H₂O. In this method, a lipid in water suspension is pushed through pores producing monodisperse vesicles in predictable size without the addition of contaminants.

3.5.6 Rapid solvent exchange

A faster, and in general more reproducible but slightly less dense, way of completing the bilayer in the flow cell is rapid solvent exchange (RSE) [15,45,46]. The substrate is incubated in an ethanolic lipid solution of 5-10 mg lipid in ethanol, depending on the used lipid. After 10 min, the cell is rapidly, and in large quantity (approximately 20x cell volume), flushed with aqueous buffer. During this exchange, the water insoluble lipid molecules complete the bilayer on top of the phytanoyl chains of the monolayer, rather than to mix

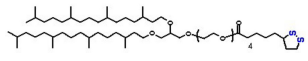
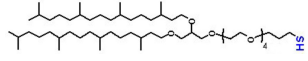
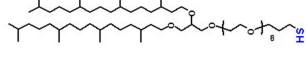
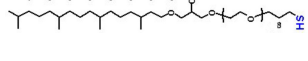
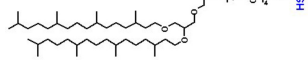


DPTL	DPTT	DPHT	D POT	DDPTT	DPHDL	CholPEG
$C_{16}H_{29}O_5S_2$	$C_{10}H_{21}O_5S$	$C_{14}H_{29}O_7S$	$C_{18}H_{37}O_9S$	$C_{10}H_{21}O_5S$	$C_{31}H_{55}O_{10}S_4$	$C_{46}H_{78}O_9S_2$
						
$0.537 \cdot 10^{-6} \text{ \AA}^{-2}$	$0.471 \cdot 10^{-6} \text{ \AA}^{-2}$	$0.495 \cdot 10^{-6} \text{ \AA}^{-2}$	$0.510 \cdot 10^{-6} \text{ \AA}^{-2}$	$0.471 \cdot 10^{-6} \text{ \AA}^{-2}$	$0.587 \cdot 10^{-6} \text{ \AA}^{-2}$	$0.517 \cdot 10^{-6} \text{ \AA}^{-2}$
5.0 nm	4.5 nm	5.2 nm	5.9 nm	4.5 nm	5.6 nm	4.8 nm

Table 3.2: Chemical structure, scattering length density (Calculated with the Scattering Length Density Calculator, <http://www.ncnr.nist.gov/resources/sldcalc.html>) and theoretical spacer length (Determined by Chem3D Ultra 6.0) of the anchors used.

The sld of inner chains is $-0.204 \cdot 10^{-6} \text{ \AA}^{-2}$, except for DDPTT, where it is $-0.164 \cdot 10^{-6} \text{ \AA}^{-2}$.

with the water and get rinsed away.

This preparation technique is suitable for forming defect-free bilayers over large substrates as have been used for neutron reflectivity measurements.

For rapid solvent exchange, 5 mg/ml DPhyPC and 10 mg/ml glyceryl trioleate in ethanol were used.

An overview of the outer lipids used for bilayer formation, either by vesicles fusion or RSE, as well as their chemical structure, theoretical length and sld can be found in table 3.3.

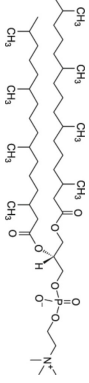
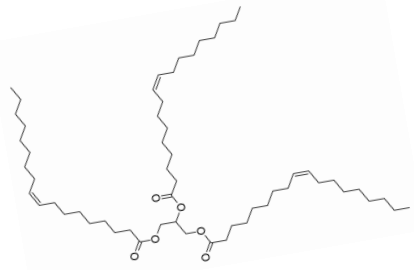
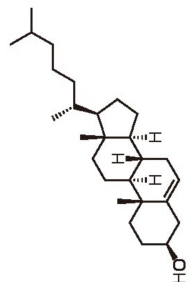
DPhyPC	Triolein	Cholesterol
$C_{46}H_{90}O_{10}PNa$	$C_{57}H_{104}O_6$	$C_{27}H_{46}O$
		
$0.253 \cdot 10^{-6} \text{ \AA}^{-2}$	Not used for NR	$0.206 \cdot 10^{-6} \text{ \AA}^{-2}$
3.0 nm	3.0 nm	2.0 nm

Table 3.3: Chemical structure, scattering length density (Calculated with the Scattering Length Density Calculator, <http://www.ncnr.nist.gov/resources/sldcalc.html>) and theoretical spacer length (Determined by Chem3D Ultra 6.0) of DPhyPC and cholesterol. Both were used for the completion of the outer bilayer.

Chapter 4

β -lactoglobulin

4.1 Introduction

Fundamental processes in food science include the interaction of proteins with various interfaces, e.g. water-oil or water-air. However, such processes are often complex. In order to facilitate a detailed analysis, model systems are used. The globular whey protein β -lactoglobulin (β lg, fig. 4.1) is the major component in bovine milk [3] and belongs to the lipocalin family that is known for specific transporter activities [94]. The protein is easily accessible and has been used in the past as model compound in investigations at the air-water or oil-water interface [95]. It has also been employed for more applied studies on the stabilisation of emulsions [7], gelation [8] and foaming [9] as well as of its influence in aroma perception [96].

In dairy products, β lg coexists with milk fat globular membranes [4], which consist of 27%(w/w) phospholipids. Therefore studies of the protein at the interface of phospholipids can give important information about processes occurring during protein-fat contacts [97–99]. However, the detailed interaction process is yet not fully understood [100] but would facilitate applications for low-fat products by adding the (charged) amphiphile to lipid-water emulsions.

In order to systematically study and differentiate between such processes, a solid supported model membrane system has been used. tBLMs are ac-

cessible to a wide variety of surface analytical tools, which allows combining techniques in order to study, for example, the adsorption of a protein to a membrane in detail.

4.1.1 Properties of β -lactoglobulin

β lg is a small globular protein with 162 residues and a molecular weight of 18.4 kDa with an elliptical diameter of 39 Å [100,101]. At room temperature, neutral pH and physiological conditions the native protein is a dimer (fig. 4.2) of two non-covalently linked monomeric molecules [102]; at concentration below 2 mg/ml the monomeric form is predominant [103]. Each monomer contains two disulfide bridges and one single thiol group which is buried in the interior of the molecule (fig. 4.1). 50% of the protein structure is made of large loops of random coils, connecting the structural elements [104]. The protein is able to interact with its environment *via* hydrophobic forces and/or sulphhydryl-disulfide interchange. The single sulfhydryl group is the major key to β lg behaviour [105].

β lg is a carrier of retinal and fatty acids and prevents the inhibition

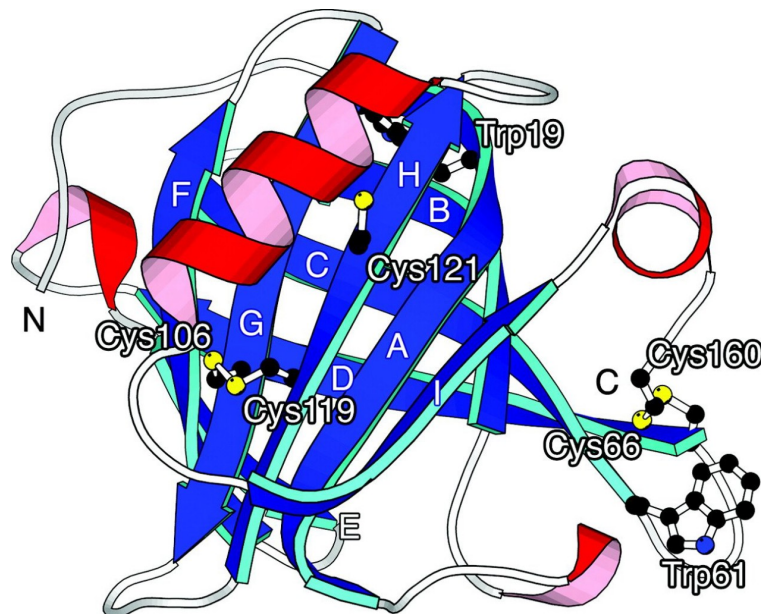


Figure 4.1: Crystal structure of β -lg, taken from [11]

of pre-duodenal lipases and facilitates the digestion of milk fat [10]. The protein is very stable under acidic conditions which makes it resistant to digestion in the human stomach and might be one of the allergens for human infant milk allergy [11]. The whey protein is useful in food applications because of its emulsifying and fat binding properties, but also due to its high nutritional quality and heat sensitivity which makes it a valuable tool for pasteurisation [106].

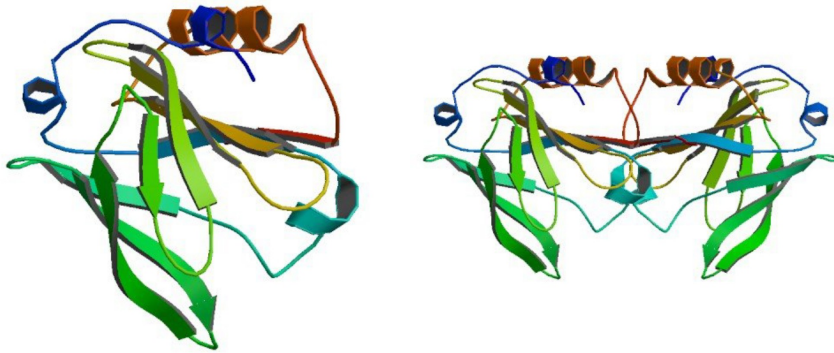


Figure 4.2: X-ray diffraction image of β lg in monomeric (left) and dimeric (right) form [107], PDB 2Q2M

4.1.2 Milk fat globule membrane

Simplified, milk is a fat in water emulsion. More than 95% of the fats are triglyceride. In un-homogenised milk, the fats exist as small globules, roughly 4 μ m in diameter. These fat globules are surrounded by a thin layer of surface-active material, which is called the milk fat globule membrane (MFGM) [4]. The MFGM is secreted from the mammary secretory cell in a tri-laminar structure:

A surface active inner layer that surrounds the intracellular fat droplet, a dense proteinaceous coat and finally a true lipid bilayer membrane originating from the secretory cell apical plasma membrane [108].

Besides phospholipids, the MFGM also consists of proteins that act as emulsifiers, preventing flocculation and coalescence and protecting the fat

against enzyme action.

Additional to casein, which aggregates proteins and calcium phosphate to nanometre-scale micelles, milk contains various other types of proteins. They are more water-soluble than the caseins and suspended in whey when the caseins coagulate into curds, therefore they are known as whey proteins. Lactoglobulin is the most abundant of them. [109] The MFGM is affected by milk processing treatments such as homogenisation, heating, cooling, etc. and consequently, many properties of dairy products are directly influenced [110].

4.1.3 β lg - lipid interactions

During milk homogenisation, the milk fat globules are reduced in size, increasing the interfacial oil-water area. To stabilise the freshly exposed lipid surface, whey proteins adsorb and by interacting with the phospholipids of the MFGM, they create a stable, highly dispersed fat phase. [5, 6] This process is probably accompanied by conformational changes of the adsorbing protein [111].

To be able to use β lg as an emulsifier, its adsorption behaviour on various surfaces has to be examined.

β -lactoglobulin has a hydrophobic binding site in its interior, but also weaker ones on its exterior [112], which bind to various hydrophobic ligands, mainly retinol and long-chain fatty acids [113, 114].

As most of those helical regions are buried in the interior of the native protein, it does not bind automatically to lipids, but needs to unfold and then participate in lipid binding to stabilise the helical conformation [115]. The role of β lg conformation in membrane association has not been elucidated and nothing is known on the lipid-dependent conformational changes in membrane-bound β lg [98].

The following experiments investigate the interactions of the whey protein β -lactoglobulin with lipids on various surface, the influence of charge and lipid packing to elucidate the state of unfolding during emulsification and the protein moieties involved.

When β lg approaches a lipid bilayer, different events could occur (fig. 4.3):

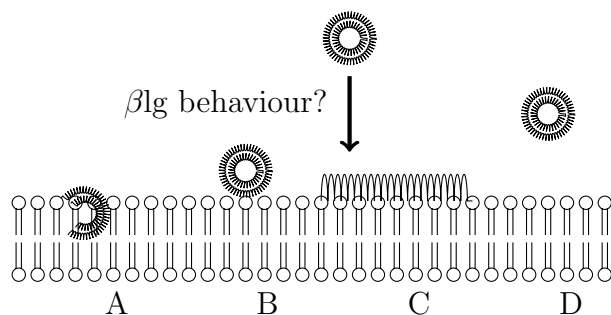


Figure 4.3: Possible β lg interaction with a lipid bilayer

- A : β lg (partly) unfolds to expose its hydrophobic core and enters the hydrophobic interior of the bilayer.
- B : The hydrophilic exterior of the protein binds to the hydrophilic outer bilayer. No protein unfolding takes place.
- C : The protein unfolds on top of the lipid layer and an aggregation layer is formed.
- D : No interactions take place.

To elucidate which scenario is the most likely, NR, SPR, EIS, isotherms and BAM experiments have been executed on various surfaces employing native and urea-denatured β lg (fig. 4.4):

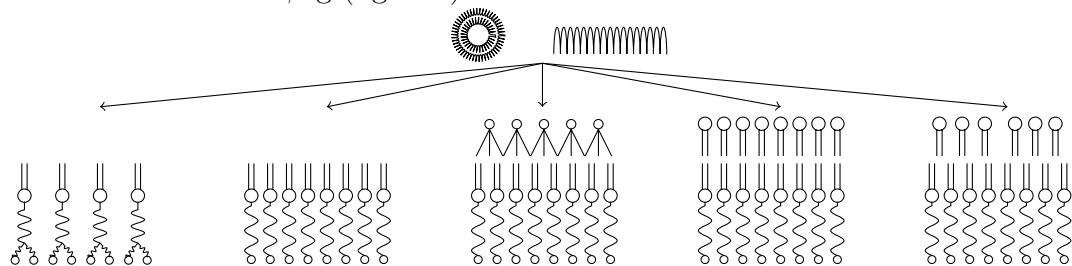


Figure 4.4: Solid supported model systems for β lg-lipid interaction investigation

- To test if the protein unfolds in proximity to the lipid layer:
 - native, globular β lg adsorption to lipid mono- and bilayers at solid interfaces and to lipid monolayers at the air-water interface
 - urea denatured, completely unfolded β lg adsorption to lipid mono- and bilayers at solid interfaces and to lipid monolayers at the air-water interface
- To evaluate the effect of the defects in the upper bilayer:
 - Cholesterol addition to Triolein and DPhyPC (RSE) bilayers
- To investigate the influence of upper layer packing density on protein adsorption and protein unfolding:
 - π -A/ π -t isotherms and BAM of β lg and DPhyPC at various surface pressures
 - β lg adsorption to DPHDL monolayers
- To examine the state of unfolding of the protein at the solid and liquid interface, as well as the influence of charge and electrostatic repulsion on the protein core stability:
 - Kinetics of β lg adsorption at pH 2, 3, 7 + 8
 - β lg adsorption to lipid mono- and bilayers at solid interfaces at pH 2 and pH 7
 - Adsorption kinetics of negatively charged DPhyPG and β lg at pH 3 + 7

4.2 Experimental

Purification procedure

β -lactoglobulin was purified from milk powder provided by Nestlé, Lisleux/France. For approximately 12 mg/ml of protein solution, 7.35 g milk powder were slowly (preferable over night) and under constant agitation dissolved in 100 ml ultra-pure water. After the powder was completely dissolved, 3.1 g trichloroacetic acid dissolved in 20 ml ultra-pure water was used as precipitant. The pH of the solution was adjusted to be below pH2. β -lg is very stable under acidic conditions [11], and it is the only part of milk that stays in solution in native condition at such low pH. The mixture was centrifuged (10000 rcf, 30 min, 20°C) and the supernatant was dialysed under constant agitation for 3 times 2 hours against water and 3 times 2 hours against PBS. (Dialysis cassette obtained from Pierce, Rockford, IL/USA) To enhance the shelf life of the protein solution, 0.02 g sodium azide was added.

For deuterated protein preparations, the last 3 dialysis steps were carried out against PBS prepared with D₂O.

Concentration and purity of the protein was checked by UV-Vis spectroscopy (Lambda900, Perkin-Elmer, Waltham, MA, USA) and differential scanning calorimetry (Mettler Toledo, Greifensee, Switzerland).

Denaturation of β -lactoglobulin

Denaturing of β lg is a two step process [106]; first the unfolding of the protein which exposes the inner hydrophobic groups and the sulfhydryl group [116] and then protein aggregation.

One method of denaturation is heat treatment in solution where the thermal motion of the protein is increased, leading to the break-up of various inter- and intramolecular bonds. This destabilisation leads to changes in the secondary and the tertiary structure. [117]

Whereas thermal denaturation can be reversible under certain circumstances, denaturation by urea over a certain exposure time is not [118,119]. During

this process the protein undergoes SH-SS interchange reactions (and possibly -SH oxidation) which leads to a complete unfolding of the protein [120,121].

Urea denaturation

For the experiments with denatured β -lactoglobulin, the protein was unfolded by urea denaturation [122].

After the normal purification procedure, the supernatant was first dialysed for 2h against PBS with 6M Urea, and finally against normal PBS, as described above.

Choice of lipids for bilayer formation

Additional to experiments on hydrophobic monolayers, investigations were also carried out on hydrophilic bilayers as they represent the environment the whey protein encounters in milk.

The major fat in milk is Triolein ($C_{57}H_{104}O_6$). It is a unsaturated fat and triglyceride (Sec. 3, fig. 3.3, middle).

Phosphatidylcholines are the major acyl chains in bovine milk phospholipids [123], which validates their choice as second lipid used. The double-stranded DPhyPC (Sec. 3, fig. 3.3, left) was used to form the upper part of bilayers due to its similarity to the lipid part of the thiolipids of the monolayer.

Due to their different chemical structures, systems formed with Triolein and DPhyPC vary in their upper part (fig. 4.5).

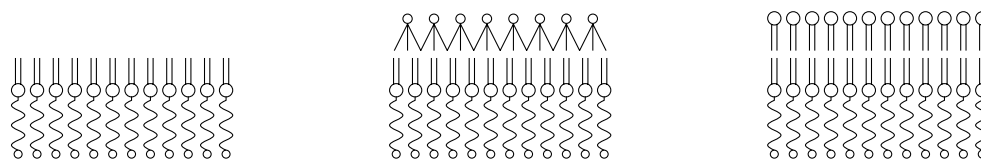


Figure 4.5: Schematic illustration of model membranes used: DPTL (left), DPTL + Triolein (middle), DPTL + DPhyPC (right)

4.3 Results

4.3.1 Pre-investigations

Fluctuations on monolayers

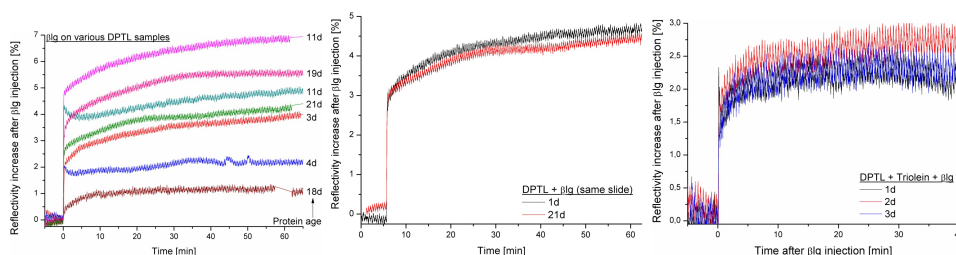


Figure 4.6: Slide effects on β Ig kinetics.

- left) Variation of kinetics for β Ig with different purification dates
- middle) β Ig kinetics of 1d and 21d old protein on same slide, no variation observable
- right) No variation on bilayers \rightarrow Triolein bilayers cushions slide effects

The reproducibility of experimental data is always a big concern, especially when working with biological or biomimetic systems. Different parameters such as the age of the protein or its concentration have been screened by measuring adsorption kinetics of the protein at a monolayer or bilayer. When β Ig was exposed to a DPTL monolayer, a strong scattering was observed (fig. 4.6, left). However, the scattering did not correlate with the age of the protein, i.e. the time after purification. The different results showed inhomogeneities in different DPTL monolayers preparations. Differences in the assembly processes or already in the substrate preparation might lead to different monolayer properties. However, when different spots on the same substrate were used no significant differences in the adsorption kinetics were detected (fig. 4.6, middle). Similarly, different protein preparations showed similar adsorption on a bilayer (fig. 4.6, right).

For studies on monolayers, comparisons were drawn from experiments under different conditions on the same slide or, if not applicable, a sufficient amount of measurements conducted to allow for good statistics.

Protein concentration

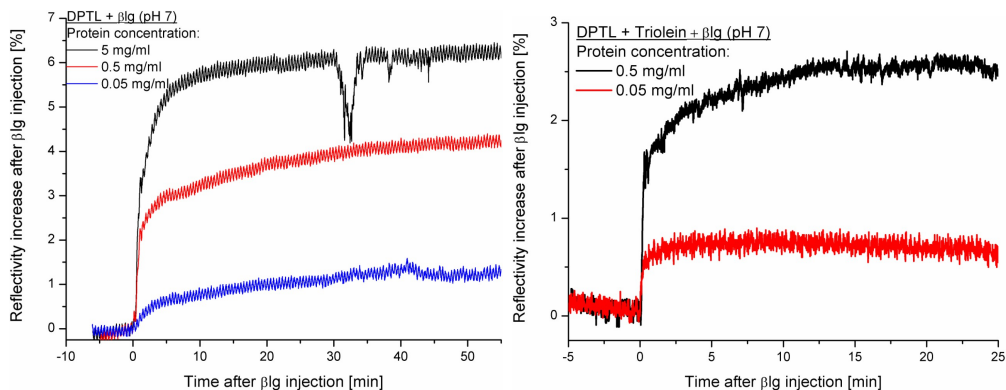


Figure 4.7: Effect of protein concentration on β Ig kinetics on mono- and bilayers. Lower protein concentrations led to thinner layers. (*Left figure: Temporary decrease in reflectivity increase due to external impact.*)

As can be seen in fig. 4.7, changes in the concentration of injected protein resulted in differences in the layer thickness on both mono- and bilayers. This can be primarily attributed to the fact that β Ig if it unfolds is able to form protein-protein aggregates if enough protein is present [124]. The second reason could be that for low concentrations, only protein patches are formed, and only higher amounts led to a complete layer.

Fitting with Winspall gave values of 1.6 nm (0.05 mg/ml), 3 nm (0.5 mg/ml) and 3.7 nm (5 mg/ml) for native β Ig on a DPTL monolayer. The value for 0.5 mg/ml corresponds well for the protein laying flattened on the monolayer, as it would be expected. Additionally, experiments with completely unfolded protein (see section 4.3.3) showed a layer thickness of about 5 nm, where we expected a high amount of protein-protein aggregation, resulting in thicker layers than for partly unfolded protein.

For the following experiments, a concentration of 0.5 mg/ml protein in buffer was used as this seemed to result in a one protein thick layer.

4.3.2 β lg interaction with mono- and bilayers

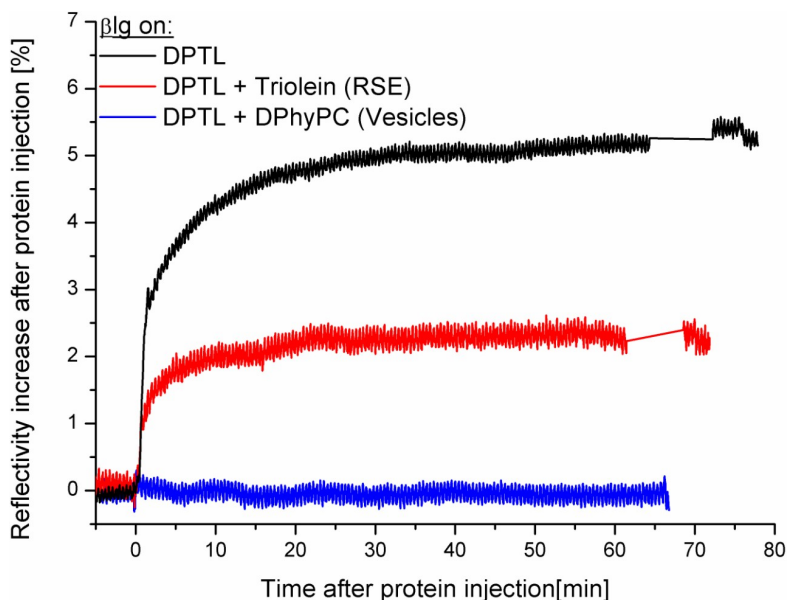


Figure 4.8: Comparison between β lg layers formed on top of DPTL, DPTL + Triolein, DPTL + DPhyPC (vesicles). β lg formed thicker layers on top of the monolayers compared to the bilayers. A thicker layer was formed on an incomplete bilayer made from Triolein compared to a very dense layer formed by vesicle fusion (DPhyPC).

The interaction of β lg with a mono- and bilayer has been probed using different techniques presented earlier. As discussed in 4.1.3, different scenarios could be envisioned. Using SPR, adsorption kinetics have been investigated. On a dense DPTL monolayer, β lg typically led to a dense protein layer ($n=1.41$) of about 3 nm. However, when exposed to a well-packed DPhyPC bilayer, no adsorption could be detected. In contrast, a Triolein bilayer showed a protein layer of about 2 nm. (fig. 4.8)

The quality and packing density of the different bilayers was probed using EIS. Bilayers were formed either by vesicle fusion or by RSE. All bilayer systems showed reasonable electrical sealing properties (Table 4.1 and 4.2, fig. 4.9, 4.10 and 4.11).

However, the Triolein layer was not as stable as a DPhyPC bilayer. This was caused by the lower packing density of the outer leaflet due to the tripod

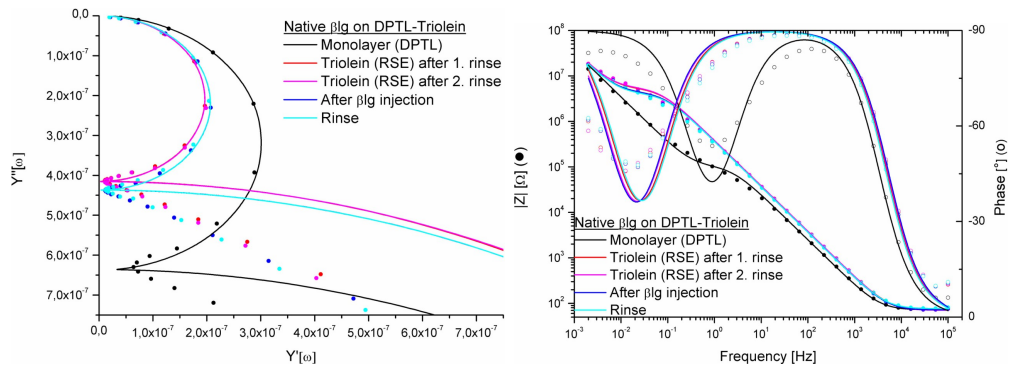


Figure 4.9: Bode + admittance plot: DPTL + Triolein + β Ig. The formation of a sealing bilayer with Triolein can be accomplished as R was 5 x higher and C decreased by factor 0.6. β Ig addition led to an increase in capacitance by 10%. The decrease in resistance by 21% was probably due to the destabilisation of the Triolein layer.

	Monolayer	Bilayer	Rinse	β Ig	Rinse
R [M Ω]	0.94	4.81	5.01	3.94	3.68
C [μ F]	0.73	0.45	0.45	0.49	0.49

Table 4.1: Fitted EIS data values for DPTL + Triolein + β Ig

structure of the Triolein molecule. For example, the resistance of a Triolein bilayer could decrease by 50% over 24h (\approx time period of one experiment), but increases of the same amount could also be monitored.

SPR experiments with denatured β Ig (fig. 4.3.3) exhibited thicker protein layers compared to native protein. If the protein has an effect on the resistance this should be even more pronounced in EIS measurements with denatured β Ig compared to native protein. Those measurements showed no significant change in resistance, compared to studies with native β Ig. Changes in resistance over time are therefore more likely caused by re-organisation of lipids in the bilayer than by β Ig. Additionally, the protein holds solvent so that it does not present a real barrier for mobile charges.

In addition to the SPR data, the β Ig adsorption was also followed by EIS, where the addition of a layer should be seen at least in the capacitance values.

To affirm that the changes observed after β lg injection were in fact caused by the protein, and not by the bilayer “swimming away” an additional rinsing step was executed before protein injection. Only if the capacitance was stable after rinsing, the protein was added. All changes could thus be attributed to lipid-protein interaction.

The impedance data for β lg on a Triolein bilayer showed a small increase (10%) in capacitance after protein addition (fig. 4.9).

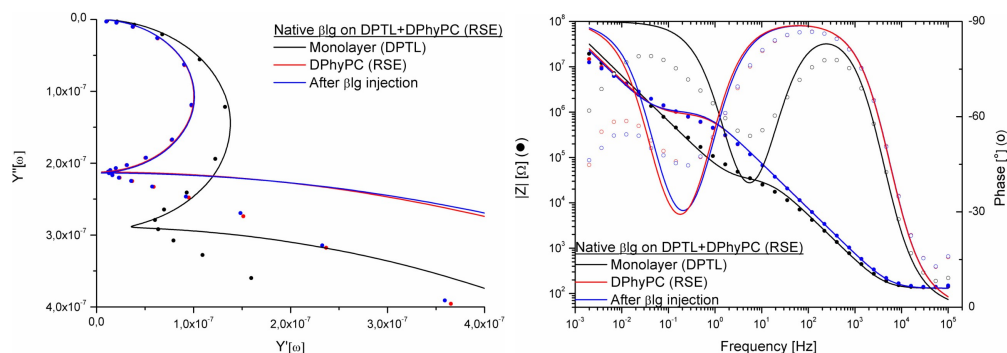


Figure 4.10: Bode + admittance plot: DPTL + DPhyPC(RSE) + β lg. No change in capacitance was observable after β lg addition. The increase in resistance by 11.5% was probably due to reorganisation in the rather poor bilayer.

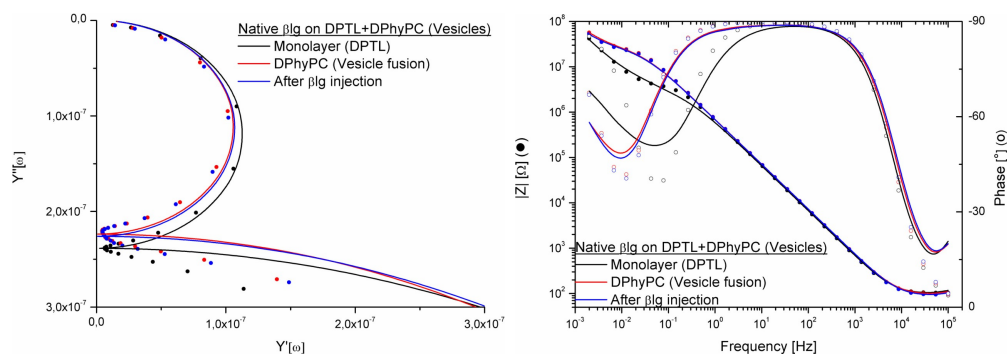


Figure 4.11: Bode + admittance plot: DPTL + DPhyPC (vesicles) + β lg. No changes were observable in the capacitance after β lg addition. The resistance decreased by 5% over 24h.

	Monolayer	Bilayer	β lg
RSE (fig. 4.10)			
R [M Ω]	0.37	0.87	0.97
C [μ F]	3.35	2.25	2.25
Vesicles (fig. 4.11)			
R [M Ω]	3.45	22.05	21.05
C [μ F]	2.75	2.55	2.55

Table 4.2: Fitted EIS data values for DPTL + DPhyPC + β lg

The addition of the protein to a DPhyPC bilayer showed no changes on bilayers formed with either vesicles or by RSE (fig. 4.10 + fig. 4.11). The EIS data thus supported the findings by SPR, i.e. the formation of a β lg layer on a triolein bilayer and no interaction with a DPhyPC bilayer. The increase in capacitance for the Triolein bilayer might also indicate a partial insertion of the protein into the layer.

Additional NR experiments were performed to investigate possible incorporation of β lg into the monolayer or bilayer structure. β lg was added to a monolayer in D₂O and CM4 and obtained spectra were compared to those of the bare monolayer. The obtained neutron reflectivity profiles showed small changes in the intensity at smaller Q after the addition of β lg. If the 4 stacks of data were fitted to a model where the protein lies atop of the DPTL monolayer, a protein layer with 26 Å thickness was observed (fig. 4.12).

Comparatively, the fit parameters for DPTL + β lg were altered in that way that the protein was allowed to enter the monolayer (fig. 4.13). This scenario is not very likely, as the monolayer should be too dense to allow for penetration, but the data is shown to enable comparisons to a fit where β lg was allowed to penetrate a DPhyPC bilayer (next paragraph) and a DPHDL monolayer (Sec. 4.3.5).

This fit resulted in a protein layer thickness on top of the DPTL monolayer of 8.9 nm with an sld of $3.9 \cdot 10^{-6} \text{Å}^{-2}$. Additionally, the sld of the spacer increased slightly from $0.69 \cdot 10^{-6} \text{Å}^{-2}$ to $0.74 \cdot 10^{-6} \text{Å}^{-2}$ from monolayer without to with protein. The sld of the inner lipid leaflet increased from $0.04 \cdot 10^{-6} \text{Å}^{-2}$ to $0.18 \cdot 10^{-6} \text{Å}^{-2}$. The hydration of the spacer part changed from 11% to 11.6%, the hydration in the inner lipid leaflet from 0.5% to 2.8%.

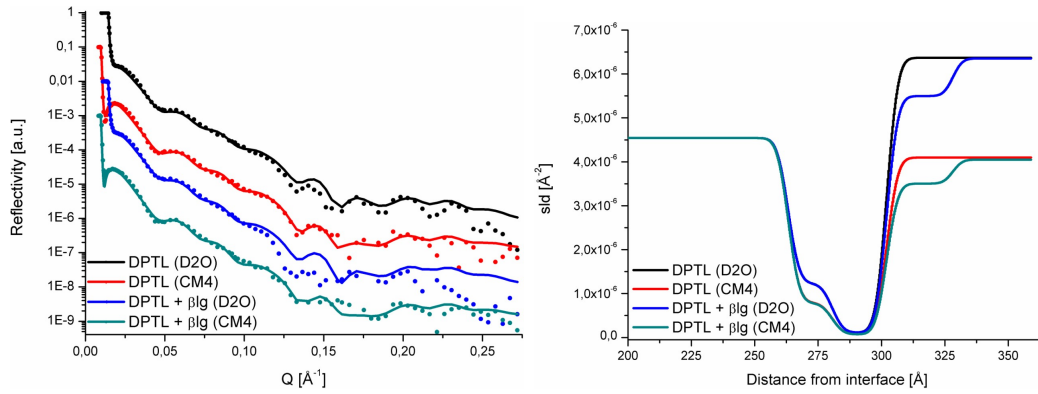


Figure 4.12: Fitted neutron reflectivity profiles (left) of DPTL (D₂O + CM4) and DPTL + β Ig and corresponding scattering length density profiles (right). β Ig was only “allowed” on top the DPTL monolayer.

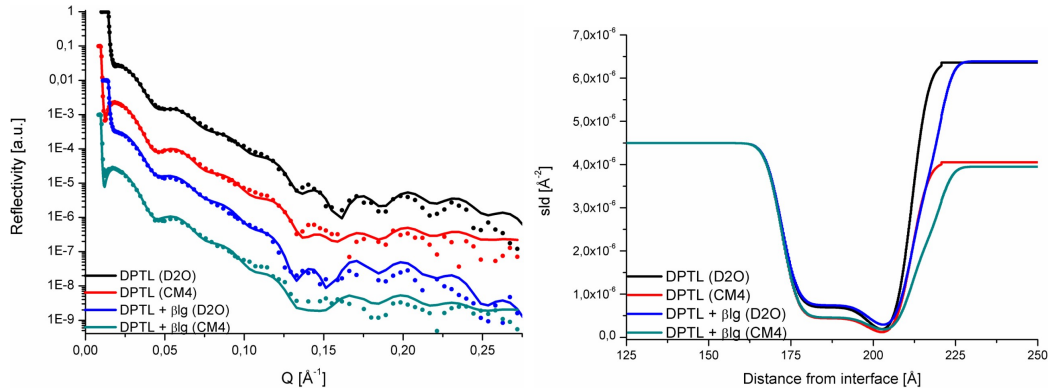


Figure 4.13: Fitted neutron reflectivity profiles (left) of DPTL (D₂O + CM4) and DPTL + β Ig and corresponding scattering length density profiles (right). β Ig was “allowed” to enter the DPTL spacer and inner alkyl chains.

β Ig added to a DPTL-DPhyPC bilayer showed a thinner protein layer than on a monolayer. If fitted with a model where bilayer penetration was allowed (but not forced), a 2 Å thick layer was formed on top DPhyPC. Additionally, the sld of the spacer part went up from $0.54 \cdot 10^{-6} \text{Å}^{-2}$ to $1.24 \cdot 10^{-6} \text{Å}^{-2}$.

Although this increase in the sld of the spacer part of the molecule suggested that the protein entered the bilayer and moved below, this is not very

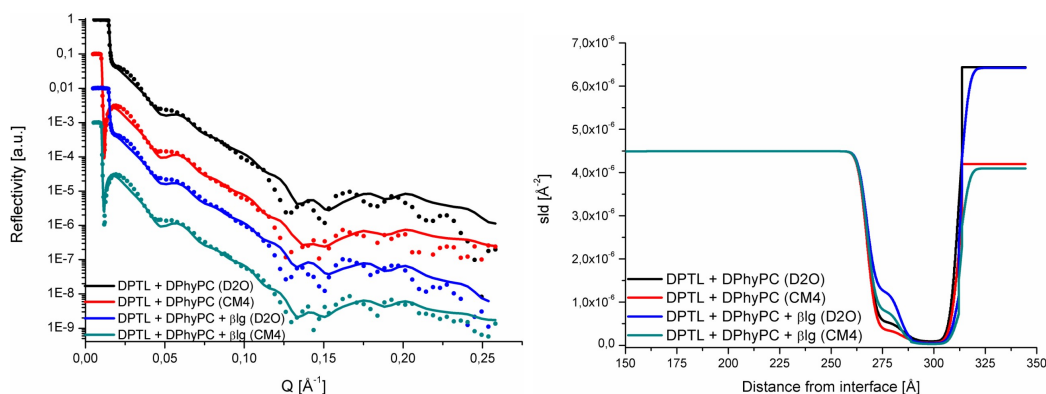


Figure 4.14: Fitted neutron reflectivity profiles (left) of DPTL + DPhyPC (D₂O + CM4) and DPTL + DPhyPC + β lg and corresponding scattering length density profiles (right). β lg was “allowed” to enter the DPTL spacer, inner and outer alkyl chains.

likely as especially DPTL forms very dense inner and outer bilayer. It is more reasonable that this result is a residue of the fitting procedure as the changes in the neutron reflectivity profiles are very subtle and the spacer, inner and outer alkyl chain layers are strongly interconnected and hard to distinguish.

Additionally, a DPTL monolayer with added protein did not exhibit this behaviour as strongly. If β lg indeed enters the spacer part of the molecule, this should be amplified on a monolayer.

In principle, the NR data thus confirm the SPR and EIS data on the protein-lipid interactions. β lg adsorbs to a hydrophobic monolayer and forms a layer of roughly 3 nm thickness. This corresponds to a complete layer of flattened protein. It seems also more likely, that protein remains on top of the monolayer rather than penetrating it. The slight interactions with the bilayer observed by NR might be due to the imperfect quality of the bilayer, formed by RSE over an area of 50 cm². Similar to a Triolein bilayer, the DPhyPC layer had probably defects and inhomogenities. Unfortunately, the formation of a Triolein bilayer in the neutron cell was not successful.

On Triolein, there are two possible mechanisms for protein adsorption:

- A The protein is in an highly unfolded state, covering the Triolein surface, but has no additional protein-protein aggregation layer.
- B The surface coverage is incomplete, with protein patches on the Triolein layer in the same or similar conformation as on the monolayer.

Neither SPR, EIS nor NR can give the exact state of unfolding of the protein, but β lg can be unfolded by urea, as done in section 4.3.3, and than compared to the scenario here.

On DPhyPC layers formed by vesicles, no interactions seemed to occur. In the literature, no interaction between the native protein and phosphocholine have been reported [98, 115, 125, 126], as well as a preference of the protein to bind to hydrophobic surfaces. On a purely hydrophilic surface, the forces acting between the surface and the protein molecule may be smaller, resulting in less conformational changes. As the protein was negatively charged at pH7, the proteins will electrostatically repel each other.

Also, the DPhyPC layer has a very high order, therefore β lg would present an energetically unfavourable defect in the bilayer.

It can be seen already, the nature of the surface present induces different conformational changes in the protein that leads to different binding behaviour.

4.3.3 Native vs. urea denatured β lg

It has been reported that native β -lactoglobulin does not interact with DPPC vesicles, but solvent denatured protein does [125]. In the native form, some helical regions are buried in the interior of the protein, which can only bind if the protein is denatured and unfolded [115].

Previous results were compared to experiments using urea-denatured β lg in order to probe the surface effect on protein denaturation. In addition to SPR and EIS experiments, studies at the air-water interface were performed. The evolution of the surface pressure after injection of β lg (2.4 mg/l) to the subphase was monitored.

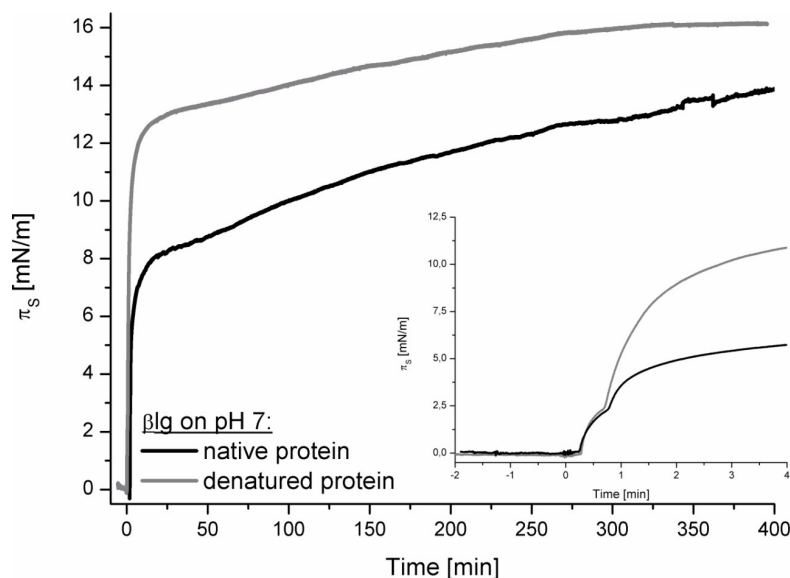


Figure 4.15: π - t isotherm of native and denatured β lg at pH7. No unfolding step was observable for denatured protein. (Inset: Diffusion of β lg to the air-water interface was similar for native and denatured protein.

π - t isotherms of completely unfolded β lg at pH 7 showed a faster increase in surface pressure and higher final pressure compared to native protein (fig. 4.15). The first step, diffusion to the surface during the first minute, was very similar and occurred for native and unfolded β lg at ca. 2.5 mN/m. The surface pressure for the native protein exhibited a second slope after 50 minutes at around 8 mN/m and ended in a plateau at around 14 mN/m

(compare also to fig. 4.38). The curve for the unfolded protein steadily increased to a plateau pressure of 16 mN/m. The second slope could thus be due to the protein denaturing at the interface.

In SPR experiments, urea denatured protein resulted in higher reflectivity increases on both mono- and bilayers compared to native β lg (fig. 4.16). Fitting the obtained scans resulted in layer thicknesses of 3 nm (native β lg) and 5 nm (denatured β lg) on DPTL monolayers. On a Triolein bilayer, native protein formed a layer of approximately 2 nm thickness compared to 4 nm, when denatured β lg was used. Whereas on bilayers made with DPhyPC vesicles no native protein layer was observable, injection of unfolded protein resulted in a 5.3 nm thick layer.

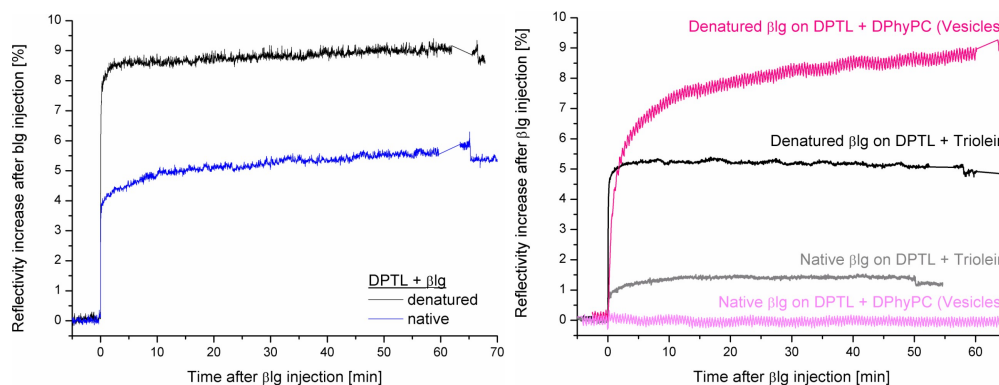


Figure 4.16: Comparison of protein layers of native and denatured β lg on top mono- and bilayers. Denatured β lg formed much denser layers than native protein due to increased protein-protein aggregation. The even higher effect on DPhyPC bilayers, compared to Triolein based ones, was due to interactions of the exposed helical regions with PC heads.

EIS measurements showed a decrease in capacitance for both bilayer systems, while the resistance was more or less stable for Triolein bilayers (around 10% increase), and marginally decreased (14%) on DPhyPC after addition of denatured β lg (fig. 4.17 and 4.18, Table 4.3 and 4.4).

Denatured β lg is able to aggregate through hydrophobic interactions or through SH/SS interchange reactions [127]. The completely unfolded protein has much more binding sites available than native protein. This will produce a dense aggregate layer.

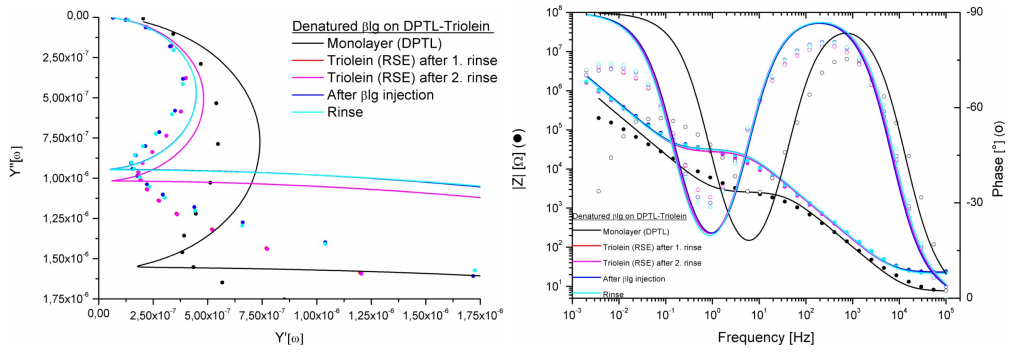


Figure 4.17: Bode + admittance plot: DPTL + Triolein + denatured β Ig. The capacitance decreased after denatured β Ig addition by 7.7% in contrast to native β Ig, where the capacitance increased by 10%.

	Monolayer	Bilayer	Rinse	β Ig	Rinse
R [M Ω]	0.003	0.027	0.027	0.031	0.030
C [μ F]	16.0	10.5	10.5	9.75	9.75

Table 4.3: Fitted EIS data values for DPTL + Triolein + β Ig (denat)

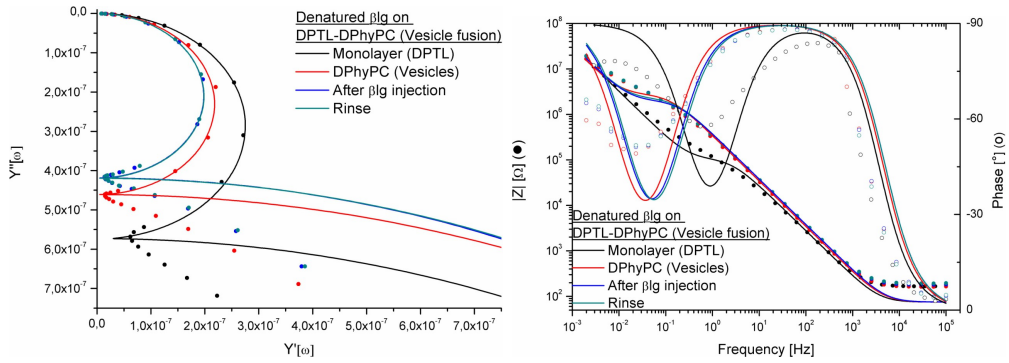


Figure 4.18: Bode + admittance plot: DPTL + DPhyPC (ves) + denatured β Ig. The capacitance decreased after denatured β Ig addition by 9.6% in contrast to native β Ig, where usually no change was observable.

	Monolayer	Bilayer	β Ig
R [M Ω]	0.13	3.27	2.87
C [μ F]	6.75	5.15	4.7

Table 4.4: Fitted EIS data values for DPTL + DPhyPC + β Ig (denat)

The higher $\Delta\pi$ of denatured protein can be explained by its structure. The hydrophobic core was completely exposed and could interact with the surface and neighbouring protein. As urea denatured β lg was already completely unfolded, no unfolding step had to take place after diffusion to the interface and aggregation/saturation could immediately start. The native protein had to unfold, leading to the second slope after 50 minutes. As the end pressures differed only by approximately 10% after 12 h, native β lg was nearly as much unfolded as urea denatured, completely unfolded protein. Additionally, modelling the thickness of the layer at the air-water interface during BA measurements, gave an adsorption layer of around 2 nm (Sec. 4.3.5).

SPR and EIS results support the formation of a dense protein layer on top of a monolayer as well as on a Triolein and DPhyPC bilayer. The increase in thickness compared to results obtained using native protein was probably due to the facilitated formation of an aggregated layer. On the Triolein bilayer, a decrease in capacitance was observed in comparison to an increase for the adsorption of the native protein. This indicates, that the denatured β lg did not penetrate the bilayer but rather formed an additional layer. The results also suggest that the native protein did not denature upon interaction with mono- or bilayers but rather remained in its native form. Most likely the protein was flattened on top of the Triolein, with some exposed moieties penetrating the bilayer, allowing for hydrophobic interactions.

The reflectivity increase during SPR measurements after injection of denatured β lg, as well as the capacitance decrease, was even more pronounced on a DPhyPC bilayer. This can be explained by interactions of the now exposed hydrocarbon chains of β lg and corresponded to experiments at the air-water interface (fig. 4.23) where β lg interacted more with DPhyPC monolayers if it was able to unfold beforehand. As no interaction between DPhyPC and the native protein could be observed, but the capacitance decreased after adding denatured β lg, an unfolding on those bilayers is highly unlikely.

4.3.4 Effect of cholesterol in the bilayer

As could be shown in section 4.3.2, native β -lactoglobulin interacted with Triolein layers but not with DPhyPC. As Triolein did not form as complete layers as DPhyPC vesicles, this could be due to defects in the bilayers that the protein was probing.

To conclude if the packing density of the upper bilayer or its chemical composition is crucial for β lg incorporation, cholesterol was added. In a Triolein layer, cholesterol should fill defects that occur due to the tripod structure of the lipid. In DPhyPC layers, defects might be caused by cholesterol as the lipid can not pack as densely as in the absence of cholesterol.

As cholesterol is also an important component in biological membranes that increases fluidity, tBLMs with mixed upper leaflets are the next step in creating more realistic artificial membrane systems.

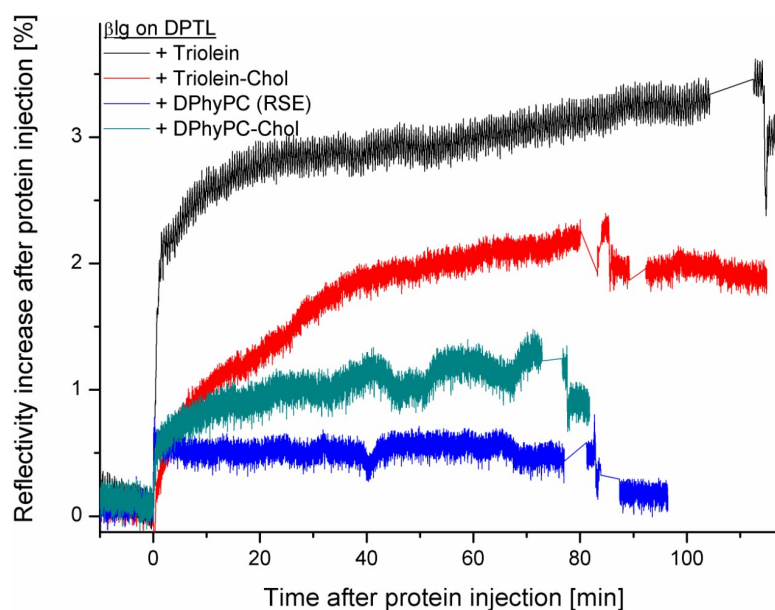


Figure 4.19: Effect of cholesterol on protein layers. Cholesterol seemed to fill defects in the Triolein layer resulting in a less dense β lg layer, but created holes in DPhyPC(RSE) layers.

Protein adsorption was studied by SPR on various bilayers (fig. 4.19). On an RSE formed DPhyPC bilayer, the protein interaction was almost completely reversible. However, the addition of cholesterol here led to a disturbed

bilayer structure and an increase in protein adsorption. For Triolein layers, adsorption could be reduced by the addition of cholesterol to the bilayers.

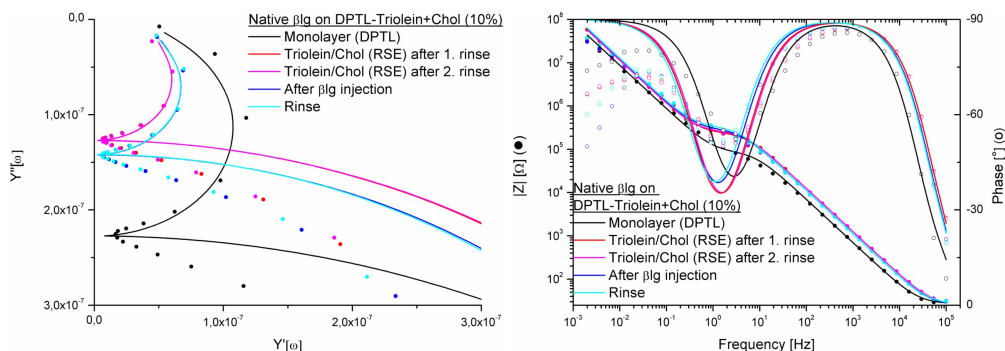


Figure 4.20: Bode + admittance plot: DPTL + Triolein-Chol (10%) + β Ig. An increase in capacitance was observable after β Ig addition. This increase was slightly smaller (7%) than in cholesterol-free Triolein layers (10%).

	Monolayer	Bilayer	Rinse	β Ig	Rinse
R [M Ω]	0.077	0.22	0.23	0.26	0.3
C [μ F]	2.6	1.4	1.4	1.6	1.6

Table 4.5: Fitted EIS data values for DPTL + Triolein-Cholesterol (10%) + β Ig

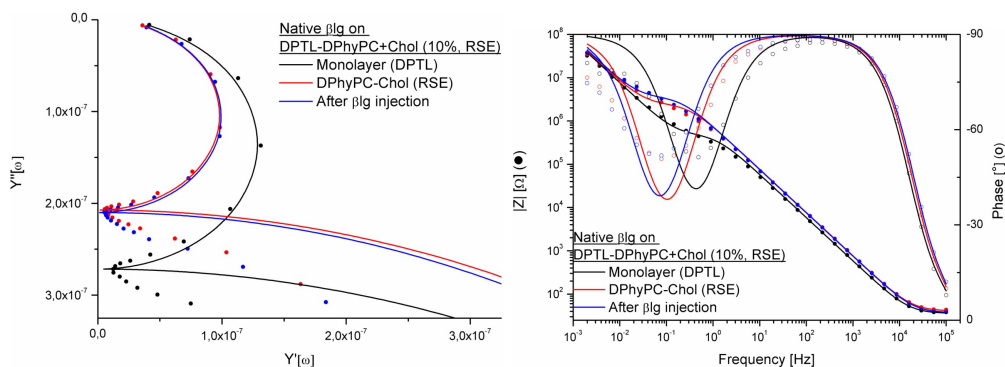


Figure 4.21: Bode + admittance plot: DPTL + DPhyPC-Chol (10%) + β Ig. A change in capacitance of 1% was observed after β Ig addition. The resistance increased by 31%.

	Monolayer	Bilayer	β lg
R [M Ω]	0.42	2.17	3.15
C [μ F]	3.15	2.325	2.35

Table 4.6: Fitted EIS data values for DPTL + DPhyPC-Cholesterol (10%) + β lg

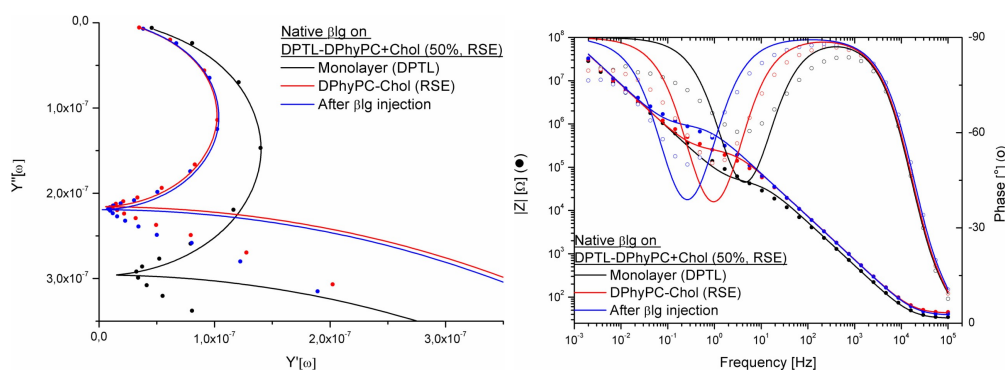


Figure 4.22: Bode + admittance plot: DPTL + DPhyPC-Chol (50%) + β lg. An increase in capacitance of 1% was observed after β lg addition. The increase in resistance was with 70% more pronounced than in bilayers with 10% cholesterol (31%) or only DPhyPC (10%). Probably the layer with 50% cholesterol was less sealing, but also more fluid, so that more re-organisation could take place.

	Monolayer	Bilayer	β lg
R [M Ω]	0.052	0.24	0.82
C [μ F]	3.45	2.425	2.45

Table 4.7: Fitted EIS data values for DPTL + DPhyPC-Cholesterol (50%) + β lg

The SPR results were supported by EIS measurements. The addition of 10% cholesterol to a Triolein bilayer showed a stabilising effect (fig. 4.20). The decrease in resistance and increase in capacitance (6.7%) after protein addition was less pronounced as for a pure Triolein layer (Increase in capacitance \approx 10%).

For DPhyPC bilayers, a perturbing effect of cholesterol has been observed. A small enhancement in β lg-DPhyPC interaction after adding 10% and 50%

cholesterol could be seen (fig. 4.21 and fig. 4.22) as the capacitance increased by 1% for both layer compositions. DPhyPC bilayers with added cholesterol did not possess the long-time stability of pure bilayers as can be seen as a shift in resistance (Plus 30% for 10% cholesterol in DPhyPC, 45% at 50%). In this state the protein was most likely able to probe some defects of the DPhyPC-cholesterol bilayers as has already been indicated by SPR experiments.

Those measurements showed that the composition of the upper leaflet has an effect on the protein-lipid interaction. β lg is attracted to less dense spots in the DPhyPC (-cholesterol) layers with the possibility of hydrophobic interaction with the underlying monolayer. However, the capacitance increase after β lg addition was much smaller (1%) as in Triolein-cholesterol layers (7%). In Triolein-cholesterol layers, cholesterol might prevent some initial protein adsorption.

4.3.5 Lipid layer packing density

To investigate the influence of the lipid packing density on protein adsorption and protein unfolding, measurements at the air-water interface were conducted. Kinetics show the surface activity of β lg in the absence and presence of DPhyPC and BAM enables us to visualise and observe the development and disappearance of phase co-existences.

β lg at the water-oil-air interface

Native protein was injected under a DPhyPC monolayer at the air-water interface that was previously compressed to different molecular areas. The barriers were kept fixed and the evolution of the surface pressure was monitored as a function of time.

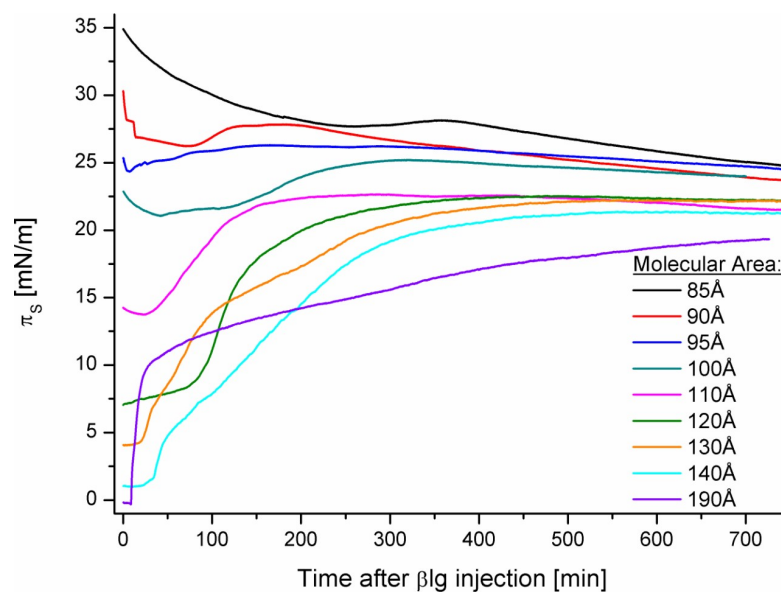


Figure 4.23: β lg incorporation at varying DPhyPC layer densities. The protein increased the surface pressure at the interface but no interaction between β lg and DPhyPC at pH7 was observable.

For initial lipid pressures below 22.5 mN/m, an increase in π could be observed after protein injection. When added to a monolayer with higher lipid pressure, the surface pressure decreased. The end pressure after β lg addition was between 22 - 25mN/M, independently from the initial lipid pressure.

β lg exhibited more surface activity in the presence of DPhyPC than at the clean air-water interface, as can be seen in fig. 4.23, where the equilibrium surface pressure was around 22 - 25 mN/m and fig. 4.15 and fig. 4.38, where the final surface pressure without lipids was below 15 mN/m at pH7.

This indicated that the protein interacted with the lipid layer. As no surface pressure increase could be observed if β lg was added over a certain initial lipid pressure (over 22.5 mN/m, around 100 Å per lipid molecule), the protein either entered the lipid monolayer at low lipid pressure, but this was prevented at higher pressure or the protein-lipid interaction were only triggered, if the β lg had air contact (e.g. caused by oxidation). A combination of those two scenarios could also be possibly.

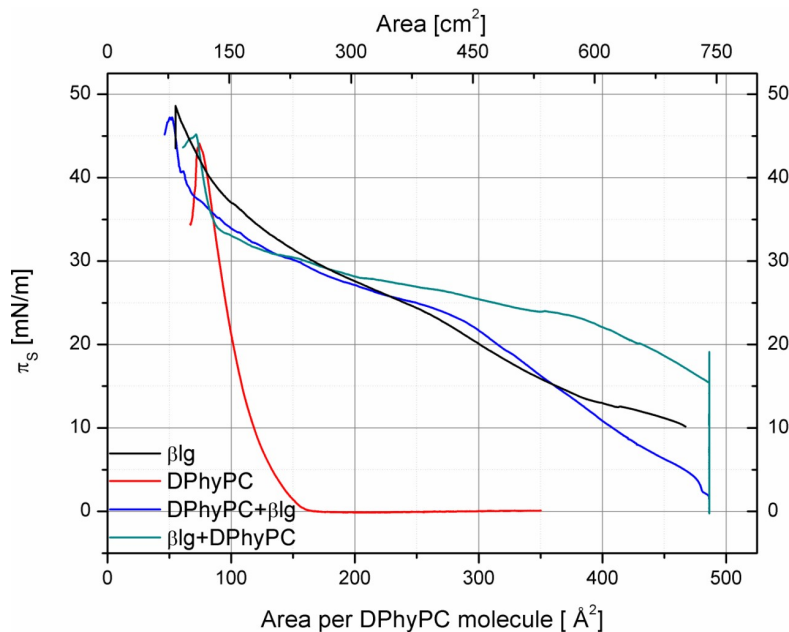


Figure 4.24: π - A_M isotherms ($v_C = 10 \text{ \AA}^2/(\text{molecule} \cdot \text{min})$) of β lg (injected into the subphase and compressed after 10 min), DPhyPC, β lg + DPhyPC (protein injected into the subphase, lipid spread on top, immediately compressed), DPhyPC+ β lg (lipid spread, afterwards protein injected into the subphase) at pH7

β -lactoglobulin itself is surface active, also in the presence of DPhyPC. Different experiments were performed, where β lg was injected to a pre-formed DPhyPC monolayer. The isotherms of the mixed monolayers were dominated

by the protein.

During compression (compression speed $v_C = 10 \text{ \AA}^2/(\text{molecule} \cdot \text{min})$), a common transition was visible at a surface pressure of 25 mN/m, however at different molecular areas. When βlg was added before DPhyPC, the transition appeared at areas of 375 \AA^2 , if added afterwards at 275 \AA^2 . This elucidates that protein and lipid compete for interface space.

If βlg was injected under a monolayer of DPhyPC that was in the gaseous phase, the collapse pressure and area were similar to a pure protein film. As the lipids were far apart, the protein could adsorb between them. During compression, those lipids did not interact as much as they would in a pure lipid film, leading to smaller collapse areas and higher collapse pressures.

(βlg : $55 \text{ \AA}^2/48.5 \text{ mN/m}$, DPhyPC + βlg : $52 \text{ \AA}^2/47.3 \text{ mN/m}$)

If DPhyPC was spread on a subphase with the protein, the collapse pressure and area were similar to that of pure lipid. (DPhyPC: $75 \text{ \AA}^2/44.2 \text{ mN/m}$, βlg + DPhyPC: $72 \text{ \AA}^2/45.1 \text{ mN/m}$) Due to the surface activity of βlg , the lipids had to cluster and aggregated already during spreading, leading to more lipid islands that dominated the phase behaviour.

BAM - experiments

The behaviour of the protein at the air-water interface was also investigated by BAM. βlg was injected to the subphase and the water surface was observed using the microscope. Simultaneously, the surface pressure was recorded. After addition of βlg , small, bright spots (smaller than $1 \mu\text{m}$) were visible at the surface (fig. 4.26, A). With time, the grey level increased, shifting from black (Grey Scale 64), to grey (Grey Scale 120) in 1 h (fig. 4.26, B). With the “BAM tools” provided by Nanofilm, those changes could be related to a film thickness at the air-water interface of 2.2 nm (Calibration factor = $2.3 \cdot 10^{-8}$, BA = 53.14).

Although the area was constant, the surface pressure increased. The increase in the first minutes after protein addition could be attributed to the diffusion of the molecule to the surface. The following increase was due to the molecule unfolding and aggregating.

β -lactoglobulin

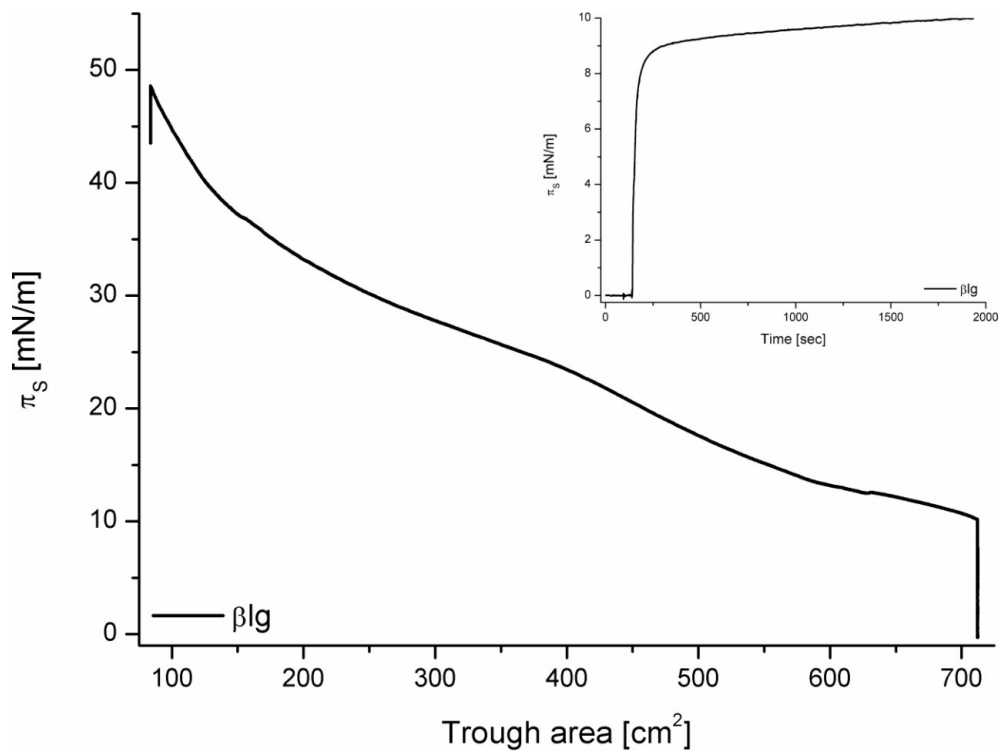


Figure 4.25: π_S - A_M isotherms of β lg at pH7 ($v_C = 10 \text{ \AA}^2/(\text{molecule} \cdot \text{min})$). (Inset: Kinetic before compression)

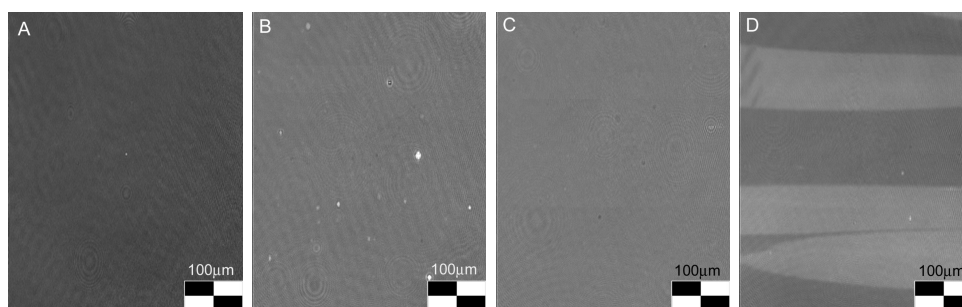


Figure 4.26: BA micrographs of β lg at various surface pressures. A 8.5 mN/m B 12.5 mN/m C 24 mN/m D 27 mN/m
The formation of an (heterogeneous) protein layer was observable in a change of greyscale. (Brighter colours relate to thicker films.)

When the protein film was compressed, block domains of varying grey scale were visible (fig. 4.26, D). As the reflected intensity is directly proportional to the film thickness, light grey domains are thicker than darker ones. As unfolding promotes protein-protein aggregation, completely unfolded proteins will cluster and form layers that reach into the subphase. If βlg has no contact to the air-water interface no denaturation and unfolding will take place. This native protein will not be able to aggregate as much as the unfolded βlg , resulting in thinner patches.

In order to monitor the influence of βlg on a DPhyPC monolayer, the protein has been added to the lipid film at different surface pressures.

DPhyPC

First, a pure DPhyPC film has been observed for comparison. DPhyPC was spread, the film was given 15 min to equilibrate and compressed at constant speed $10 \text{ \AA}^2/(\text{molecule} \cdot \text{min})$.

At the gaseous-liquid interface, foam structures were observable (fig. 4.28, A-C). After they fused, small, bright aggregates were visible that did not grow in size and stayed present until the collapse (fig. 4.28, D).

DPhyPC (0 mN/m) + βlg

DPhyPC was spread onto a pure pH 7 subphase while the trough barriers were completely open ($A_M \approx 485 \text{ \AA}^2$). 15 minutes after the spreading of the lipids, protein was injected under the monolayer and compression of the film was started immediately (compression speed $v_C = 10 \text{ \AA}^2/(\text{molecule} \cdot \text{min})$).

At the beginning of the compression, the same behaviour as for pure βlg was visible (fig. 4.30, A). At surface pressures higher 28 mN/m, the BA images changed to those observed for pure DPhyPC in liquid phase (fig. 4.30, B-D).

This abrupt change was one indication that βlg was incorporated into the lipid monolayer but expelled at higher surface pressure because the lipid-protein interactions are too weak.

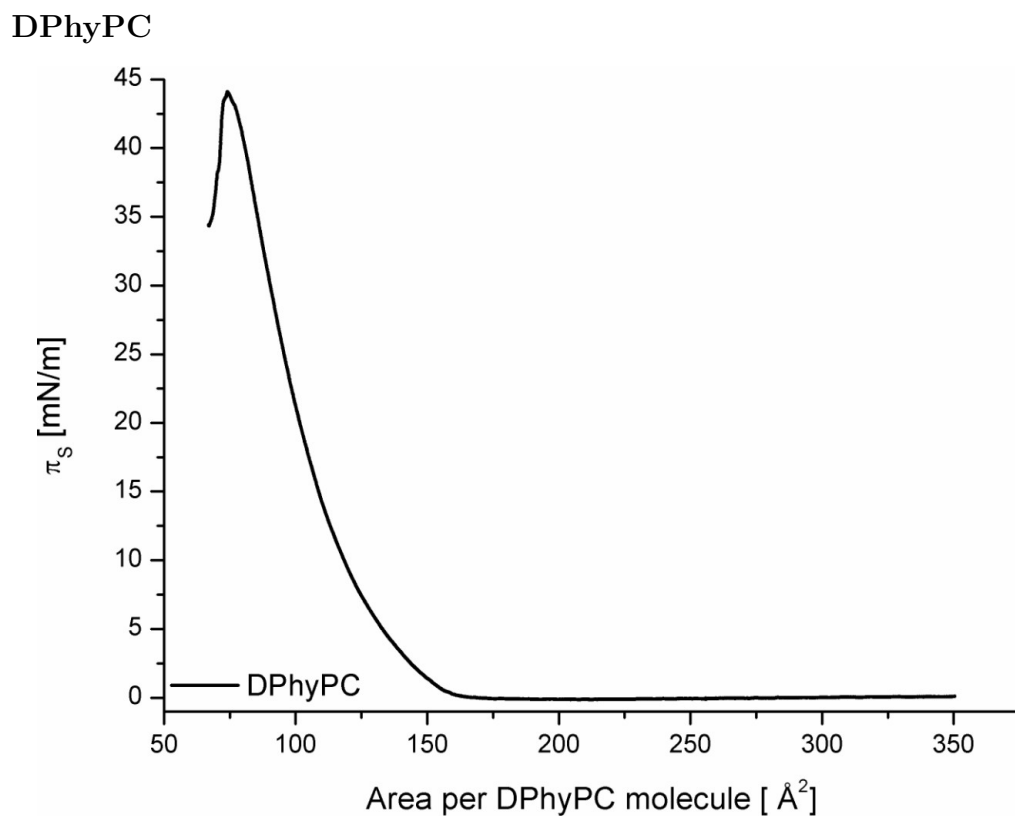


Figure 4.27: π_s - A_M isotherm of DPhyPC at pH7
 ($v_C = 10 \text{ \AA}^2/(\text{molecule} \cdot \text{min})$)

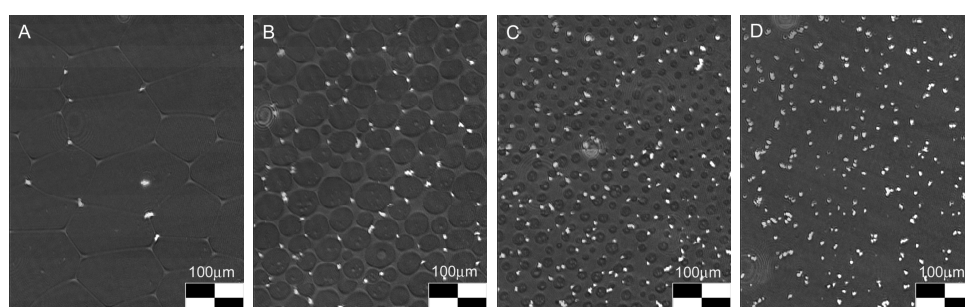


Figure 4.28: BA micrographs of DPhyPC at various surface pressures.
 A 0 mN/m ($A_M \approx 170 \text{ \AA}$) B 0 mN/m ($A_M \approx 165 \text{ \AA}$) C 0.1 mN/m ($A_M \approx 160 \text{ \AA}$)
 D 4 mN/m

DPhyPC (0 mN/m) + β lg

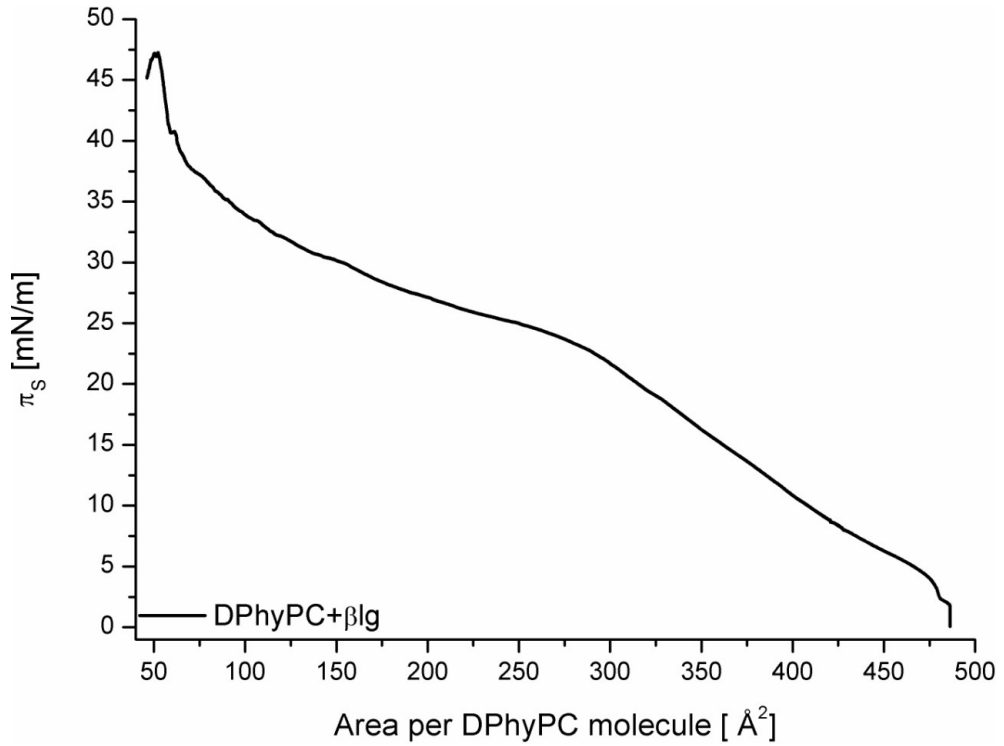


Figure 4.29: π_S - A_M isotherm of DPhyPC + β lg (added at 0 mN/m, $v_C = 10 \text{ \AA}^2/(\text{molecule} \cdot \text{min})$)

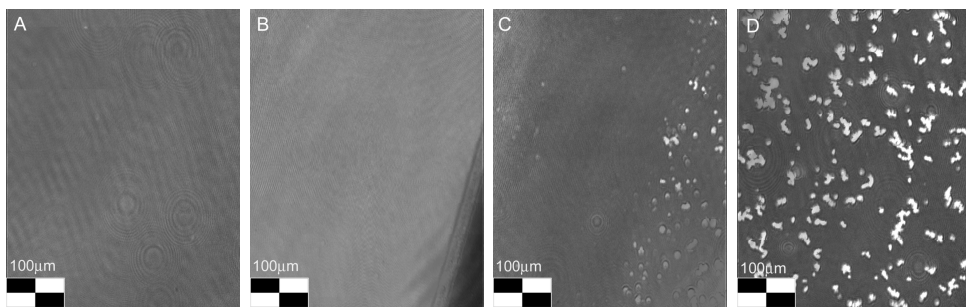


Figure 4.30: BA micrographs of DPhyPC and β lg (added at 0 mN/m) at various surface pressures

A 11 mN/m B 28.6 mN/m C 28.8 mN/m D 35 mN/m

β lg was expelled from the lipid monolayer at higher surface pressure.

DPhyPC (29 mN/m) + β lg

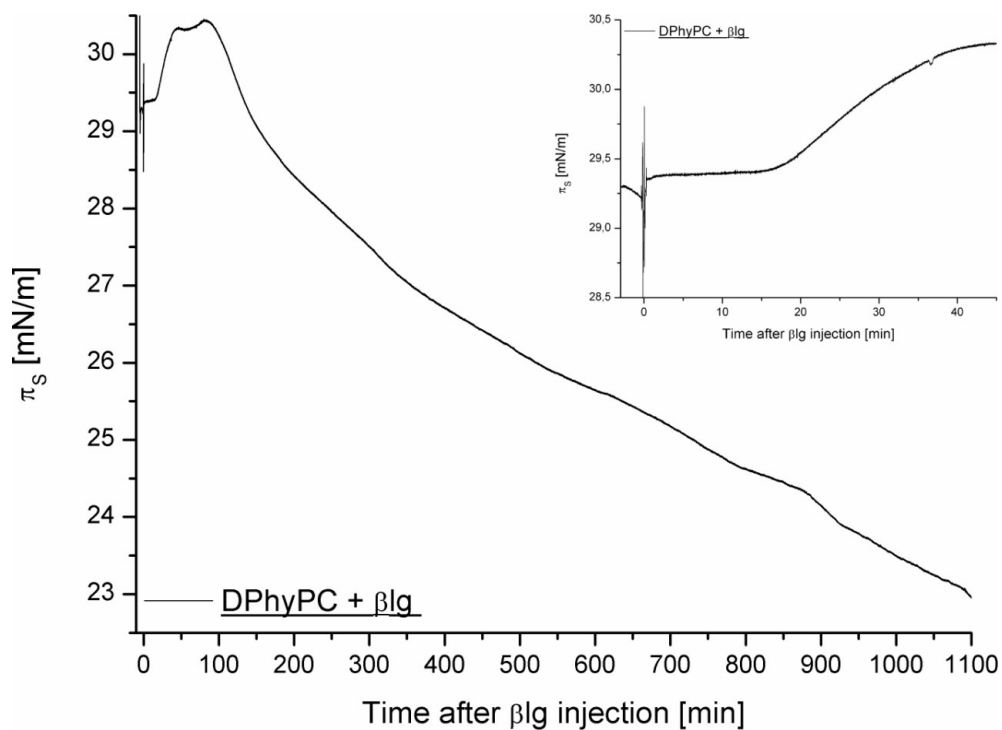


Figure 4.31: π_S -t isotherm of DPhyPC + β lg (added at 29 mN/m)
(Inset: Zoom into beginning of kinetic)

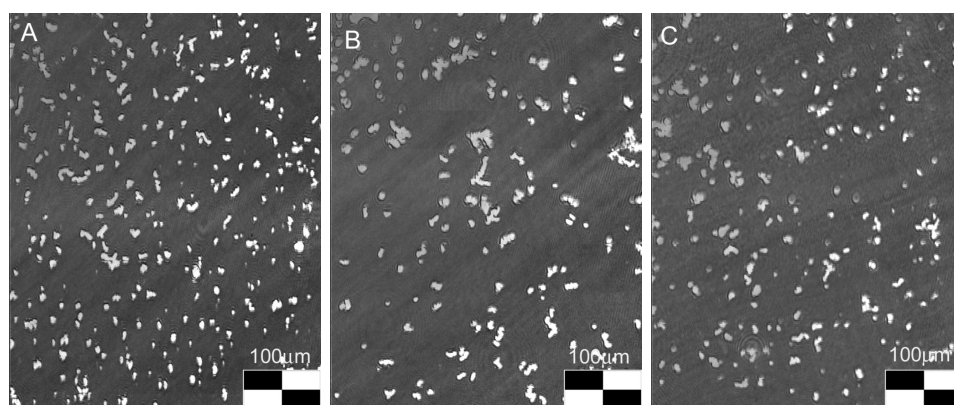


Figure 4.32: BA micrographs of DPhyPC and β lg (added at 29 mN/m) at various surface pressures
A 29.3 mN/m B 29.3 mN/m (after 45 min) C 22.2 mN/m (after \approx 19 h)

DPhyPC (29 mN/m) + β lg

A pure DPhyPC monolayer was compressed as described before. Close to $\pi=29$ mN/m the compression speed v_C was stepwise reduced to $0 \text{ \AA}^2/(\text{molecule} \cdot \text{min})$. When the surface pressure was stable, β lg was injected into the subphase and the changes in π was monitored at constant A_M .

When the lipid monolayer was already in the liquid condensed phase when β lg was added, less interaction occurred. The surface pressure increased by 1 mN/m, the background became slightly lighter and lipid aggregations seemed to go down slightly (fig. 4.32).

Probably some free space existed between the lipids where the protein could adsorb and unfold.

β lg + DPhyPC

When DPhyPC was spread on a monolayer with β lg already present in the subphase, lipid aggregation occurred immediately (fig. 4.34).

As the surface was covered with the protein layer, lipids could not spread homogeneously and had to cluster. Those aggregates seemed to be even smaller and rather round, than those observed for the previous scenarios.

The Langmuir and BAM results confirmed the previous assumptions that β lg preferentially interacts with the hydrophobic part of a lipid layer. The protein probably adsorbs to defects or voids between the lipids.

$\beta\text{lg} + \text{DPhyPC}$

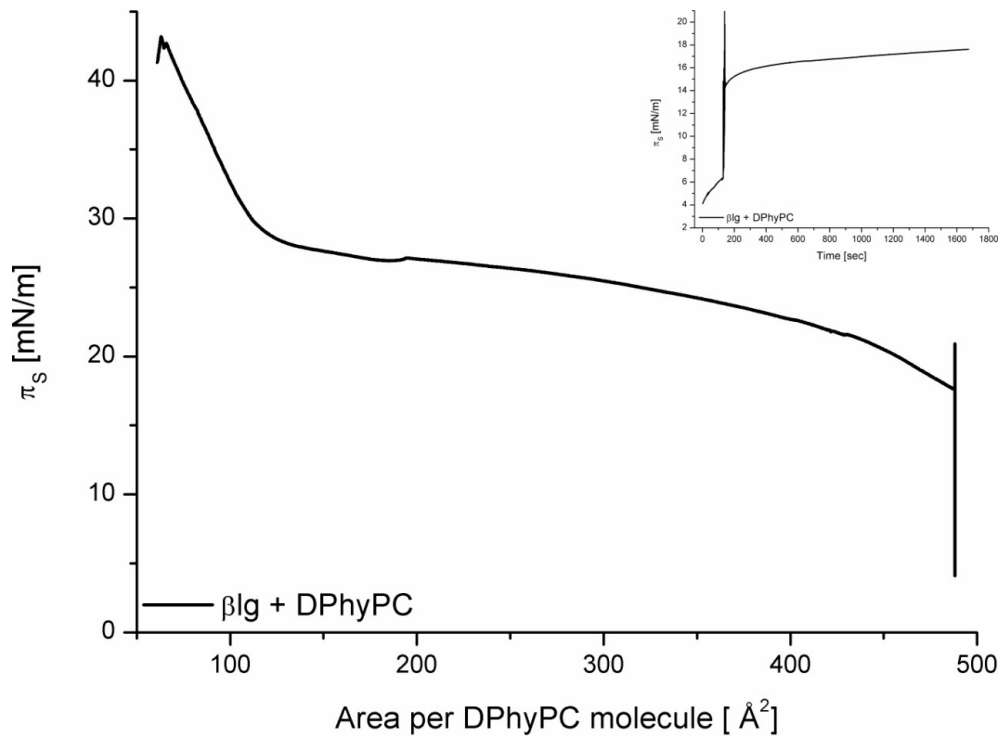


Figure 4.33: π_S - A_M isotherm of $\beta\text{lg} + \text{DPhyPC}$
 ($v_C = 10 \text{ \AA}^2/(\text{molecule} \cdot \text{min})$) (Inset: Zoom at DPhyPC spreading)

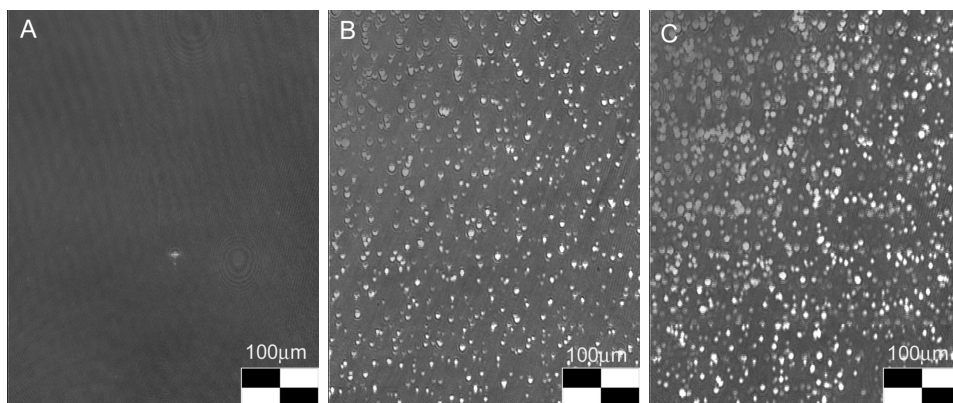


Figure 4.34: BA micrographs of βlg and DPhyPC
 A 6 mN/m (before spreading) B 16 mN/m (after spreading) C 38.5 mN/m
 Lipid aggregates formed immediately after spreading on a protein layer.

DPHDL

To investigate the influence of the lipid packing density of solid supported substrates on protein adsorption and protein unfolding, measurements on DPTL based monolayers were compared to experiments on DPHDL based monolayers. The alkyl chains of the “self-diluting” anchor lipid DPHDL are much less packed in such a monolayer than in DPTL based monolayers.

The adsorption of the protein was probed by SPR and NR.

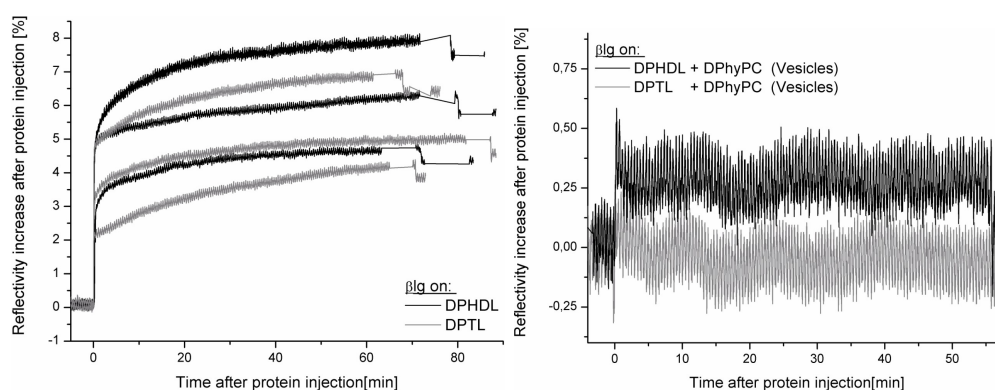


Figure 4.35: β Ig on DPHDL monolayers and DPhyPC bilayers. As DPTL and DPHDL adsorption kinetics cannot be compared directly due to substrate effects, examples for maximum, average and minimum adsorption kinetics are given (left). On DPHDL monolayers a slightly denser layer was formed. On bilayers, the anchor had no effect on the protein layer.

β Ig on a DPHDL monolayer (fig. 4.35) formed a slightly thicker layer than on DPTL, 3.4 nm (DPHDL) compared to 3 nm (DPTL). This might result from the chemical structure of DPHDL and the resulting monolayer (fig. 4.37).

On a DPHDL/DPhyPC bilayer, a slight increase in reflectivity was observed. However, this added layer could be washed away and was probably due to unspecific adsorption rather than directed protein-lipid interactions.

SPR results showed a thicker layer of adsorbed protein on DPHDL compared to DPTL, this could be due to the protein partly entering the less dense monolayer. Following this scenario, the setup protocol for fitting the DPHDL + β Ig NR data allowed the protein to enter the monolayer (fig. 4.36). The sld profiles showed that the reflected intensity of the protein went up

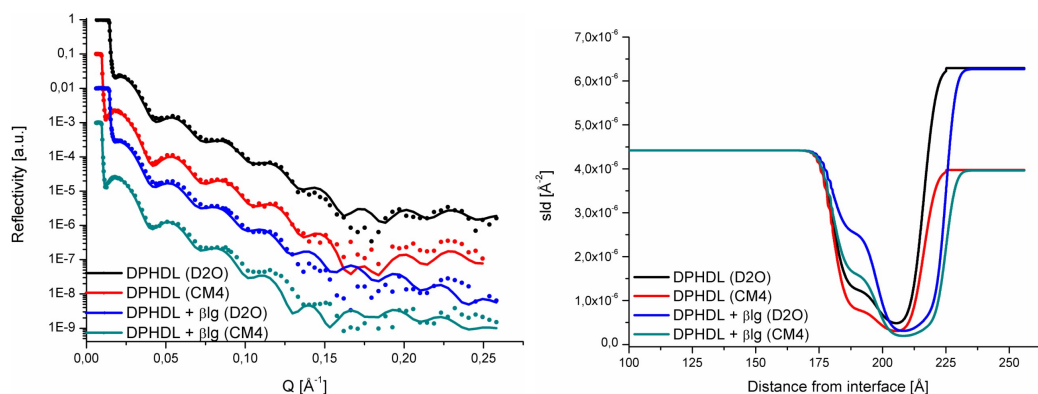


Figure 4.36: Fitted neutron reflectivity profiles (left) of DPHDL (D₂O+CM4) and DPHDL + β Ilg and corresponding scattering length density profiles (right).

(from $1.25 \cdot 10^{-6} \text{ \AA}^{-2}$ to $2.54 \cdot 10^{-6} \text{ \AA}^{-2}$), the inner leaflet values stayed nearly the same ($0.45 \cdot 10^{-6} \text{ \AA}^{-2} / 0.3 \cdot 10^{-6} \text{ \AA}^{-2}$) and a 8.4 \AA thick protein layer formed after β Ilg addition. Additionally, the volume fraction of the spacer doubled from 20% to 40%. Those changes are in very good accordance to those observed in DPTL (monolayer) after β Ilg addition, when the protein was allowed to enter the monolayer as well (8.8 \AA). Although a β Ilg layer thickness around $8 - 9 \text{ \AA}$ is not what we expected, the similarities to the fit of β Ilg on a DPTL monolayer indicated that the protein did not behave significantly different on a monolayer with much lower lipid chain density.

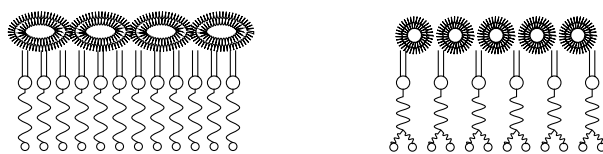


Figure 4.37: β Ilg on DPHDL/DPTL monolayers.

Additionally, the differences between β Ilg on DPTL and DPHDL monolayers were noticeable smaller than for pre-unfolded β Ilg. The protein probably did not unfold much on the monolayers. In addition, the value for the protein layer on top DPHDL corresponds nearly with the diameter of a β Ilg monomer. Possibly the protein is able to slightly penetrate the less dense DPHDL monolayer. This would result in a reduced electrostatic repulsion

between the negatively charged proteins and β lg would not have to flatten as much on the monolayer, leading to a slightly increased protein layer thickness (fig. 4.37).

4.3.6 pH influence

Hydrophobic interactions are important for proteins in general, e.g. influencing the emulsifying properties.

For β lg specifically, controlling the pH helps to determine the state of unfolding and enables to control charges present at the protein surface. β lg has been investigated at various pH values to examine the state of unfolding of the protein at solid and liquid interfaces. This is possible as the stability of the protein and therefore its ability to unfold is pH dependant. At lower pH, the protein core is very rigid and exhibits a stable conformation [128, 129]; at higher pH, β lg is more flexible and easier to unfold. This is supported by DSC measurements (Sec. 6.16) that show that the denaturation enthalpy needed to unfold the protein is higher at pH 2 compared to higher pH values.

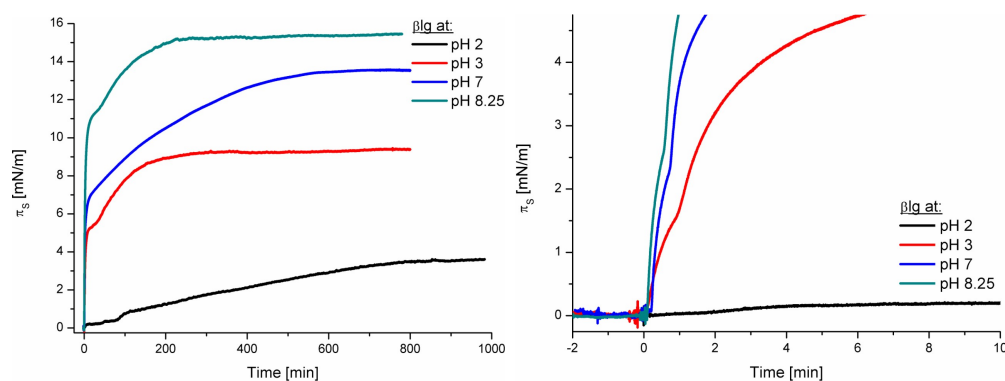


Figure 4.38: pH dependence of β lg at the air-water interface. The variance in surface pressure resulted from the difference in protein confirmation. Decreasing pH increased the rigidness of the β lg core, limiting unfolding and protein aggregation.

A clear tri-step action while the protein was adsorbing at the interface was visible:

1. Diffusion to the air-water interface
2. Unfolding + Aggregation
3. Saturation

In order to probe the influence of the pH on the adsorption of the protein, π -t isotherms were measured using subphases with pH values between 2 and 8.25.

The surface pressure increase of β lg at the air-water interface was inversely

proportional to the pH of the used subphase; $\Delta\pi$ was smallest at pH 2 and strongest at pH 8 (fig. 4.38).

The difference in the final surface pressure can be explained by the different unfolding states of the protein at the observed pH. The more unfolded the protein was, the higher was $\Delta\pi$. (Compare to section 4.3.3.) Also protein-protein aggregation was promoted in a more unfolded protein due to more available binding sites.

A tri-step action of β lg was clearly visible (fig. 4.38):

1. Diffusion of the protein to the air-water interface
2. Unfolding of β lg and protein-protein aggregation
3. Saturation

It became apparent that the time the protein needed to diffuse to the air-water interface was different and increased with decreasing pH (fig. 4.38, Inset).

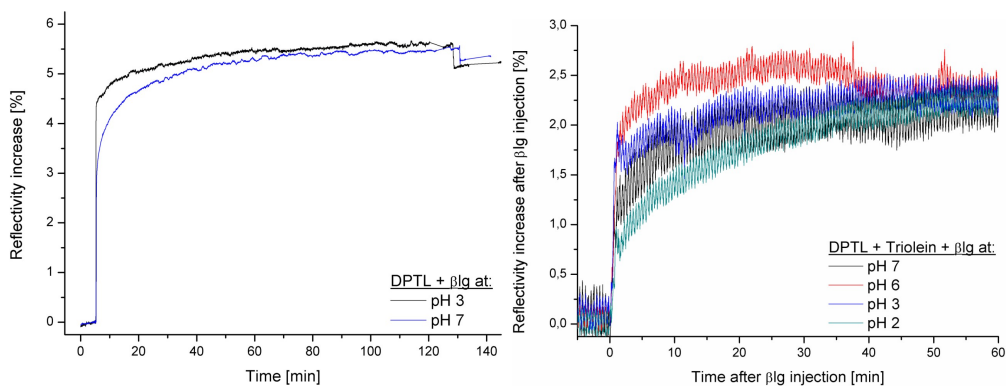


Figure 4.39: pH effects on protein layers. No difference between β lg layers formed on top DPTL at pH7 and pH3 could be observed. This was also the case for layers on top Triolein for various pH's.

However, SPR measurements showed no difference in layer thickness at different pH, neither on DPTL monolayers nor on Triolein bilayers. (fig. 4.39) The same conclusion can be drawn from EIS data (fig. 4.40), where also no effect of pH was visible, the capacitance increase was around 11% at pH3 as well as at pH7.

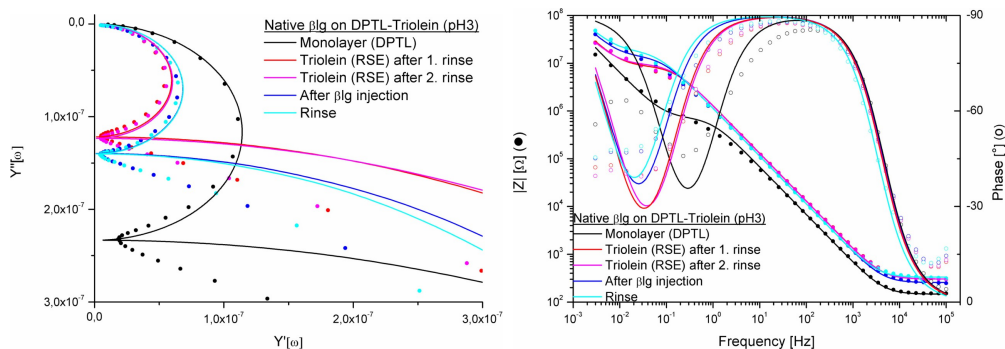


Figure 4.40: Bode + admittance plot: DPTL + Triolein + β Ilg at pH3. An increase in capacitance was visible after β Ilg addition. This was on average 10%, the same mean value as for β Ilg at pH7.

	Monolayer	Bilayer	Rinse	β Ilg	Rinse
R [M Ω]	0.66	4.5	6.4	8.7	10.8
C [μ F]	2.58	1.45	1.475	1.55	1.55

Table 4.8: Fitted EIS data values for DPTL + Triolein + β Ilg at pH 3

No difference in adsorption to either DPTL monolayers or Triolein bilayers at pH 3 and pH 7 was observable. This is a strong indication that if the protein unfolds on top of a monolayer or a bilayer, this unfolding is only small as the core stability should influence extensive unfolding.

4.3.7 Comparison DPhyPC - DPhyPG

To evaluate the influence of charge and electrostatic repulsion on the protein core stability, experiments have been performed with negatively charged DPhyPG at the air-water interface in the presence of positively (pH 3) and negatively (pH 7) charged β lg.

The measurements in this section were executed by Chloé Champagne, ENSBANA, Dijon/France during an internship from June - September 2008.

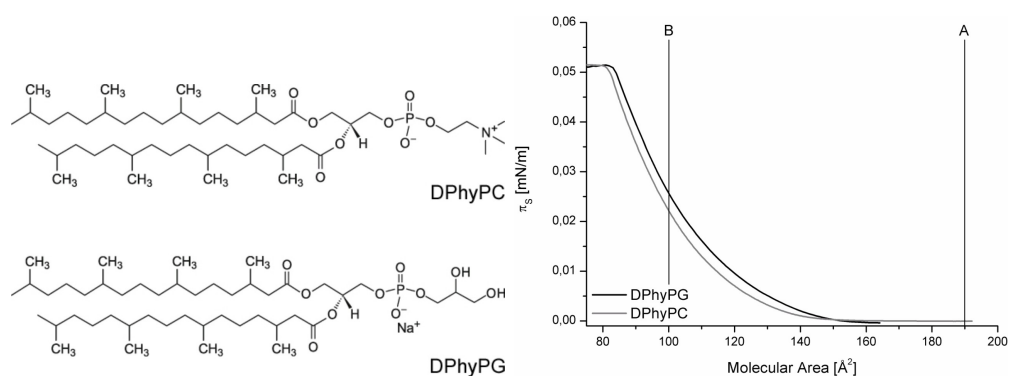


Figure 4.41: Chemical structure + π_S - A_M isotherm of DPhyPC/DPhyPG ($v_C = 10 \text{ \AA}^2/(\text{molecule} \cdot \text{min})$)

Lines indicate A_M of β lg addition, A = 190 \AA^2 and B = 100 \AA^2 .

The π -A isotherms of the zwitterionic DPhyPC and the negatively charged DPhyPG were similar in their phase behaviour (fig. 4.41). DPhyPC was slightly shifted to smaller areas due to less electrostatic repulsion between the lipids.

The kinetics of β -lactoglobulin added under a monolayer made of DPhyPC and DPhyPG at pH3 and pH7 varied significantly (fig. 4.42).

At pH7 and low lipid pressure, negatively charged β lg interacted with DPhyPC monolayers as previously observed (compare section 4.3.5), π increased over time when β lg was added at low surface pressure, but decreased at high π . Results for DPhyPG at low surface pressure were comparable. Also at high lipid pressure no severe differences could be observed between DPhyPG and DPhyPC.

At pH3, the positively charged protein interacted more with the negatively charged DPhyPG monolayers than the zwitterionic DPhyPC, observable in

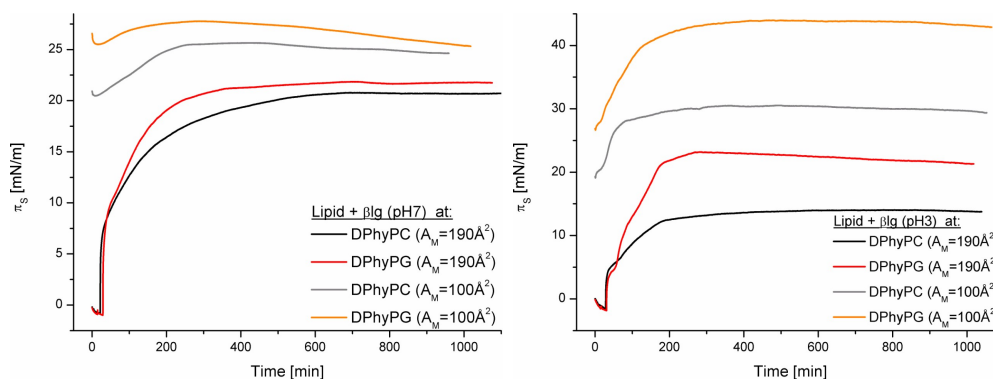


Figure 4.42: Interactions of β lg with DPhyPC and DPhyPG at low and high lipid area. Surface pressure increase after protein addition was comparable in the presence of zwitterionic lipid DPhyPC and negatively charged protein (pH7) and positively charged protein (pH3) at low area per lipid molecule. No difference was visible at pH7 between zwitterionic or negatively charged lipids at low area per lipid molecule. No interaction was observable at pH7 with neither zwitterionic nor negatively charged lipid at high area per lipid molecule. Favourable interactions were observed for positively charged β lg at pH3 and negatively charged DPhyPG.

higher surface pressure increases, both at low and high lipid pressure ($\Delta\pi \approx 12$ mn/m below DPhyPC, $\Delta\pi \approx 20$ mn/m below DPhyPG).

The increase in surface pressure at low lipid pressure at pH3 was comparable to the increase at pH7 and can be explained by the protein diffusing to the interface, unfolding and thereby lowering the surface tension. At high initial surface pressure, only little interfacial area was available to the protein. At pH7 only a small increase was observable, indicating no significant protein-lipid interaction. It seemed the protein has to be unfolded to be able to interact with the phospholipids. The similar behaviour of β lg in the presence of DPhyPC and DPhyPG is an indication that the interaction between the protein and the lipids are not only electrostatic, as this should result in more repulsion at the DPhyPG layer and therefore, in a variation of surface pressure increase.

Beneath a DPhyPC layer, the total surface pressure increase at high areas was lower for β lg at pH3 than at pH7. At pH3, the protein core was more stable, leading to less unfolding and smaller $\Delta\pi$ after β lg injection.

In contrast to pH7, $\Delta\pi$ was similar at low and high surface pressure at pH3. At this pH, the protein experienced much stronger electrostatic interactions than at pH7, this may weaken the intra-molecular forces that stabilise the native structure, promotes unfolding and protein-lipid interactions. As this electric field would be stronger in the presence of DPhyPG, this also explains the higher surface pressure increase for the negative charged lipid.

4.4 Summary

By means of SPR, EIS, π -A isotherms, BAM and NR the globular whey protein β -lactoglobulin and its interaction with various lipids was investigated.

On a monolayer, a dense one molecule thick protein layer could be observed with SPR and NR. Comparison between DPTL and DPHDL indicated that the protein party entered the alkyl chains if the lipid packing density allowed it to avoid protein-protein contact and flattening (fig. 4.43).

The pH of the bulk solvent controls the unfolding tendency of the protein. Different pH values yet did not influence the adsorption kinetics. However, completely unfolded β lg led to significantly different layer thicknesses. Thus, the protein does not or only slightly unfold when exposed to a lipid monolayer.

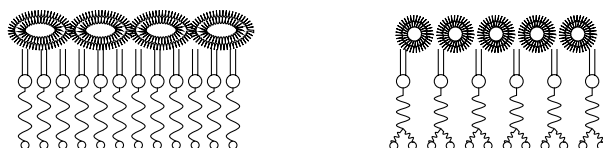


Figure 4.43: β lg adsorption to DPTL (left) and DPHDL (right) monolayers.

On a bilayer (fig. 4.44), the native protein probed defects in the upper layer and penetrated it if possible. As results for native and pre-unfolded protein varied significantly, a complete unfolding on top a bilayer is highly unlikely.

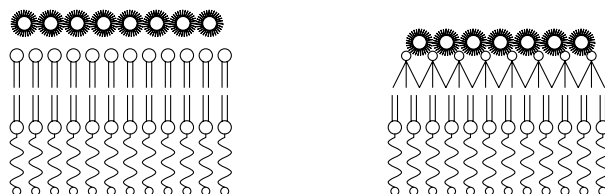


Figure 4.44: Schematic illustration of native protein adsorption to model membranes: DPTL + DPhyPC (left) and DPTL + Triolein (right)

Urea denatured protein formed a much thicker layer (fig. 4.45) than the native protein due to the high protein-protein interaction leading to protein

aggregation. Additionally, interactions between DPhyPC and unfolded β lg were promoted due to exposed hydrocarbon regions of the protein.

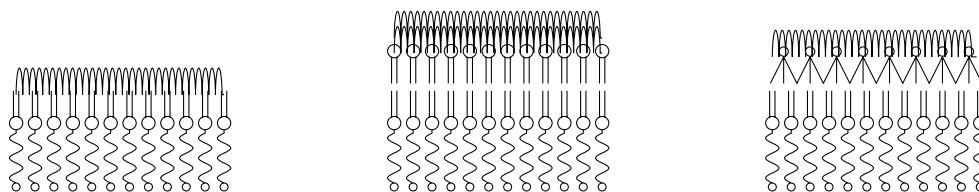


Figure 4.45: Schematic illustration of denatured protein adsorption to model membranes: DPTL monolayer (left), DPTL + DPhyPC (middle), DPTL + Triolein (right)

The protein core stability increased with decreasing pH, which could be observed in π -t isotherms. At pH 2, the protein lowered the surface tension considerable less than β lg at pH 8, due to the fact that the hydrophobic core was more stable at lower pH and the protein did not unfold as much (fig 4.46).

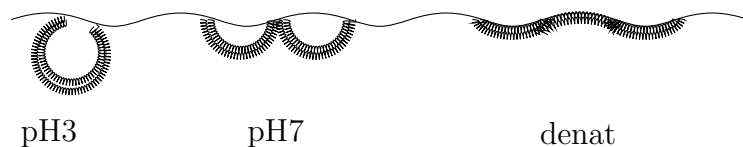


Figure 4.46: Schematic illustration of β lg at the air-water interface at different pH

The adsorption of β lg to solid supported mono- and bilayers did not show any pH dependence. At the air-water interface, the protein is exposed to oxygen and probably to a higher surface energy, which led to an enhanced unfolding compared to the oil-water interface. This is also supported by the isotherms measured for DPhyPC/ β lg mixtures. Although the decrease in surface tension was higher in films where DPhyPC and β lg are present compared to pure protein films, this effect was more pronounced at high lipid area where β lg was able to diffuse to the interface and unfold. β lg seemed only able to interact with phospholipids if in the unfolded state.

This could either be achieved by denaturation at the air-water interface or due to electrostatic interactions that weaken the intra-molecular forces of the protein.

This trend could also be shown by BAM. Lipid aggregates were formed at much smaller molecular area and surface pressure if the protein was present from the beginning of the compression, compared to only pure lipid. Still, β lg was expelled from the lipid layer at higher surface pressure and the protein had no effect on lipid aggregations if introduced after their formation.

The interactions between β lg and phospholipids are driven by hydrophobic as well as by electrostatic interactions. The latter were investigated by exposing the protein at different pH values to zwitterionic DPhyPC and negatively charged DPhyPG lipids. The strongest interaction was observed between positively charged β lg at pH 3 and DPhyPG ((fig. 4.47).

The protein lipid interaction with DPhyPC did not show a significant pH dependence and are probably governed by hydrophobic forces.

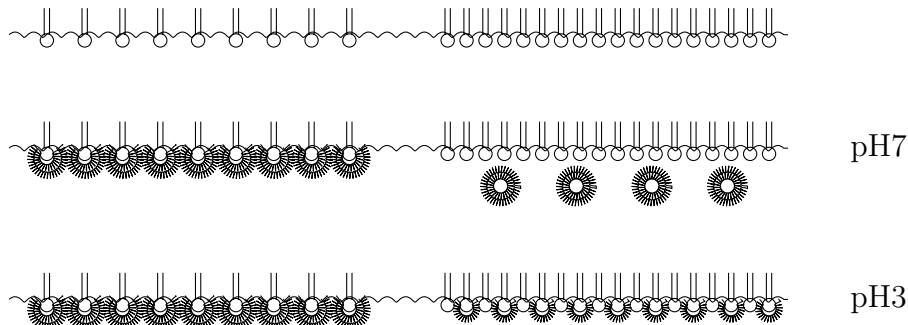


Figure 4.47: Schematic illustration of β lg at the air-water-lipid interface at different pH and lipid packing

Furthermore, π -t isotherms could show that β lg approached the air-water interface in a tri-step action (fig. 4.48). First it quickly diffused to the surface, than it unfolded and aggregated. The degree of unfolding was influenced by the pH and therefore by the rigidness of the globular molecule.

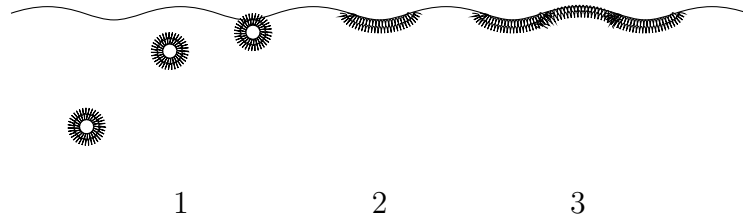


Figure 4.48: Schematic illustration of β lg at the air-water/air-lipid interface Tri-step action

The work described in this manuscript could elucidate the question how the whey protein β lg interacts with various lipids. Additionally, the importance of pre-denaturation for those interactions could be shown as only in the unfolded state the protein is able to interact with phospholipids. As they are one major compound in the milk fat globular membrane, interactions between phospholipids and β lg is of great importance for food science applications.

Chapter 5

Model membranes

5.1 DPTL

A lipid bilayer that is decoupled from a solid substrate has an increased stability and can cover small surface roughness features. It also provides an ion and water reservoir underneath the membrane. Inspired by the properties of archaea bacteria membranes, Cornell et al. [15] presented a first approach to tethered bilayer lipid membranes (tBLMs) in 1997. They used lipids made of branched hydrocarbon units which are in a fluid phase at ambient conditions. Therefore, the problems of membranes assembled from straight aliphatic chains longer than 12 C atoms, such as crystal defects [130] are minimised.

In 2003, Schiller et al. [131] synthesised the first lipids used for tBLMs in Mainz. In contrast to Cornell's lipids, 2,3-di-O-phytanyl-sn-glycerol-1-tetraethylene glycol-d,l-a-lipoic acid ester lipid (DPTL, Table 5.1) contains two phytanyl chains bound to the spacer through a chiral glycerol unit to ensure a stable insertion of the molecules into the lipid membrane. DPTL can be covalently bound to gold substrates *via* a lipoic acid anchor. This enables the use of surface analytical techniques such as SPR, QCM, NR, AFM, etc., and electrochemical methods.

tBLMs prepared with DPTL show good electrical sealing properties and allowed for the incorporation of various peptides and proteins [13, 14].

The structure of a DPTL based mono- and bilayer has been investigated by neutron reflectivity measurements (fig. 5.1). The analysis of the data resulted in a monolayer thickness of 3.9 nm. The theoretical lengths of DPTL in a stretched configuration determined by Chem3D Ultra 6.0 is 5 nm. This indicates a non-stretched conformation, as also shown by IR measurements [132]. Most probably the spacer adopts a rather helical structure. The sld of the spacer part was simulated to be $0.54 \cdot 10^{-6} \text{ \AA}^{-2}$, which was in very good accordance to the theoretical value of $0.537 \cdot 10^{-6} \text{ \AA}^{-2}$ (NCNR Scattering Length Density Calculator) and implies a surface coverage of 99.5%. The ethylene glycol part of the molecule allowed only for a hydration of about 5%. The completion of the mono- to a bilayer led to a dense distal layer with an sld of $0.54 \cdot 10^{-6} \text{ \AA}^{-2}$ and a low hydration of 3.5%. The inner layer was even less hydrated (1%).

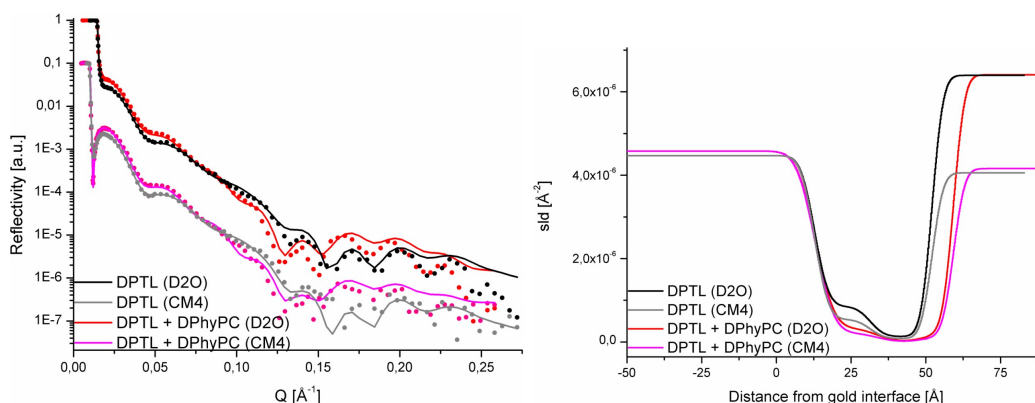


Figure 5.1: Fitted neutron reflectivity profiles (left) of DPTL (D₂O+CM4) and DPTL + DPhyPC and corresponding scattering length density profiles (right).

Monolayer and bilayer data were measured on two different samples.

5.2 Anchor modifications

As mentioned previously, the space beneath an artificial membrane is crucial for its functionality and should provide, e.g. space for sub-membrane moieties of incorporated proteins. Although it was possible to incorporate

smaller peptides into tBLMs formed with DPTL as spacer, more complex proteins such as the exotoxin α -hemolysin are difficult to incorporate into a dense bilayer [14]. Therefore, anchor molecules with different spacer groups were synthesised and investigated (fig. 5.2).

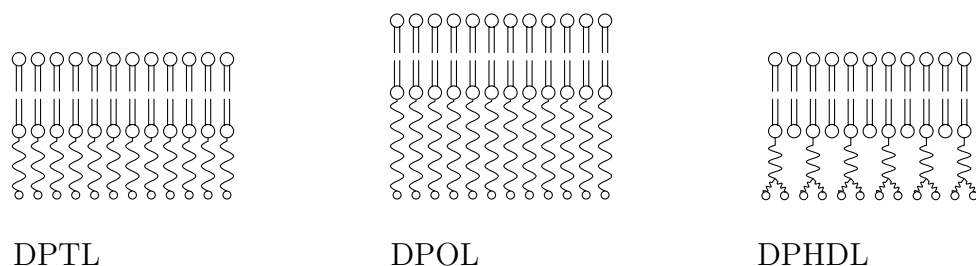


Figure 5.2: Schematics of different anchor/spacer architectures

Additionally, different anchor groups have been used allowing the assembly of the membrane on various substrates. For example, silane anchors have been utilised to form membranes on glass or oxide substrates. Using a universal synthesis procedure, a large variety of anchor lipids has been developed. [17, 133]

Here, the structures of seven different molecules have been investigated. All molecules can be anchored on gold substrates. DPTL, DPHDL and CholPEG have lipoic acid moieties, while DPTT, DPHT, DPOT and DDPTT have a short thiol anchors (Table 5.1).

The different lipids vary mainly in their spacer part, which leads to different electrochemical properties [25] (Table 5.2).

Valinomycin

Valinomycin is a small depsipeptide that transports ions across a lipid bilayer [134]. Due to its high selectivity for potassium ions over sodium ions, the peptide has been used to probe the functionality of the investigated bilayers. Only an intact bilayer should show a high electrical resistance and a decrease of this resistance in case of a successful peptide incorporation.

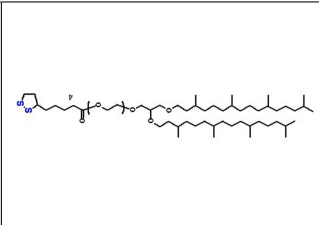
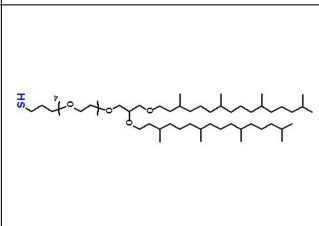
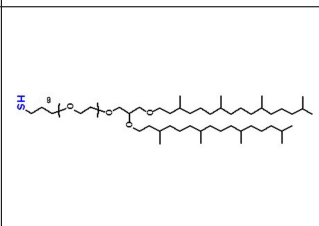
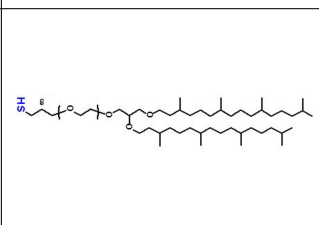
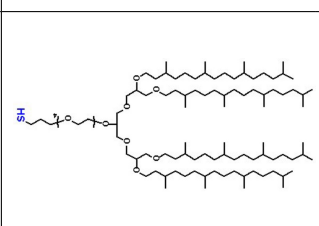
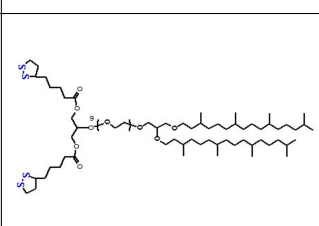
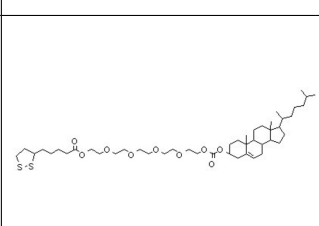
DPTL	DPTT	DPHT	DPOT	DDPTT	DPHDL	CholPEG
$C_{16}H_{29}O_5S_2$	$C_{10}H_{21}O_5S$	$C_{14}H_{29}O_7S$	$C_{18}H_{37}O_9S$	$C_{10}H_{21}O_5S$	$C_{31}H_{55}O_{10}S_4$	$C_{46}H_{78}O_9S_2$
						
$0.537 \cdot 10^{-6} \text{ \AA}^{-2}$	$0.471 \cdot 10^{-6} \text{ \AA}^{-2}$	$0.495 \cdot 10^{-6} \text{ \AA}^{-2}$	$0.510 \cdot 10^{-6} \text{ \AA}^{-2}$	$0.471 \cdot 10^{-6} \text{ \AA}^{-2}$	$0.587 \cdot 10^{-6} \text{ \AA}^{-2}$	$0.517 \cdot 10^{-6} \text{ \AA}^{-2}$
5.0 nm	4.5 nm	5.2 nm	5.9 nm	4.5 nm	5.6 nm	4.8 nm

Table 5.1: Chemical structure, scattering length density (Calculated with the Scattering Length Density Calculator, <http://www.ncnr.nist.gov/resources/sldcalc.html>) and theoretical spacer length (Determined by Chem3D Ultra 6.0) of the anchors used.
The sld of inner chains is $-0.204 \cdot 10^{-6} \text{ \AA}^{-2}$, except for DDPTT, where it is $-0.164 \cdot 10^{-6} \text{ \AA}^{-2}$.

	DPTL*	DPTT*	DPHT*	DPOT	DPHDL*	DDPTT
R [$M\Omega\text{cm}^2$] (Mono)	1 - 10	0.5 - 5	0.6 - 5	0.01	0.01 - 0.3	0.73
C [μFcm^{-2}] (Mono)	0.7 - 1.4	0.7 - 1.2	0.7 - 1.2	0.94	0.8 - 4	1.07
R [$M\Omega\text{cm}^2$] (Bi)	3 - 55	3 - 15	2 - 35	0.09	0.2 - 6.5	1.53
C [μFcm^{-2}] (Bi)	0.6 - 1.1	0.6 - 0.85	0.6 - 0.85	0.8	0.6 - 0.8	0.79

Table 5.2: Overview of EIS data for DPTL, DPTT, DPHT, DPHDL and DDPTT.

* Data taken from Thesis by Inga Vockenroth [25].

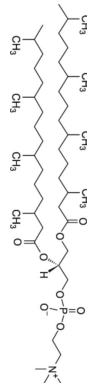
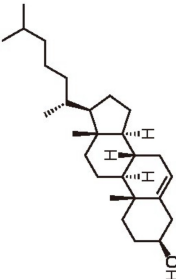
DPhyPC	Cholesterol
$\text{C}_{46}\text{H}_{90}\text{O}_{10}\text{PNa}$	$\text{C}_{27}\text{H}_{46}\text{O}$
	
$0.253 \cdot 10^{-6} \text{ \AA}^{-2}$	$0.206 \cdot 10^{-6} \text{ \AA}^{-2}$
3.0 nm	2.0 nm

Table 5.3: Chemical structure, scattering length density (Calculated with the Scattering Length Density Calculator, <http://www.ncnr.nist.gov/resources/sldcalc.html>) and theoretical spacer length (Determined by Chem3D Ultra 6.0) of DPhyPC and cholesterol. Both were used for the completion of the outer bilayer.

5.3 DPTT – DPHT – DPOT

DPTT - DPHT - DPOT (Table 5.1) is a class of anchor molecules very similar to DPTL, but equipped with a thiol instead of a lipioic acid anchor. The length of the ethylene glycol part of the molecule can be varied to control the thickness of the space beneath the lipid membrane. Electrical impedance measurement [25] showed slightly diminished bilayer sealing of DPTT/DPHT compared to DPTL. Neutron reflectivity measurements were performed to elucidate the structure of a DPTT/DPHT/DPOT based mono- and bilayer.

DPTT

NR measurements and subsequent fitting of a DPTT based mono- and bilayer (fig. 5.3) resulted in a monolayer thickness of 3 nm which was 2/3 of the theoretical value of 4.5 nm. The measured sld of the spacer ($0.8 \cdot 10^{-6} \text{ \AA}^{-2}$) differed slightly from the theoretical value ($0.47 \cdot 10^{-6} \text{ \AA}^{-2}$). The hydration of the ethylene glycol part of the molecule was simulated to be 13%.

Bilayer completion on DPTT monolayers was excellent and led to a dense distal layer with nearly the same sld for the lower ($0.1 \cdot 10^{-6} \text{ \AA}^{-2}$) and the upper ($0.11 \cdot 10^{-6} \text{ \AA}^{-2}$) lipid leaflet and hydration (1.6% and 1.8%). The roughness of the system was 9.6%.

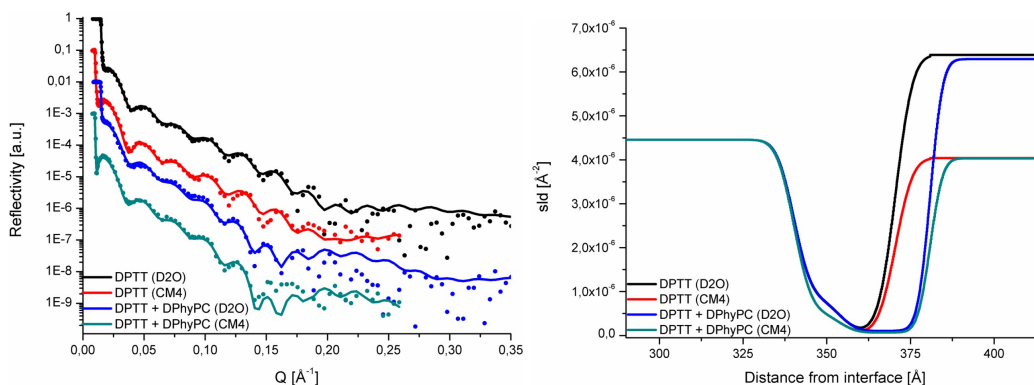


Figure 5.3: Fitted neutron reflectivity profiles (left) of DPTT (D₂O+CM4) and DPTT + DPhyPC and corresponding scattering length density profiles (right).

DPHT

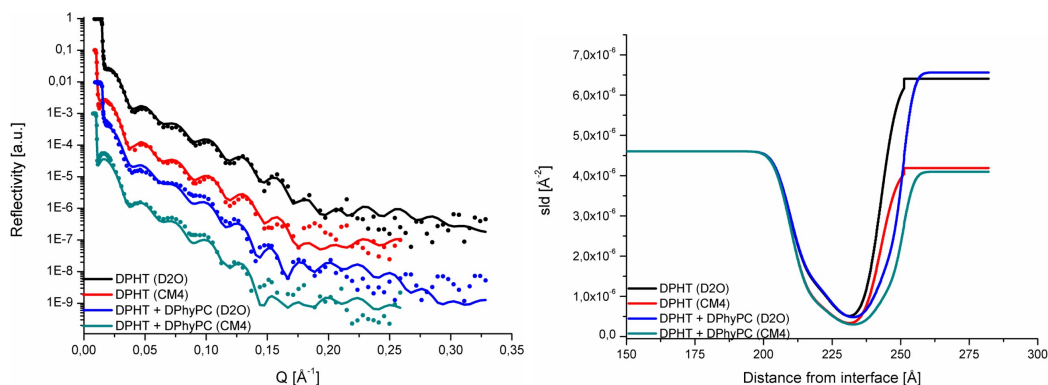


Figure 5.4: Fitted neutron reflectivity profiles (left) of DPHT (D₂O+CM4) and DPHT + DPhyPC and corresponding scattering length density profiles (right).

The structure of a DPHT based mono- and bilayer has been investigated by neutron reflectivity measurements (fig. 5.4). The thickness of the monolayer could be simulated to 3.3 nm, compared to 5.2 nm of the theoretical value. The ethylene glycol part of the molecule incorporated 21% water, the alkyl chains 6%. The roughness of the system was 11.2 Å.

The theoretical sld value for DPHT is $0.5 \cdot 10^{-6} \text{Å}^{-2}$, the experimental value was $1.4 \cdot 10^{-6} \text{Å}^{-2}$.

Bilayer formation on DPHT was not as good as on DPTT, as the sld of the outer lipid layer was $2.4 \cdot 10^{-6} \text{Å}^{-2}$ and also more hydrated than the inner one.

DPOT

Fitted NR measurements of DPOT (fig. 5.5) resulted in approximately 40% water incorporation in the ethylene glycol part of the molecule which had a length of 5.2 nm. This comes close to 5.9 nm which is the theoretical value. The surface roughness of the monolayer was 24 Å, which was in contrast to the values for DPTT (10 Å) and DPHT (11 Å) and indicated a corrugated monolayer.

Bilayer formation was rather poor on DPOT layer, as the measured sld

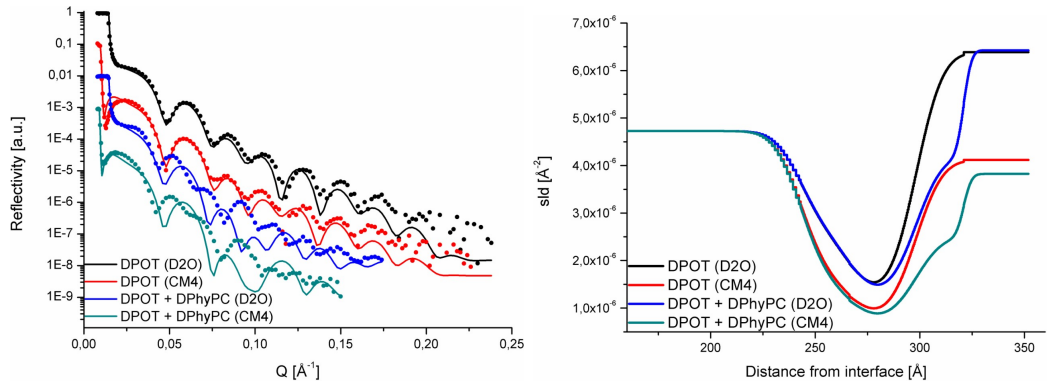


Figure 5.5: Fitted neutron reflectivity profiles (left) of DPOT (D₂O+CM4) and DPOT + DPhyPC and corresponding scattering length density profiles (right).

($4.2 \cdot 10^{-6} \text{ \AA}^{-2}$) of the outer bilayer was very high and did not exhibit the values expected for a dense lipid layer ($0 - 1 \cdot 10^{-6} \text{ \AA}^{-2}$).

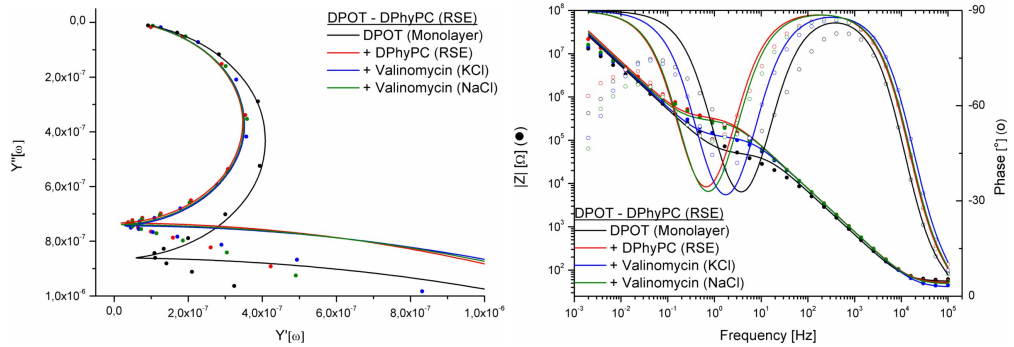


Figure 5.6: Electrical impedance measurements of DPOT + DPhyPC + Valinomycin in KCl and NaCl. Only small influences were observable after peptide addition. C increased by 1.3%, R decreased by 67% in KCl.

	Monolayer	Bilayer	Valinomycin (KCl)	Valinomycin (NaCl)
R [$\text{M}\Omega\text{cm}^2$]	0.01	0.09	0.03	0.08
C [μFcm^{-2}]	0.94	0.8	0.81	0.8

Table 5.4: Fitted EIS data values for DPOT

This was also reflected in EIS measurements (Table 5.4). Although the capacitance of the monolayer ($0.94 \mu\text{Fcm}^{-2}$) and bilayer ($0.8 \mu\text{Fcm}^{-2}$) was in

the range of DPHT ($0.7 - 1.2 \mu\text{Fcm}^{-2}$ /monolayer, $0.6 - 0.85 \mu\text{Fcm}^{-2}$ /bilayer [25]), the resistance of the DPOT monolayer ($0.01 \text{ M}\Omega\text{cm}^2$) and bilayer ($0.09 \text{ M}\Omega\text{cm}^2$) did not reach the $\text{M}\Omega$ range as DPHT bilayers did.

The capacitance values suggest that an upright monolayer was formed but the resistance values indicate that this layer was not sealing, neither as monolayer nor as bilayer.

EIS data for Valinomycin showed a decrease in resistance ($0.09 \text{ M}\Omega\text{cm}^2$ [NaCl] to $0.03 \text{ M}\Omega\text{cm}^2$ [KCl]) of the membrane in the presence of KCl and recovery ($0.08 \text{ M}\Omega\text{cm}^2$) after NaCl rinsing. This demonstrated that a bilayer had to be present, otherwise a drop in resistance after KCl flushing and recovery after NaCl rinsing would not be observable.

It is highly likely that DPOT, due to its long spacer part, experienced problems during the self-assembly process, leading to an inhomogeneous monolayer. EIS and NR indicated that a bilayer can be formed on top DPOT, but as the monolayer was probably not as ordered as DPTT or DPHT, and therefore rougher, the bilayer could not compensate all defects.

Comparison DPTT – DPHT – DPOT

	DPTT	DPHT	DPOT
Spacer length [\AA]	30.3	33.1	55.2
Spacer sld [$\cdot 10^{-6} \text{\AA}^{-2}$]	0.8	1.4	2.6
Water incorporation (Spacer)	13%	21%	40%
Water incorporation (Alkyl chains)	1.6%	6.4%	19.9%
Surface roughness [\AA]	9.6	11.2	23.7

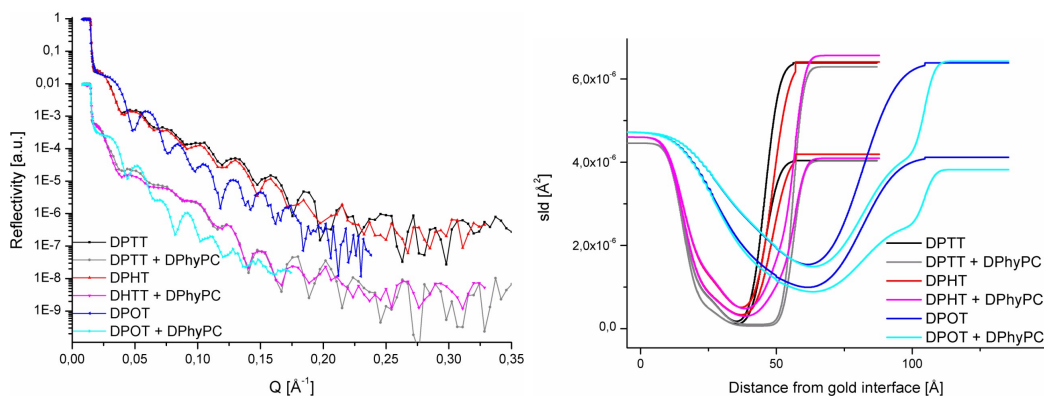


Figure 5.7: Neutron reflectivity profiles (left) of DPTT, DPHT, DPOT, DPTT + DPhyPC, DPHT + DPhyPC and DPOT + DPhyPC and corresponding scattering length density profiles (right).

Cr and Au were evaporated on DPTT and DPHT during one procedure, resulting in similar chromium and gold layers. DPTT and DPHT were measured on AndR, DPOT on NG7.

The thiol tethered anchors, DPTT - DPHT - DPOT (fig. 5.7), showed thinner monolayer thicknesses in the experiment than theoretically determined. For DPTT and DPHT, the experimental values were $\approx 2/3$ of the theory value, DPOT was around 90%. An upright configuration of the molecules provided, all three spacers were not completely stretched, as has also been observed for DPTL. Most probably the spacers adopted a rather helical structure.

If DPOT was actually more elongated than DPTT/DPHT in the tBLM architecture or if this was a residue of the poorer fit quality, compared to DPTT

and DPHT, cannot be decided by NR alone. But as EIS measurements gave similar capacitance values for DPOT as for DPHT, a layer that was by a factor 1.7 thicker is highly unlikely as this should be reflected in the capacitance which is reciprocally proportional to the systems thickness.

The measured sld of the spacer of DPTT/DPHT/DPOT differed more from the theoretical value than it did for DPTL. This indicated that the surface coverage of the monolayer was not as high as for DPTL, or that the layer was not as densely packed. EIS measurements [25] that showed much higher resistance values (1-10 $M\Omega\text{cm}^2$) for DPTL monolayers than for DPTT/DPHT (0.5-5 $M\Omega\text{cm}^2$) support these observations. Additionally, the hydration of the ethylene glycol part of the molecule was 13% for DPTT, compared to 5% for DPTL, although DPTT is slightly smaller and for the same chain packing, similar water incorporation could be expected.

The hydration of the spacer increased with increased spacer length. An increment in spacer length by factor 1.5 increased the water incorporation by nearly factor 1.5 as well.

The alkyl chains reflect the same trend, increasing the spacer length increased the hydration. This was probably due to less dense packing of the layers due to problems during self-assembly. This is supported by the surface roughness of the system, which increased with spacer length as well. During self-assembly, molecules first adsorb very quickly and unordered to the surface, followed by a much slower re-organisation [135]. Possibly, the longer chains of DPHT and DPOT hinder this second step and prevent absolute coverage and homogeneous monolayers.

The higher surface roughness also influenced the bilayer formation. On DPTT, a perfect bilayer in terms of sld and hydration was formed, whereas on DPHT and DPOT the second layer sld shifted to values close to the bulk solvent and became more “watery”. EIS measurements support this, as the resistance of DPOT bilayers did not increase as much as for DPTT/DPHT. But still a bilayer has to present, as valinomycin was able to incorporate in all three architectures, although the resistance decrease after KCl rinsing was diminished in DPOT systems.

5.4 DPHDL

DPHDL (Table 5.1) was synthesised [133] as a so called “self -diluting” molecule. The lipid has a bulky anchor that should result in less dense packing of the inner alkyl chains. During vesicle fusion or RSE, the free spaces in the inner bilayer should be filled by mobile lipids. Such an architecture should be much more fluid and enable the incorporation of peptides/proteins with big sub-membrane moieties. In fact, this has already been shown by Vockenroth et al. [14].

Neutron reflectivity measurements shall elucidate how well this “filling” of the inner bilayer works. In addition, to enhanced protein incorporation, DPHDL based bilayer should also have a bigger water reservoir underneath the membrane. How big the hydration of the spacer part is will also be addressed.

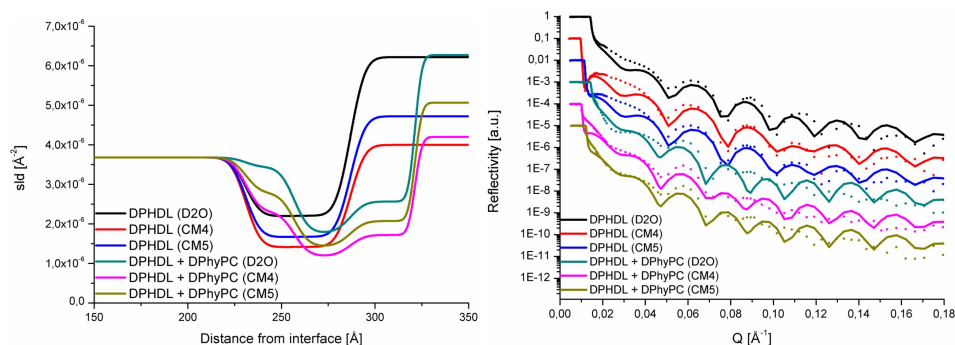


Figure 5.8: Fitted neutron reflectivity profiles (left) of DPHDL (D₂O, CM5 + CM4) and DPHDL + DPhyPC and corresponding scattering length density profiles (right).

The structure of a DPHDL based mono- and bilayer has been investigated by neutron reflectivity measurements (fig. 5.8). The analysis of the data resulted in a monolayer thickness of 5.6 nm, which was the theoretical predicted value. The sld of the spacer part of the molecule was with $2.2 \cdot 10^{-6} \text{\AA}^{-2}$ significantly higher than the theoretical predicted value of $0.59 \cdot 10^{-6} \text{\AA}^{-2}$. The same sld was observed for the alkyl chains of the molecule. Also, during monolayer experiments, the hydration of the monolayer was 35% for both anchor and alkyl chain part.

After the completion of the bilayer by RSE, the sld as well as the hydration went up for the lower spacer part ($3.4 \cdot 10^{-6} \text{Å}^{-2}$, 65%). In the inner bilayer chains, the hydration decreased to 28% and the sld went down ($1.8 \cdot 10^{-6} \text{Å}^{-2}$). The sld of the outer bilayer chains was with $2.6 \cdot 10^{-6} \text{Å}^{-2}$ slightly higher.

The sld of the inner lipids went down after bilayer completion indicating intercalating of the mobile lipids with the inner alkyl chains. Also the formation of a bilayer can be clearly seen, although the slds after bilayer completion were higher than theoretically expected. Additionally, the sld of the spacer part of the molecules went up after RSE, as well as the hydration, presumable due to solvent trapping.

5.5 DDPTT

To assemble tBLMs with even higher sealing abilities than DPTL/DPTT, DDPTT (Table 5.1) was synthesised [133]. This molecule has two diphytanoyl chains in the inner bilayer compared to one for all the other anchor lipids. This extended hydrophobic part should enable denser bilayers. However, EIS measurements [133] showed a diminished sealing in DDPTT based bilayers. NR was executed to investigate the structural composition of a DDPTT layer and elucidate where potential improvements are.

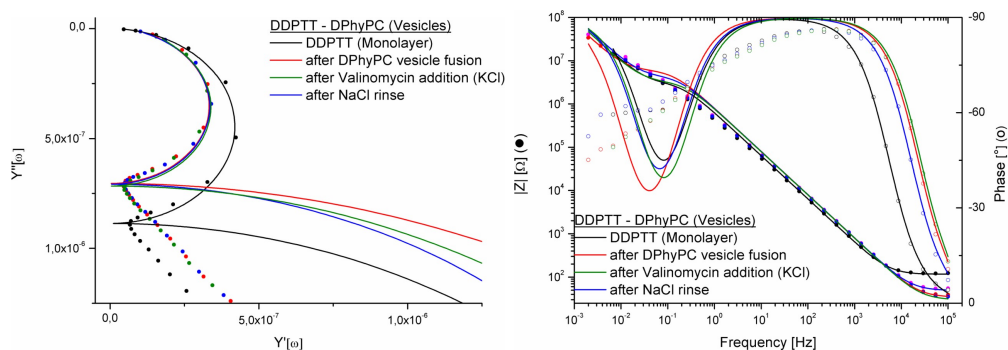


Figure 5.9: Electrical impedance measurements of DDPTT + DPhyPC + Valinomycin in KCl and NaCl. Only small influences were observable after peptide addition. C increased by 1.3%, R decreased by 31.4% in KCl.

	Monolayer	Bilayer	Valinomycin (KCl)	Valinomycin (NaCl)
R [$M\Omega\text{cm}^{-2}$]	0.73	1.53	1.05	1.09
C [μFcm^{-2}]	1.07	0.78	0.79	0.78

Table 5.6: Fitted EIS data values for DDPTT

EIS measurements (fig. 5.9) of DDPTT monolayers were comparable to DPTT [25]. DPTT monolayers showed resistances between 0.5 - 5 $M\Omega\text{cm}^{-2}$ and capacitances between 0.7 - 1.2 μFcm^{-2} . The resistance of a DDPTT monolayer was measured to be 0.73 $M\Omega\text{cm}^{-2}$ and the capacitance 1.07 μFcm^{-2} . Also the bilayer capacitance was similar (0.6 - 0.85 μFcm^{-2} [DPTT], 0.7 μFcm^{-2} [DDPTT]), but the bilayer resistance was lower (3 - 15 $M\Omega\text{cm}^{-2}$ [DPTT], 1.05 $M\Omega\text{cm}^{-2}$ [DDPTT]). Additionally, valinomycin incorporation in DPTT

based architectures led to a decrease in resistance in KCl by factor 15, in DDPTT only factor 1.5 was observed. The recovery of the bilayers after NaCl rinse was similar, 73% (DPTT) and 71% (DDPTT) of the original value.

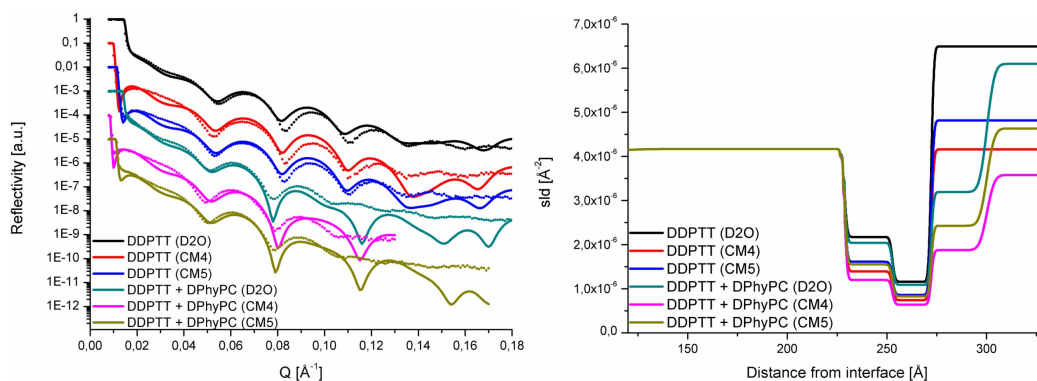


Figure 5.10: Fitted neutron reflectivity profiles (left) of DDPTT (D₂O, CM5 + CM4) and DDPTT + DPhyPC and corresponding scattering length density profiles (right).

NR measurements (fig. 5.10) and subsequent fitting of DDPTT based mono- and bilayers resulted in a monolayer thickness of 4.35 nm, nearly the theoretical predicted value of 4.5 nm. The sld of the ethylene glycol was $2 \cdot 10^{-6} \text{Å}^{-2}$, which was considerably higher than the theoretical expected value of $0.47 \cdot 10^{-6} \text{Å}^{-2}$. Also the alkyl sld was with $1.1 \cdot 10^{-6} \text{Å}^{-2}$ much higher than the theoretical value of $-0.16 \cdot 10^{-6} \text{Å}^{-2}$. These variations suggest either an insufficient monolayer or a misguided fit. As EIS measurements showed a monolayer with similar values than for DPTT, and considering the NR profiles, the latter case might be more reasonable. The structure of DDPTT might be too inhomogeneous to be successfully described by a layer model. The hydration of the spacer part was with 17.5% between DPTT (13%) and DPHT (21%). Bilayer formation was not as good as on DPTT, as has also been shown by EIS, but still a denser layer could be built, compared to DPOT.

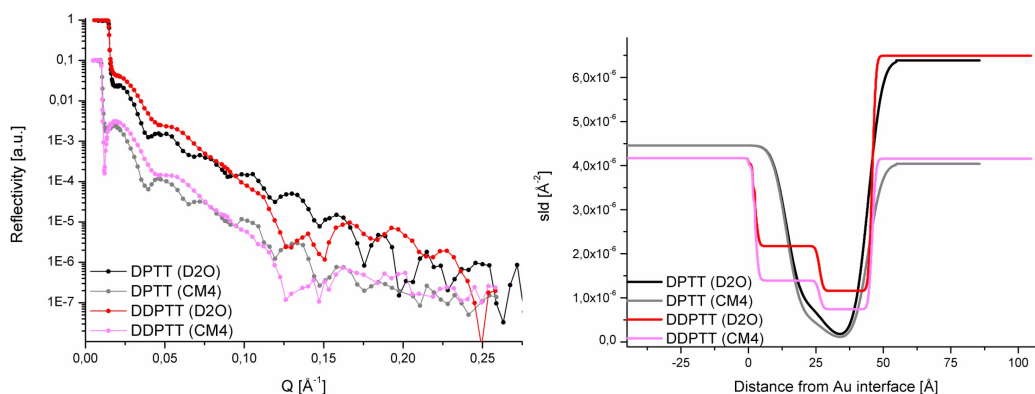


Figure 5.11: Neutron reflectivity profiles (left) of DPTT, DDPTT, DPTT + DPhyPC and DDPTT + DPhyPC and corresponding scattering length density profiles (right).

Cr and Au were evaporated on DPTT and DDPTT substrates during independent procedures, resulting in different chromium and gold layers. DPTT was measured on AndR, DDPTT on NG-7.

5.5.1 Comparison: DPTT vs. DDPTT

DDPTT exhibited a much more pronounced spacer and inner alkyl part than DPTT (fig. 5.11). The spacer part was much more hydrated and while DPTT showed hardly any hydration (1%) of the inner alkyl chains, DDPTT demonstrated 11%. Differences in sld between the spacer and the alkyl part were not as pronounced for DPTT than they were for DDPTT. This is probably due the higher amount of diphytanoyl chains per anchor and therefore a much higher alkyl chain packing density in DDPTT.

5.6 CholPEG

In addition to the ion and water reservoir beneath the bilayer, membrane fluidity is a vital factor for membrane functionality. To enhance membrane mobility, a cholesterol-pentaethyleneglycol spacer (CholPEG, Table 5.1) was synthesised [19] and mixed with DPTL molecules. We therefore combine the sealing abilities of our anchor molecules with the possible increase in fluidity by adding a cholesterol linker.

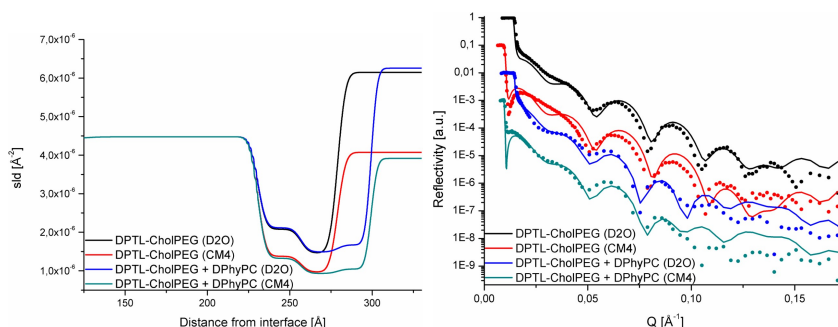


Figure 5.12: Fitted neutron reflectivity profiles (left) of DPTL-CholPEG (D₂O + CM4) and DPTL-CholPEG + DPhyPC and corresponding scattering length density profiles (right).

NR measurements (fig. 5.12) of DPTL monolayer with 10% CholPEG added to the self-assembly solution were executed and fitted. The analysis of data resulted in a monolayer thickness of 4.8 nm. This was the theoretically approximated length for the CholPEG. The sld of the spacer part was $2.1 \cdot 10^{-6} \text{ \AA}^{-2}$, which was considerable higher than the expected value for DPTL ($0.54 \cdot 10^{-6} \text{ \AA}^{-2}$) which has the same anchor as CholPEG. The inner alkyl chain sld was with $1.46 \cdot 10^{-6} \text{ \AA}^{-2}$ closer to the expected value of $0.52 \cdot 10^{-6} \text{ \AA}^{-2}$, but still higher. Completion of the bilayer by DPhyPC RSE was successful, the sld of the outer chain layer being only slightly higher ($1.67 \cdot 10^{-6} \text{ \AA}^{-2}$) than the inner layer. Hydration of the system was very high, with 33% water incorporation in spacer part of the molecule and 25% in the bilayer.

EIS measurements (fig. 5.13) of DPTL-CHolPEG were different from e.g. DPTL as they exhibited a pronounced swelling behaviour. The capacitance

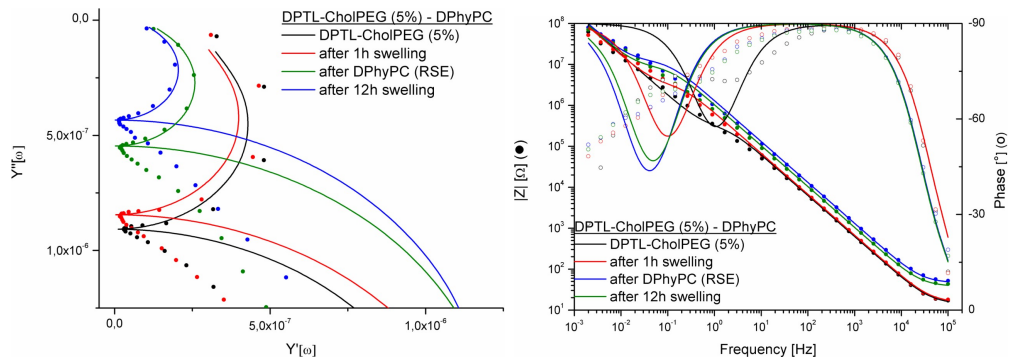


Figure 5.13: Electrical impedance measurements of DPTL-CholPEG (5%) + DPhyPC . An effect of monolayer swelling can clearly be seen as the resistance increased by factor of 10, and the capacitance decreased by 11% over 1 h. Also after RSE re-organisation took place in the bilayer, as the resistance decreased gradually by 30% over 12 h, and the capacitance increased by 21%.

	Monolayer (0 h)	Monolayer (1 h)	Bilayer (1.5 h)	Bilayer (12 h)
R [$M\Omega\text{cm}^{-2}$]	0.06	0.7	2.95	2.06
C [μFcm^{-2}]	1.27	1.12	0.51	0.66

Table 5.7: Fitted EIS data values for DPTL-CholPEG (5%)

decreased in 1 h in NaCl by 11%, the resistance increased by factor of 10. Even after RSE, the bilayer displayed re-organisation, as the resistance decreased gradually by 30% over 12 h, and the capacitance increased by 21%.

5.6.1 Comparison: DPTL vs. DPTL-CholPEG

DPTL monolayers with 10% CholPEG resulted in thicker layers than pure DPTL (4.8 nm compared to 3.9 nm), but higher slds even though similar values were theoretically expected.

Also the hydration of the monolayer was much higher if CholPEG molecules were introduced.

Additionally, EIS measurements for DPTL monolayers with 5% CholPEG showed more re-organisation in monolayers as well as bilayers.

These observations can be explained by a diminished packing density of

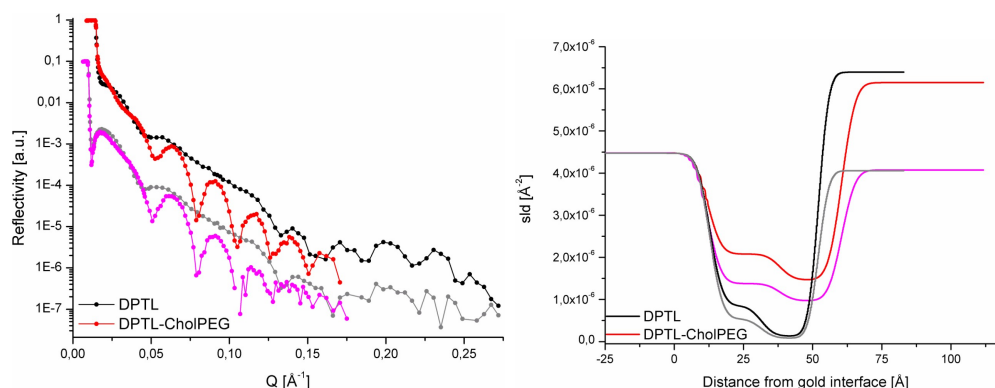


Figure 5.14: Neutron reflectivity profiles (left) of DPTL, DPTL-CholPEG, DPTL + DPhyPC and DPTL-CholPEG + DPhyPC and corresponding scattering length density profiles (right).

Cr and Au were evaporated on DPTL and DPTL-CholPEG substrates during independent procedures, resulting in different chromium and gold layers. DPTL was measured on NG-1, DPTL-CholPEG on AndR.

the DPTL molecules due to CholPEG incorporation. As CholPEG takes up space of the DPTL molecules, and is not a ‘free space’ like for DPHDL, bilayer formation does not create a much more sealing bilayer. All this shows that monolayers with cholesterol in the spacer part incorporate more water, showed more mobility and exhibited only slightly less electrical sealing.

5.7 Cholesterol

Another approach to increase the membrane fluidity was the addition of cholesterol (Table 5.3) to the RSE solution. The idea is that cholesterol dilutes the upper bilayer of the membrane which makes it easier for proteins with big sub-membrane moieties to be incorporated. Also such lipid-cholesterol bilayers would be closer to a biological membrane and might trigger events of cholesterol affine membrane proteins [136].

NR measurements (fig. 5.15) of a DPTL monolayer where instead of pure DPhyPC, DPhyPC + 10% Cholesterol was used for bilayer formation showed an increased hydration of the inner and outer alkyl chains as well as of the spacer part. Whereas DPTL + DPhyPC exhibited 1% (inner leaflet) and

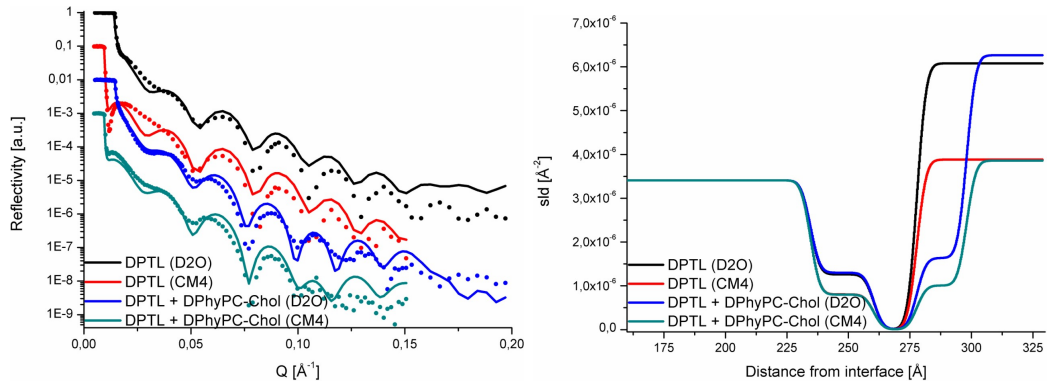


Figure 5.15: Fitted neutron reflectivity profiles (left) of DPTL (D₂O+CM4) and DPTL + DPhyPC-Cholesterol and corresponding scattering length density profiles (right).

3.5% (outer leaflet) hydration, DPTL + DPhyPC-Cholesterol showed 21% for both. Also the hydration of the spacer increased from 5% (DPhyPC) to 15% (DPhyPC-Cholesterol).

Hence, cholesterol in the outer lipid chains clearly had a positive effect on the hydration of the whole bilayer. Possibly the less dense inner and outer layers allowed for diffusion between the bilayer and the spacer part. Therefore, the spacer hydration was more similar to a monolayer (compare to Sec. 4.3.2, fig. 4.12, hydration of the monolayer = 11.6%) than in a bilayer with a sealing outer layer.

EIS measurements of DPTL monolayers with DPhyPC-Chol (Sec. 4.3.4, fig. 4.21 + fig. 4.22) showed, depending on the amount of cholesterol in the outer layer, lower resistances (middle kΩ to lower MΩ). This, together with the higher bilayer sld of $1.6 \cdot 10^{-6} \text{ \AA}^{-2}$ compared to the theoretical value of DPhyPC-Chol between $0.2\text{-}0.25 \cdot 10^{-6} \text{ \AA}^{-2}$ indicates a more watery bilayer.

5.8 Summary

A variety of anchor lipids has been investigated by neutron reflectivity as well as electrical impedance spectroscopy.

DPTL, which has a lipoic acid anchor, showed the best surface coverage and sealing properties, but the hydration of the spacer part was only of about 5%. This can be probably attributed to the width of anchor and the attached alkyl chains, which are very similar and hence enabled very dense layers.

The group of thiol anchor lipids, DPTT-DPHT-DPOT, showed an increased water incorporation but did not exhibit the same excellent surface coverage as DPTL. Furthermore, it could be demonstrated that elongating the ethylene glycol part of molecule decreases the stability of the monolayers which directly influences the stability of the bilayers, both in terms of electrical sealing as well as lipid packing density.

Probably the longer ethylene glycol chains hinder each other during self-assembly, preventing the formation of a homogeneous, dense bilayer.

This effect could also be observed for the double diphytanoyl chained lipid DDPTT. Synthesised with especially high sealing bilayers in mind, it hardly reached the $M\Omega$ range in resistance. DPTL and DPTT meet the demand of a bilayer system with $M\Omega$ resistance much better and should be preferred.

If a large ion and water reservoir is necessary, DPHDL is recommended even though it suffers from slightly lower resistances. It could be shown that the spaces in the less densely packed alkyl chain layer could be filled with mobile lipids after the bilayer formation. The large hydration of over 50% should enhance protein incorporation even if they feature bigger moieties.

Another possibility of more biocompatibility is the addition of cholesterol, either to the monolayers or to the bilayers. Enlarged hydration could be achieved for both methods with only slight drawbacks in electrical sealing and membrane stability.

Eventually one has to state that, so far, excellence in one membrane feature can only be gained by disadvantages in other parts of the architecture. One promising way seems to be the formation of mixed bilayers on DPTL base, either with an additional compound in the mono- or bilayers. The

key to a successful fabrication of such multi-component systems will be the assembly as constrictions between the different molecules has to be avoided. Especially here, the substrate will be of great importance, as even small defects influence the self-assembly process. Investigations should therefore not only concentrate on synthesising the ‘perfect’ anchor lipid, but also creating the ‘most defect-free’ surface possible.

Appendix

6.1 Abbreviations

AC	Alternating current
β -lg	β -lactoglobulin
C	Capacitance
CA	Contact angle
CholPEG	Cholesterol-polyethylene glycol-lipoic ester
DC	Direct current
DDPTT	1,3-di-(2',3'-di-O-phytanyl-glycerol)-glycerol-2-tetraethylene glycol-3''-mercaptopropyl ether lipid
DPHDL	2-(2',3'-di-O-phytanyl-glycerol-1'-hexaethylene glycol)-glycerol-1,3-di-O-D,L-lipoic acid ester lipid
DPHT	2,3-di-O-phytanyl-glycerol-1-hexaethylene glycol-3'-mercaptopropyl ether lipid
DPTL	2,3-di-O-phytanyl-sn-glycerol-1-tetraethylene glycol-D,L-lipoic acid ester lipid
DPTT	2,3-di-O-phytanyl-glycerol-1-tetraethylene glycol-3'-mercaptopropyl ether lipid
DPOT	2,3-di-O-phytanyl-glycerol-1-octaethylene glycol-3'-mercaptopropyl ether lipid
DPhyPC	Diphytanyl phosphatidylcholine
DPhyPG	Diphytanyl phosphatidylglycerol
DSC	Differential scanning calorimetry
EIS	Electrical impedance spectroscopy
FRAP	Fluorescence recovery after photo bleaching
LB	Langmuir - Blodgett
LM	Langmuir monolayer
MFGM	Milk fat globule membrane

MilliQ	ultra-pure water filtered with a Millipore (Billerica, MA/USA) device
NR	Neutron reflectivity
SA	Self-assembly
SAM	Self assembled monolayer
sBLM	supported Bilayer Lipid Membrane
sld	scattering length density
SP	Surface plasmon
SPR	Surface plasmon resonance
tBLM	tethered bilayer lipid membrane
QCM	Quartz crystal microbalance
R	Resistance
RSE	Rapid solvent exchange
tsg	template stripped gold
v_C	compression speed

6.2 Chemicals

Name	Formula	Manufacturer	Purity
Trichloroacetic acid	CCl_3COOH	Serva, Heidelberg/Germany	–
Ethanol	$\text{C}_2\text{H}_5\text{OH}$	Sigma-Aldrich, Munich/Germany	absolute
Triolein	$\text{C}_{57}\text{H}_{104}\text{O}_6$	Sigma-Aldrich, Munich/Germany	practical grade, $\approx 65\%$
Deuterated water	D_2O	Aldrich, Munich/Germany	$\geq 99\%$
DPhyPC	$\text{C}_{46}\text{H}_{90}\text{O}_{10}\text{PNa}$	Avanti Polar Lipids, Alabaster, AL/USA	
Sodium chloride	NaCl	Sigma-Aldrich, Munich/Germany	$\geq 99.5\%$
Sodium phosphate (dibasic)	Na_2HPO_4	Fluka, Munich/Germany	$\geq 99\%$
Sodium phosphate (monobasic)	NaH_2PO_4	Fluka, Munich/Germany	$\geq 99\%$
Sodium azide	NaN_3	Acros, Geel/Belgium	

6.3 DSC

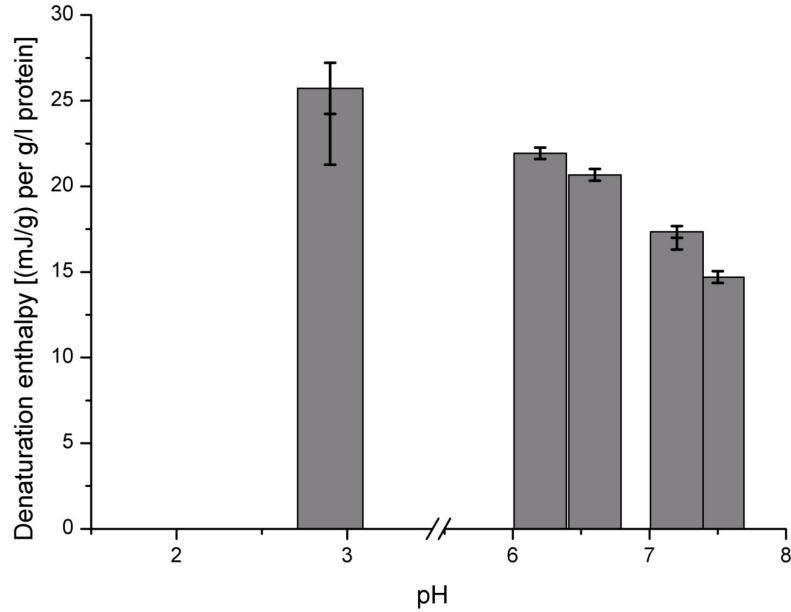


Figure 6.16: DSC at various pH.
Data courtesy of Camille Loupiac, Ensbanda/Dijon.

6.4 EIS values

	R	C
DPTL + Triolein + native β lg (pH7)	- (57.5±7.9)%	+ (10.9±6.1)%
DPTL + DPhyPC (RSE) + native β lg	+ 10.1%	0
DPTL + DPhyPC (Vesicles) + native β lg	- 4.7%	0
DPTL + Triolein-Chol-10% + native β lg	- (11.3±13.6)%	+ (6.7±3.8)%
DPTL + DPhyPC-Chol-10% + native β lg	+ (30.3±1.5)%	- (3.5 ±3.5)%
DPTL + DPhyPC-Chol-50% + native β lg	+ (45±25.8)%	+ (3.3±2.2)%
DPTL + Triolein + native β lg (pH3)	- (86.2±7.7)%	+ (10.8±4.4)%
DPTL + Triolein + denat β lg	- 14.1%	- 7.7%
DPTL + DPhyPC (Vesicles) + denat β lg	+ 11.8%	- 9.6%

Table 6.10: Overview of EIS data

6.5 GaRefl setup.c protocols

Example of DPTT + DPhyPC

Protocol taken from the GaRefl manual [74] and modified.

```
#include <stdio.h>
#include <assert.h>
#include "refl.h"
#include "reflcalc.h"
#define MODELS 4
/* initialising non-standard fitting variables */
double global_rough, rough_au_cr, rho_DPTT_spacer, rho_alkyl, rho_bi,
vf_spacer , vf_alkyl, vf_bi;
/*===== CONSTRAINTS =====*/
void constr_models(fitinfo *fit)
{
int i,k;
fitpars *pars = &fit[0].pars;

for (i=0; i<pars_count(pars); i++)
{
if (pars_peek(pars,i)==pars_max(pars,i))
{pars_poke(pars,i,pars_min(pars,i)+0.99*(pars_max(pars,i)-
pars_min(pars,i)));}
if (pars_peek(pars,i)==pars_min(pars,i))
{pars_poke(pars,i,pars_min(pars,i)+0.01*(pars_max(pars,i)-
pars_min(pars,i)));}
}
/* Rescue the free parameters from the model. */
for (i=0; i < fit[1].pars.n; i++)
fit[1].pars.value[i] = *(fit[1].pars.address[i]);
/* Go through all layers copying parameters from model 0 to other models
*/
tied_parameters(fit);
```

```

/* copy the global roughness to all interfaces not SIOX interfaces*/
for (i=0; i < MODELS; i++) {
for (k=1;k <it[i].m.n-1; k++) fit[i].m.rough[k]=global_rough;
fit[i].m.rough[3]=rough_au_cr;
}
/* Restore the free parameters to the model. */
for (i=0; i <fit[1].pars.n; i++){
(fit[1].pars.address[i]) = fit[1].pars.value[i];
}
for (i=0; i <2; i++) {
fit[i].m.rho[4]=vf_spacer*rho_DPTT_spacer+(1-
vf_spacer)*fit[i].m.rho[fit[i].m.n-1];
fit[i].m.rho[5]=vf_alkyl*rho_alkyl+(1-vf_alkyl)*fit[i].m.rho[fit[i].m.n-1];
fit[i].m.rho[6]= fit[i].m.rho[fit[i].m.n-1];
}
for (i=2; i <MODELS; i++) { fit[i].m.rho[4]=vf_spacer*rho_DPTT_spacer+(1-
vf_spacer)*fit[i].m.rho[fit[i].m.n-1];
fit[i].m.rho[5]=vf_alkyl*rho_alkyl+(1-vf_alkyl)*fit[i].m.rho[fit[i].m.n-1];
fit[i].m.rho[6]=vf_bi*rho_bi+(1-vf_bi)*fit[i].m.rho[fit[i].m.n-1];
}
}
/*===== INITIAL SETUP=====*/
fitinfo* setup_models(int *models)
{
static fitinfo fit[MODELS];
int i;
fitpars *pars = &fit[0].pars;
fitpars *freepars = &fit[1].pars;
models = MODELS;

for (i=0; i < MODELS; i++) fit_init(&fit[i]);

/* Load the data for each model */

```

```

fit_data(&fit[0], "723.ref");
fit_data(&fit[1], "724.ref");
fit_data(&fit[2], "725.ref");
fit_data(&fit[3], "726.ref");

/* Initialize instrument parameters for each model.*/
for (i=0; i < MODELS; i++) {
#include "reflcalc.h"
const double L = 5.0042,dLoL=0.020,d=1890.0;
double Qlo,Tlo, dTlo,dToT,s1,s2;
Qlo=0.0154,Tlo=0.35;
s1=0.175, s2=s1;
dTlo=resolution_dT(s1,s2,d);
dToT=resolution_dToT(s1,s2,d,Tlo);
data_resolution_fv(&fit[i].dataA,L,dLoL,Qlo,dTlo,dToT);
fit[i].beam.lambda = L;
interface_create(&fit[i].rm, "erf", erf_interface, 100);
}
/*===== MODEL =====*/
/* Add layers: d (thickness, Å), rho (Nb, Å-2), mu (absorption, Å), rough
(interlayer roughness, Å) */
for (i=0; i < MODELS; i++) {
model_layer(&fit[i].m, 0.00000, 2.07e-6, 0.0e-8, 7.000); /* 0 substrate */
model_layer(&fit[i].m, 39, 3.72e-6, 0.0e-8, 7.000);/* 1 oxide */
model_layer(&fit[i].m, 22.5, 4.29e-6, 0.0e-8, 16.000); /* 2 Cr */
model_layer(&fit[i].m, 138.000, 4.56e-6, 0.0e-8, 9.000); /* 3 Au */
model_layer(&fit[i].m, 16.0, 0.5e-6, 0.0e-8, 7.000); /* 4 DPTT spacer */
model_layer(&fit[i].m, 20.0, -0.1e-6, 0.0e-8, 7.000); /* 5 DPTT alkyl */
model_layer(&fit[i].m, 15.0000, 0-6, 0.0e-8, 7.000); /*6 bi */
model_layer(&fit[i].m, 100.000, 6.35e-6, 0.0e-8, 7.000); /* 7 Solvent */
}
global_rough=7;

```

```

/*correct solvent layers for different models*/
/* fit[3].m.d[3] = ... */
/*===== FIT PARAMETERS =====*/
/* Specify which parameters are your fit parameters. Parameters are fitted
to be the same in all datasets by default */
pars_add(pars, "d_oxide", &(fit[0].m.d[1]), 5, 50);
pars_add(pars, "d_Cr", &(fit[0].m.d[2]), 15., 30);
pars_add(pars, "d_gold", &(fit[0].m.d[3]), 130., 160.);
pars_add(pars, "d_DPTT_spacer", &(fit[0].m.d[4]), 5., 24.);
pars_add(pars, "d_DPTT_alkyl", &(fit[0].m.d[5]), 15., 25.);
pars_add(pars, "d_bi", &(fit[0].m.d[6]),5., 25.);

pars_add(pars, "vf_DPTT_spacer", &(vf_spacer), 0, 1);
pars_add(pars, "vf_alkyl", &(vf_alkyl), 0, 1);
pars_add(pars, "vf_bi", &(vf_bi), 0.5, 1);

pars_add(pars, "rho_CrOx", &(fit[0].m.rho[1]), 3. 5e-6, 4.0e-6);
pars_add(pars, "rho_Cr", &(fit[0].m.rho[2]), 4.0e-6, 4.5e-6);
pars_add(pars, "rho_Au", &(fit[0].m.rho[3]), 4.4e-6, 4.8e-6);
pars_add(pars, "rho_DPTT_spacer", &(fit[0].m.rho[4]), 0.25e-6, 2.5e-6);
pars_add(pars, "rho_alkyl", &(fit[0].m.rho[5]), -0.2e-6, 0.75e-6);
pars_add(pars, "rho_bi", &(fit[0].m.rho[6]), -0.2e-6, 0.75e-6);

pars_add(pars, "rho_solv_0", &(fit[0].m.rho[fit[0].m.n-1]), 6.0e-6, 6.4e-6);
pars_add(pars, "rho_solv_1", &(fit[1].m.rho[fit[1].m.n-1]), 3.75e-6, 4.25e-6);
pars_add(pars, "rho_solv_2", &(fit[2].m.rho[fit[2].m.n-1]), 6.0e-6, 6.4e-6);
pars_add(pars, "rho_solv_3", &(fit[3].m.rho[fit[3].m.n-1]), 3.75e-6, 4.25e-6);

pars_add(pars, "global_rough", &(global_rough), 5.0, 10.0);
pars_add(pars, "rough_au_cr", &(rough_au_cr), 10.0, 30.0);

pars_add(pars, "background_0", &(fit[0].beam.background), 1e-9, 2.5e-6);
pars_add(pars, "background_1", &(fit[1].beam.background), 1e-9, 2.5e-6);

```

```

pars_add(pars, "background_2", &(fit[2].beam.background), 1e-9, 2.5e-6);
pars_add(pars, "background_3", &(fit[3].beam.background), 1e-9, 2.5e-6);

/* Build a list of 'free parameters' in fit[1].pars. These are
parameters for which the values are allowed to differ from those
in model 0. By default all values in all models are the same unless
specified here. The range data is not used here, so set it to [0,1].
*/
pars_add(freepars, "rho_solv_1", &(fit[1].m.rho[fit[1].m.n-1]), 0, 1);
pars_add(freepars, "rho_solv_2", &(fit[2].m.rho[fit[2].m.n-1]), 0, 1);
pars_add(freepars, "rho_solv_3", &(fit[3].m.rho[fit[3].m.n-1]), 0, 1);

constraints = constr_models;
return fit;
}

```


Acknowledgements

Bibliography

- [1] E. Sackmann. *Handbook of Biological Physics*, volume 1, chapter Biological Membranes Architecture and Function, pages 1–62. Elsevier Science B.V., 1995.
- [2] J.N. Israelachvilli, S. Marčelja, and R.G. Horn. Physical principles of membrane. *Quarterly Reviews of Biophysics*, 13(2):121–200, 1980.
- [3] A.H. Palmer. The preparation of a crystalline globulin from the albumin fraction of cow’s milk. *J. Biol. Chem.*, 104:359–372, 1934.
- [4] S. Patton and T.W. Keenan. The milk fat globule membrane. *Biochimica et Biophysica Acta*, 415:273–309, 1975.
- [5] P. Walstra. *Physical chemistry of milkfat globules*, volume Developments in dairy chemistry. Applied Science Publishers, 1983.
- [6] D.G. Cornell and D.L. Patterson. Interaction of phospholipids in monolayers with β -lactoglobulin. *Journal of agricultural and food chemistry*, 37:1455–1459, 1989.
- [7] J.L. Klemaszewski, K.P. Das, and J.E. Kinsella. Formation and coalescence stability of emulsions stabilized by different milk proteins. *Journal of Food Science*, 57(2):366–371, 1992.
- [8] D.M. Mulvihill and J.E. Kinsella. Gelation of β -lactoglobulin: Effects of sodium chloride and calcium chloride on the rheological and structural properties of gels. *Journal of Food Science*, 53(1):231–236, 1988.

- [9] J.P. Davis, D. Doucet, and E.A. Foegeding. Foaming and interfacial properties of hydrolyzed β -lactoglobulin. *Journal of Colloid and Interface Science*, 288(2):412–422, 2005.
- [10] L. Ragona, L. Zetta, F. Fogolari, H. Molinari, D.M. Pérez, P. Puyol, K. De Kruif, F. Löhr, and H. Rüterjans. Bovine β -lactoglobulin: Interaction studies with palmitic acid. *Protein Science*, 9(7):1347–1356, 2000.
- [11] M. Yagi, K. Sakurai, C. Kalidas, C.A. Batt, and Y. Goto. Reversible Unfolding of Bovine β -Lactoglobulin Mutants without a Free Thiol Group. *J. Biol. Chem.*, 278(47):47009–47015, 2003.
- [12] I. Köper, S.M. Schiller, F. Giess, R. Naumann, and W. Knoll. *Advances in Planar Lipid Bilayers and Liposomes*. Elsevier, 2006. Chapter 2: Functional Tethered Biomolecular Lipid Membranes (tBLMs).
- [13] I.K. Vockenroth, P.P. Atanasova, J.R. Long, A.T.A. Jenkins, W. Knoll, and I. Köper. Functional incorporation of the pore forming segment of achr m2 into tethered bilayer lipid membranes. *Biochimica et Biophysica Acta (BBA) - Biomembranes*, 1768(5):1114–1120, 2007.
- [14] I.K. Vockenroth, P.P. Atanasova, A.T.A. Jenkins, and I. Köper. Incorporation of alpha hemolysin in different tethered bilayer lipid membrane architectures. *Langmuir*, 24:496–502, 2008.
- [15] B.A. Cornell, V.L.B. Braach-Maksvytis, L.G. King, P.D.J. Osman, B. Raguse, L. Wiczorek, and R.J. Pace. A biosensor that uses ion-channel switches. *Nature*, 287:580–583, 1997.
- [16] E.T. Castellana and P.S. Cremer. Solid supported lipid bilayers: From biophysical studies to sensor design. *Surface Science Reports*, 61:429444, 2006.
- [17] V. Atanasov, P.P. Atanasova, I.K. Vockenroth, N. Knorr, and I. Köper. A molecular toolkit for highly insulating tethered bilayer lipid mem-

- branes on various substrates. *Bioconjugate Chemistry*, 17:631–637, 2006.
- [18] P.P. Atanasova, V. Atanasov, and I. Köper. Anchor-lipid monolayers at the air-water interface; prearranging. *Langmuir*, 23:7672–7678, 2007.
- [19] Synthesised by Claire Rossi. Unpublished.
- [20] M. Bloom and O.G. Mouritsen. *The Evolution of Membranes*. Handbook of Biological Physics. Elsevier Science B.V., 1995.
- [21] S.J. Singer and G.L. Nicolson. The Fluid Mosaic Model of the Structure of Cell Membranes. *Science*, 175(4023):720–731, 1972.
- [22] M. Montal and P. Mueller. Formation of Bimolecular Membranes from Lipid Monolayers and a Study of Their Electrical Properties. *Proceedings of the National Academy of Sciences of the United States of America*, 69(12):3561–3566, 1972.
- [23] N. Malmstadt, T.J. Jeon, and J.J. Schmidt. Long-lived planar lipid bilayer membranes anchored to an in situ polymerized hydrogel. *Advanced Materials*, 20(1):84–89, 2008.
- [24] O. Purruicker, H. Hillebrandt, K. Adlkofer, and M. Tanaka. Deposition of highly resistive lipid bilayer on silicon-silicon dioxide electrode and incorporation of gramicidin studied by ac impedance spectroscopy. *Electrochimica Acta*, 47(5):791 – 798, 2001.
- [25] Inga Vockenroth. *Investigations of tethered bilayer lipid membranes for their potential use in biosensing devices*. PhD thesis, University of Bath, 2007.
- [26] A.A. Brian and H.M. McConnell. Allogeneic stimulation of cytotoxic T cells by supported planar membranes. *Proceedings of the National Academy of Sciences of the United States of America*, 81(19):6159–6163, 1984.

- [27] H.M. McConnell, T.H. Watts, R.M. Weis, and A.A. Brian. Supported planar membranes in studies of cell-cell recognition in the immune system. *Biochimica et Biophysica Acta (BBA) - Reviews on Biomembranes*, 864(1):95 – 106, 1986.
- [28] T.M. Bayerl and M. Bloom. Physical properties of single phospholipid bilayers adsorbed to micro glass beads. a new vesicular model system studied by 2h-nuclear magnetic resonance. *Biophysical Journal*, 58(2):357 – 362, 1990.
- [29] C. Reich, M.B. Hochrein, B. Krause, and B. Nickel. A microfluidic setup for studies of solid-liquid interfaces using x-ray reflectivity and fluorescence microscopy. *Review of Scientific Instruments*, 76(9):095103, 2005.
- [30] T.L. Fare. Electrical characterization of dipalmitoylphosphatidylethanolamine and cadmium stearate films on platinum surfaces in aqueous solutions. *Langmuir*, 6:1172, 1990.
- [31] D.A. Stenger, T.L. Fare, D.H. Cribbs, and K.M. Rusin. Voltage modulation of a gated ion channel admittance in platinum-supported lipid bilayers. *Biosensors and Bioelectronics*, 7(1):11 – 20, 1992.
- [32] A. Gilardoni, E. Margheri, and G. Gabrielli. Potassium ion selective membranes built by the langmuir-blodgett technique. *Colloids and Surfaces*, 68(4):235 – 241, 1992.
- [33] J. Spinke, J. Yang, H. Wolf, M. Liley, H. Ringsdorf, and W. Knoll. Polymer-supported bilayer on a solid substrate. *Biophysical Journal*, 63(6):1667 – 1671, 1992.
- [34] A.L. Plant, M. Gueguetchkeri, and W. Yap. Supported phospholipid/alkanethiol biomimetic membranes: insulating properties. *Biophysical Journal*, 67(3):1126 – 1133, 1994.
- [35] C. Steinem, A. Janshoff, W.P. Ulrich, M. Sieber, and H.J. Galla. Impedance analysis of supported lipid bilayer membranes: a scrutiny of

- different preparation techniques. *Biochimica et Biophysica Acta (BBA) - Biomembranes*, 1279(2):169 – 180, 1996.
- [36] H.T. Tien and Z. Salamon. Formation of self-assembled lipid bilayers on solid substrates. *Bioelectrochemistry and Bioenergetics*, 22(3):211 – 218, 1989.
- [37] K. Seifert, K. Fendler, and E. Bamberg. Charge transport by ion translocating membrane proteins on solid supported membranes. *Biophysical Journal*, 64(2):384 – 391, 1993.
- [38] E.L. Florin and H.E. Gaub. Painted supported lipid membranes. *Biophysical Journal*, 64(2):375–383, 1993.
- [39] J.J. Ramsden. Partition coefficients of drugs in bilayer lipid membranes. *Cellular and Molecular Life Sciences*, 49(8):688 – 692, 1993.
- [40] T. Cassier, A. Sinner, A. Offenhuser, and H. Mhwald. Homogeneity, electrical resistivity and lateral diffusion of lipid bilayers coupled to polyelectrolyte multilayers. *Colloids and Surfaces B: Biointerfaces*, 15(3-4):215 – 225, 1999.
- [41] J.Y. Wong, J. Majewski, M. Seitz, C.K. Park, J.N. Israelachvili, and G.S. Smith. Polymer-cushioned bilayers. i. a structural study of various preparation methods using neutron reflectometry. *Biophysical Journal*, 77(3):1445 – 1457, 1999.
- [42] M.A. Holden, S.Y. Jung, T. Yang, E.T. Castellana, and P.S. Cremer. Creating fluid and air-stable solid supported lipid bilayers. *Journal of the American Chemical Society*, 126(21):6512–6513, 2004.
- [43] E. Kalb, S. Frey, and L.K. Tamm. Formation of supported planar bilayers by fusion of vesicles to supported phospholipid monolayers. *Biochimica et Biophysica Acta (BBA) - Biomembranes*, 1103(2):307 – 316, 1992.
- [44] A.L. Plant. Self-assembled phospholipid/alkanethiol biomimetic bilayers on gold. *Langmuir*, 9:2764, 1993.

- [45] G. Valincius, D.J. McGillivray, W. Febo-Ayala, D.J. Vanderah, J.J. Kasianowicz, and M. Lösche. Enzyme activity to augment the characterization of tethered bilayer membranes. *J. Phys. Chem. B*, 110(21):10213 – 10216, 2006.
- [46] D.J. McGillivray, G. Valincius, D.J. Vanderah, W. Febo-Ayala, J.T. Woodward, F. Heinrich, J.J. Kasianowicz, and M. Lösche. Molecular-scale structural and functional characterization of sparsely tethered bilayer lipid membranes. *Biointerphases*, 2(1):21–33, 2007.
- [47] S.J. Johnson, T.M. Bayerl, D.C. McDermott, G.W. Adam, A.R. Rennie, R.K. Thomas, and E. Sackmann. Structure of an adsorbed dimyristoylphosphatidylcholine bilayer measured with specular reflection of neutrons. *Biophysical Journal*, 59(2):289 – 294, 1991.
- [48] B.W. Koenig, S. Krueger, W.J. Orts, C.F. Majkrzak, N.F. Berk, J.V. Silverton, and K. Gawrisch. Neutron reflectivity and atomic force microscopy studies of a lipid bilayer in water adsorbed to the surface of a silicon single crystal. *Langmuir*, 12(5):1343–1350, 1996.
- [49] M. Kühner, R. Tampé, and E. Sackmann. Lipid mono- and bilayer supported on polymer films: composite polymer-lipid films on solid substrates. *Biophysical Journal*, 67(1):217 – 226, 1994.
- [50] E. Sackmann. Supported Membranes: Scientific and Practical Applications. *Science*, 271(5245):43–48, 1996.
- [51] J. Majewski, J.Y. Wong, C.K. Park, M. Seitz, J.N. Israelachvili, and G.S. Smith. Structural studies of polymer-cushioned lipid bilayers. *Biophysical Journal*, 75(5):2363 – 2367, 1998.
- [52] B. Raguse, V. Braach-Maksvytis, B.A. Cornell, L.G. King, P.D.J. Osman, R.J. Pace, and L. Wiczorek. Tethered lipid bilayer membranes: Formation and ionic reservoir characterization. *Langmuir*, 14(3):648–659, 1998.

- [53] M.L. Wagner and L.K. Tamm. Tethered polymer-supported planar lipid bilayers for reconstitution of integral membrane proteins: Silane-polyethyleneglycol-lipid as a cushion and covalent linker. *Biophysical Journal*, 79(3):1400 – 1414, 2000.
- [54] F. Giess, M.G. Friedrich, J. Heberle, R.L Naumann, and W. Knoll. The protein-tethered lipid bilayer: A novel mimic of the biological membrane. *Biophysical Journal*, 87(5):3213 – 3220, 2004.
- [55] G.C. Terstappen and A. Reggiani. In silico research in drug discovery. *Trends in Pharmacological Sciences*, 22(1):23 – 26, 2001.
- [56] V. Hlady and J. Buijs. Protein adsorption on solid surfaces. *Current Opinion in Biotechnology*, 7:72–77, 1996.
- [57] M. Malmsten. Formation of adsorbed protein layers. *Journal of Colloid and Interface Science*, 207:186199, 1998.
- [58] K. Nakanishi, T. Sakiyama, and K. Imamura. On the adsorption of proteins on solid surfaces, a common but very complicated phenomenon. *The Society for Biotechnology, Japan*, 91(3):233–244, 2001.
- [59] M. Sarikaya, C. Tamerler, A.K.Y. Jen, K. Schulten, and F. Baneyx. Molecular biomimetics: nanotechnology through biology. *Nature Materials*, 2(9):577 – 585, 2003.
- [60] J.J. Gray. The interaction of proteins with solid surfaces. *Current Opinion in Structural Biology*, 14(1):110 – 115, 2004.
- [61] P. Vadgama. Surface biocompatibility. *Annu. Rep. Prog. Chem., Sect. C: Phys. Chem.*, 101:14–52, 2005.
- [62] M. Malmsten. Protein adsorption at phospholipid surfaces. *Journal of Colloid and Interface Science*, 172(1):106 – 115, 1995.
- [63] E. Ostuni, B.A. Grzybowski, M. Mrksich, C.S. Roberts, and G.M. Whitesides. Adsorption of proteins to hydrophobic sites on mixed self-assembled monolayers. *Langmuir*, 19(5):1861–1872, 2003.

- [64] A.V. Makievski, V.B. Fainerman, M. Bree, R. Wüstneck, J. Krägel, and R. Miller. Adsorption of proteins at the liquid/air interface. *The Journal of Physical Chemistry B*, 102(2):417–425, 1998.
- [65] Y.F. Maa and C.C. Hsu. Protein denaturation by combined effect of shear and air-liquid interface. *Biotechnology and Bioengineering*, 54(6):503–512, 1997.
- [66] H. Möhwald. Phospholipid and phospholipid-protein monolayers at the air/water interface. *Annual Review of Physical Chemistry*, 41(1):441–476, 1990.
- [67] C.J. Beverung, C.J. Radke, and H.W. Blanch. Protein adsorption at the oil/water interface: characterization of adsorption kinetics by dynamic interfacial tension measurements. *Biophysical Chemistry*, 81(1):59 – 80, 1999.
- [68] A. Fillery-Travis, E.N.C. Mills, and P. Wilde. Protein-lipid interactions at interfaces. *Grasas y Aceites*, 51(1-2):50–55, 2000.
- [69] J.K. Bienlein and R. Wiesendanger. *Einführung in die Struktur der Materie*. Vieweg+Teubner, 2003.
- [70] H. Stöcker. *Taschenbuch der Physik: Formeln, Tabellen, Übersichten*. Deutsch (Harri), 2004.
- [71] W. Demtröder. *Experimentalphysik, Bd. 3. Atome, Moleküle und Festkörper*. Springer, Berlin, 2005.
- [72] C.F. Majkrzak, N.F. Berk, S. Krueger, J.A. Dura, M. Tarek, D. Tobias, V. Silin, C.W. Meuse, J. Woodward, and A.L. Plant. First-principles determination of hybrid bilayer membrane structure by phase-sensitive neutron reflectometry. *Biophysical Journal*, 79(6):3330–3340, 2000.
- [73] L.G. Parratt. Surface studies of solids by total reflection of x-rays. *Phys. Rev.*, 95(2):359–369, Jul 1954.

- [74] P.A. Kienzle, M. Doucet, D.J. McGillivray, K.V. O'Donovan, N.F. Berk, and C.F. Majkrzak. *Ga Refl.* NIST NCNR, 2000-2006. <http://www.ncnr.nist.gov/reflpak>.
- [75] J. Homola. Surface plasmon resonance sensors for detection of chemical and biological species. *Chemical Reviews*, 108(2):462–493, 2008.
- [76] E. Kretschmann. Die Bestimmung optischer Konstanten von Metallen. *Zeitschrift für Physik*, 241:313–324, 1971.
- [77] W. Knoll, F. Yu, T. Neumann, S. Schiller, and R. Naumann. Supramolecular functional interfacial architectures for biosensor. *Phys. Chem. Chem. Phys.*, 5:51695175, 2003.
- [78] AF thanks Jakub Dostalek for fruitful discussions and suggestions on this topic.
- [79] R.J. Marsh, R.A.L. Jones, and M. Sferrazza. Adsorption and displacement of a globular protein on hydrophilic and hydrophobic surfaces. *Colloids and Surfaces B: Biointerfaces*, 23(1):31–42, 2002.
- [80] J.R. Macdonald and W.R. Kenan. *Impedance Spectroscopy: Emphasizing Solid Materials and Systems*. Wiley-Interscience, 1987.
- [81] G. Wiegand. *Fundamental principles of the electric properties of supported lipid membranes investigated by advanced methods of impedance spectroscopy*. PhD thesis, TU München, 2000.
- [82] K.S. Birdi. *Lipid and biopolymer monolayers at liquid interfaces*. Plenum Press, 1989.
- [83] M.C. Petty. *Langmuir-Blodgett films – An introduction*. Cambridge University Press, 1996.
- [84] D.A. Pink. Theoretical models of monolayer, bilayers and biological membranes. in: *Biomembrane structure and function* (edited by D. Chapman), 1984.

- [85] P.R. Bergethon. *The physical basics of biochemistry*. Springer Verlag, 2000.
- [86] H. Möhwald. Phospholipid Monolayers. in: *Handbook of Biological Physics* (edited by R. Lipowsky and E. Sackmann), 1:161–211, 1984.
- [87] NIMA Technology. Langmuir–Blodgett Troughs – Operating Manual. 1998.
- [88] M. Kaganer, H. Möhwald, and P. Dutta. Structure and phase transitions in langmuir monolayers. *Rev. Mod. Phys.*, 71(3):779819, 1999.
- [89] V.G. Bordo and H.G. Rubahn. *Optics and Spectroscopy at Surfaces and Interfaces*. Wiley-VCH, 2005. (First edition).
- [90] H. Vogel. *Gerthsen Physik*. Springer Verlag, 1997. (Nineteenth edition).
- [91] S. Henon and J. Meunier. Microscope at the Brewster angle: Direct observation of first-order phase transitions in monolayers. *Review of Scientific Instruments*, 62–4:936–939, 1990.
- [92] R. Naumann, S.M. Schiller, F. Giess, B. Grohe, K.B. Hartman, I. Kärcher, I. Köper, J. Lübben, K. Vasilev, and W. Knoll. Tethered lipid bilayers on ultraflat gold surfaces. *Langmuir*, 19:5435–5443, 2003.
- [93] M.J. Hope, M.B. Bally, G. Webb, and P.R. Cullis. Production of large unilamellar vesicles by a rapid extrusion procedure. characterization of size distribution, trapped volume and ability to maintain a membrane potential. *Biochem Biophys Acta*, 812:5565, 1985.
- [94] R.Jost. Functional characteristics of dairy proteins. *Trends in Food Science & Technology*, 4:283288, 1993.
- [95] M.A. Bos and T. Nylander. Interaction between β -lactoglobulin and phospholipids at the air/water interface. *Langmuir*, 12(11):2791–2797, 1996.

- [96] A.M. Seuvre, M.A. Espinosa Diaz, and A. Voilley. Retention of aroma compounds by β -lactoglobulin in different conditions. *Food Chemistry*, 77(4):421–429, 2002.
- [97] J.W.P. Boots, V. Chupin, J.A. Killian, R.A. Demel, and B. de Kruijff. Interaction mode specific reorganization of gel phase monoglyceride bilayers by β -lactoglobulin. *Biochimica et Biophysica Acta (BBA) - Biomembranes*, 1420(1-2):241–251, 1999.
- [98] T. Lefèvre and M. Subirade. Interaction of β -lactoglobulin with phospholipid bilayers: a molecular level elucidation as revealed by infrared spectroscopy. *International Journal of Biological Macromolecules*, 28(1):59–67, 2000.
- [99] P.A.T. Martins, E. Gomes, W.L.C. Vaz, and M.J. Moreno. Binding of phospholipids to β -lactoglobulin and their transfer to lipid bilayers. *Biochimica et Biophysica Acta (BBA) - Biomembranes*, 1778(5):1308–1315, 2008.
- [100] G. Kontopidis, C. Holt, and L. Sawyer. Invited review: β -lactoglobulin: Binding properties, structure, and function. *Journal of dairy science*, 87(4):785–796, 2004.
- [101] M. Verheul, J.S. Pedersen, S.P.F.M. Roefs, and K.G. de Kruif. Association behavior of native β -lactoglobulin. *Biopolymers*, 49(1):11–20, 1999.
- [102] H.A. McKenzie and W.H. Sawyer. Effect of ph on β -lactoglobulin. *Nature*, 214:1101–1104, 1967.
- [103] J.K. Zimmerman, G.H. Barlow, and I.M. Klotz. Dissociation of β -lactoglobulin near neutral ph. *Archives of Biochemistry and Biophysics*, 138:101–109, 1970.
- [104] H.L. Monaco, G. Zanotti, P. Spadon, M. Bolognesi, L. Sawyer, and E.E. Eliopoulos. Crystal structure of the trigonal form of bovine beta-

- lactoglobulin and of its complex with retinol at 2.5 Å resolution. *Journal of Molecular Biology*, 197(4):695 – 706, 1987.
- [105] H.A. McKenzie, G.B. Ralston, and D.C. Shaw. Location of sulfhydryl and disulfide groups in bovine β -lactoglobulins and effects of urea. *Biochemistry*, 11(24):4539–4547, 1972.
- [106] J.N. De Wit. Thermal Stability and Functionality of Whey Proteins. *J. Dairy Sci.*, 73(12):3602–3612, 1990.
- [107] L. Vijayalakshmi, R. Krishna, R. Sankaranarayanan, and M. Vijayan. An asymmetric dimer of β -lactoglobulin in a low humidity crystal form - structural changes that accompany partial dehydration and protein action. *Proteins: Structure, Function, and Bioinformatics*, Volume 71(1):241–249, 2008.
- [108] J.M. Evers, R.G. Haverkamp, S.E. Holroyd, G.B. Jameson, D.D.S. Mackenzie, and O.J. McCarthy. Heterogeneity of milk fat globule membrane structure and composition as observed using fluorescence microscopy techniques. *International Dairy Journal*, 18(12):1081 – 1089, 2008.
- [109] J.N. deWit and G. Klarenbeek. Effects of Various Heat Treatments on Structure and Solubility of Whey Proteins. *J. Dairy Sci.*, 67(11):2701–2710, 1984.
- [110] H. Singh. The milk fat globule membrane—a biophysical system for food applications. *Current Opinion in Colloid & Interface Science*, 11(2-3):154 – 163, 2006.
- [111] M.C. Phillips. Sensory evaluation guide for testing food and beverage products. *Food Technology*, 35(11):50–59, 1981.
- [112] S. Ikeda, E.A. Foegeding, and C.C. Hardin. Phospholipid/fatty acid-induced secondary structural change in β -lactoglobulin during heat-induced gelation. *Journal of Agricultural and Food Chemistry*, 48(3):605–610, 2000.

- [113] M.D. Perez and M. Calvo. Interaction of β -lactoglobulin with retinol and fatty acids and its role as a possible biological function for this protein: a review. *Journal of Dairy Science*, 78(5):978–988, 1995.
- [114] L. Sawyer, S. Brownlow, I. Polikarpov, and S. Wu. β -lactoglobulin: Structural studies, biological clues. *Int. Dairy Journal*, 8:65–72, 1998.
- [115] E.M. Brown, R.J. Carroll, P.E. Pfeffer, and J. Sampugna. Complex formation in sonicated mixtures of β -lactoglobulin and phosphatidylcholine. *Lipids*, 18(2):111–118, 1983.
- [116] H. Labouré, E. Cases, and P. Cayot. Heat induced β -lactoglobulin polymerization: role of the change in medium permittivity. *Food Chemistry*, 85(3):399 – 406, 2004.
- [117] S. Damodaran and A. Paraf. *Food Proteins and Their Applications*. CRC Press, 1997.
- [118] P.L. Privalov and G.I. Makhatadze. Heat capacity of proteins ii. partial molar heat capacity of the unfolded polypeptide chain of proteins: Protein unfolding effects. *Journal of molecular biology*, 213:385–391, 1990.
- [119] R.K.O. Apenten, S. Khokhar, and D. Galani. Stability parameters for β -lactoglobulin thermal dissociation and unfolding in phosphate buffer at ph 7.0. *Food Hydrocolloids*, 16(2):95 – 103, 2002.
- [120] H.A. McKenzie and G.B. Ralston. The denaturation of proteins: Two state? reversible or irreversible? *Cellular and Molecular Life Sciences*, 27(6):617–624, 1971.
- [121] Y.L. Xiong and J.E. Kinsella. Mechanism of urea-induced whey protein gelation. *Journal of Agricultural and Food Chemistry*, 38(10):1887–1891, 1990.
- [122] T.A. Dar, L.R. Singh, A. Islam, and F. Anjum. Guanidinium chloride and urea denaturations of β -lactoglobulin a at ph 2.0 and 25 c. *Biophysical Chemistry*, 127:140148, 2007.

- [123] W.R. Morrison, E.L. Jack, and L.M. Smith. Fatty acids of bovine milk glycolipids and their specific distribution in the diacylglycerophospholipids. *Journal of the American Oil Chemists' Society*, 42(12):1142–1147, 1965.
- [124] A.H. Clark, D.H.P. Saunderson, and A. Sugett. Infrared and laser-Raman spectroscopic studies of thermally-induced globular protein gels. *International Journal of Peptide and Protein Research*, 17(3):353–364, 1981.
- [125] E.M. Brown, J. Sampugna, P.E. Pfeffer, and R.J. Carroll. Interaction of phosphatidylcholine with β -lactoglobulin. *Biophysical Journal*, 37(1):71–72, 1982.
- [126] A. Kristensen, T. Nylander, M. Paulsson, and A. Carlsson. Calorimetric studies of interactions between β -lactoglobulin and phospholipids in solutions. *International Dairy Journal*, 7(1):87 – 92, 1997.
- [127] K. Shimada and J.C. Cheftel. Sulfhydryl group/disulfide bond interchange reactions during heat-induced gelation of whey protein isolate. *Journal of Agricultural and Food Chemistry*, 37(1):161–168, 1989.
- [128] M. Shimizu, M. Saito, and K. Yamauchi. Emulsifying and structural properties of β -lactoglobulin at different pHs. *Agricultural and Biological Chemistry*, 49:189–194, 1984.
- [129] L. Ragona, F. Pusterla, L. Zetta, H.L. Monaco, and H. Molinari. Identification of a conserved hydrophobic cluster in partially folded bovine β -lactoglobulin at pH 2. *Folding and Design*, 2(5):281–290, 1997.
- [130] H. Lang, C. Duschl, and H. Vogel. A new class of thiolipids for the attachment of lipid bilayers on gold surfaces. *Langmuir*, 10(1):197–210, 1994.
- [131] S.M. Schiller, R. Naumann, K. Lovejoy, H. Kunz, and W. Knoll. Archaea analogue thiolipids for tethered bilayer lipid membranes on ultrasmooth gold surfaces. *Angewandte Chemie*, 42:208–211, 2003.

- [132] J. Kunze, J. Leitch, A.L. Schwan, R.J. Faragher, R. Naumann, S. Schiller, W. Knoll, J.R. Dutcher, and J. Lipkowski. New method to measure packing densities of self-assembled thiolipid monolayers. *Langmuir*, 22(12):5509–5519, 2006.
- [133] Petia Atanasova. *A molecular approach towards tethered bilayer lipid membranes: Synthesis and characterization of novel anchor lipids*. PhD thesis, Universität Mainz, 2007.
- [134] L. Rose and A.T.A. Jenkins. The effect of the ionophore valinomycin on biomimetic solid supported lipid dppte/epc membranes. *Bioelectrochemistry*, 70(2):387 – 393, 2007.
- [135] C.D. Bain and G.M. Whitesides. Formation of monolayers by the coadsorption of thiols on gold: Variation in the length of the alkyl chain. *Journal of the American Chemical Society*, 111:7164–7175, 1989.
- [136] K. Simons and E. Ikonen. Functional rafts in cell membranes. *Nature*, 387:569–572, 1997.